ABSTRACT

ERNST, ANDREW FRANCES. Morphology and Function of the Ovipositor Mechanism in Ceraphronoidea (Hymenoptera) and a Phylogeny of the Megaspilinae (Hymenoptera: Ceraphronoidea: Megaspilidae) Based on Molecular Data. (Under the direction of Dr Andrew R. Deans and Dr Brian M. Wiegmann).

Chapter one presents a description of the ovipositor structure of Ceraphronoidea. Six representatives were chosen from Ceraphronidae and Megaspilidae, including Lagynodinae and Megaspilinae. Descriptions are presented in both free text and as characters and character states, using logically defined terms taken from the Hymenoptera Anatomy Ontology, Phenotypic Quality Ontology, and Biospatial Ontology. Variation within Ceraphronoidea and comparison of functional morphology with other Hymenopteran groups are discussed. The configuration and functional interaction of sclerites and muscles does not display much variation across Ceraphronoidea, however the orientation and shape of sclerites display phylogenetically informative variation. The presence and absence of annuli and characters associated with the range of motion of the first valvulae may be indicative of the nature of the oviposition substrate. The unique method used to retract the valvulae into the resting position using the S7-first valvula muscle is an autapomorphy for Ceraphronoidea. The divided first valvula of Trassedia which allows for a greater range of motion of the first valvula is an autapomorphy for Trassedia. The lack of annuli in Trassedia indicate a potential grouping with Ceraphronidae.

Chapter two addresses the phylogeny of megaspiline genera using DNA sequence data from all seven currently accepted generic concepts. Two genera, Dendrocerus and Conostigmus are diverse in comparison to other genera which contain no more than four described species. The monophyly of Dendrocerus and Conostigmus with respect to one

another, and the validity of the remaining genera are tested phylogenetically. Sections of two ribosomal rDNA genes, 16S and 28S, as well as ribosomal protein coding gene 23 and COI are sequenced from 42 ingroup taxa and 16 outgroup taxa. Data are analyzed utilizing model based maximum likelihood (ML) and Bayesian inference (BI). The results from both the ML and BI analyses show Megaspilus, Creator, and Platyceraphron nested within Dendrocerus, with that clade monophyletic with respect to the rest of Megaspilinae. Trichosteresis is nested within Conostigmus, with Conostigmus forming a paraphyletic grade at the base of Megaspilinae. Trassedia groups with Ceraphronidae.

Morphology and Function of the Ovipositor Mechanism in Ceraphronoidea (Hymenoptera) and a Phylogeny of the Megaspilinae (Hymenoptera: Ceraphronoidea: Megaspilidae) Based on Molecular Data

by
Andrew Frances Ernst

A thesis submitted to the Graduate Faculty of
North Carolina State University
in partial fulfillment of the
requirements for the degree of
Master of Science

Entomology

Raleigh, North Carolina

2012

APPROVED BY:

_____	_____
Andrew R Deans	Brian M Wiegmann
Committee Co-Chair	Committee Co-Chair

_____
Coby Schal

DEDICATION

This work is dedicated to my family and friends who have been so supportive through all my endeavors and to my wonderful lab mates Patricia Mullins and Heather Campbel, and the rest of the Deans lab who have made this such an enjoyable experience.

BIOGRAPHY

Andrew Frances Ernst was born in Fresno California on November 7th 1982 to Joline and Lee Ernst. At the age of seven, his family moved to southern California where he eventually graduated from Indio High School with a great deal of interest in agricultural science. He then attended College of the Desert (COD), completing his AS majoring in Environmental Horticulture. During his time at COD he worked at a local retail nursery, Moller's Garden Center, and at the Agriculture Department at COD with Jeffery Place, Valerie Lowe and Kurt Leuschner. During his time at College of the Desert, Andrew took a general entomology course with Kurt where he took a field trip to the entomology department at the University of California Riverside (UCR). After this experience, Andrew decided to transfer to UCR to pursue a BS in Entomology.

Soon after arriving at UCR, Andrew realized he needed a job. After meeting with some of the professors and staff in the Entomology Department he was hired as a student assistant in the UCR Entomology Museum working with Dr Serguei Triapitsyn and Dr Douglas Yanega. His job was process critical point dried parasitic Hymenoptera. After Gaining experience processing material for the museum, Andrew was hired by Dr John Heraty to work in the Hymenoptera systematics lab in the Entomology Department. From this experience he gained a great deal of respect for the diversity of Hymenoptera and decided to apply to graduate school with Hymenoptera systematics in mind. Andrew was accepted to North Carolina State University to work with Dr Andrew R Deans to work on this…

ACKNOWLEDGMENTS

I would like to acknowledge the help I've gotten through my entire graduate experience from Dr. István Mikó. His advice concerning the morphology of Ceraphronoidea, help in determining specimens, dissection methods and imaging methods was crucial to my work. I would also like to extend my thanks to Dr. Barbara Sharanowski, who educated me in laboratory methods and gave me an excellent foundation in understanding methods in molecular phylogenetics. I would like to thank Eva Johannas for teaching me how to use the confocal laser scanning microscope, and for her advice in aquireing the best images possible. I also thank Brian Cassel for his advice in troubleshooting problems in the laboratory, and Dr. Lars Vilhelmsen for his advice and expertise concerning the hymenopteran ovipositor. I thank Steven Turner for his help accessing computing resources for analysis.

TABLE OF CONTENTS

Page

List of Tables vii

List of Figures viii

CHAPTER 1 Morphology and function of the ovipositor mechanism in Ceraphronoidea (Hymenoptera) 1

Introduction 1

Materials and methods 2

Taxa examined 2

Specimen preparations 3

Imaging 4

Terminology used for descriptions 4

Results 5

First valvifer 5

Second valvifer 9

First valvula 11

Second valvula 12

Third valvula 13

Abdominal tergum 9 14

Muscles 15

Discussion 18

Functional morphology.....18

Variation in Ceraphronoidea.....20

Additional features unique to Ceraphronoidea 23

Conclusion 23

REFERENCES 25

CHAPTER 2 Phylogenetics of Megaspilinae (Hymenoptera: Ceraphronoidea: Megaspilidae) based on molecular data.....48

Introduction.....48

Taxonomic history.....48

Materials and methods 51

Taxon sampling.....51

Nucleotide sampling and laboratory protocols 51

Sequence alignment and phylogenetic analyses 54

Results.....56

Model based analyses 57

Discussion.....61

REFERENCES 65

LIST OF TABLES

Chapter 1

Table 1. Specimens observed for morphological description including specimen identifiers, preparation techniques, imaging method and collecting locality . 31

Table 2. Labels linked to anatomical concepts including URI links to ontologies..... 32

Chapter 2

Table 1. List of taxa including country in which the specimen was collected 71

Table 2. List of primers used for PCR amplification of gene regions including the sequence of the primers (5'-3') and the source where primers were found.... 72

Table 3. List of gene regions sampled including the PCR thermal cycler protocols used 73

Table 4. List of taxa, including genes representing taxa in the dataset..... 73

Table 5. List of genes used, including the aligned length in bases, base compositions given in proportions, and models of evolution determined using jModeltest (Posada 2008)..... 74

Table 6. List of datasets including the number of generations to reach an average standard deviation of split frequencies (ASDSF) MrBayes runs, and the effective sample sizes (ESS) calculated from Tracer 1.5.0 (Rambaut and Drummond 2007)..... 75

LIST OF FIGURES

Chapter 1

Figure 1. Photos taken of the ovipositor structure of *Conostigmus abdominalis*, *Trassedia luapi*, *Megaspilus armatus*, *Ceraphron* AFEsp4, *Lagynodes* AFEsp1, and *Aphanogmus* AFEsp1 41

Figure 2. Photos taken of the ovipositor structure of *Conostigmus abdominalis*, *Aphanogmus* AFEsp1, *Trassedia luapi*, and *Megaspilus armatus* 43

Figure 3. Photos taken of the ovipositor structure of *Ceraphron* AFEsp4, *Conostigmus abdominalis*, and *Megaspilus armatus* 45

Figure 4. Photos taken of the ovipositor structure of *Conostigmus abdominalis*, *Megaspilus armatus*, and *Ceraphron* AFEsp4 47

Chapter 2

Figure 1. Most likely tree from the maximum likelihood analysis of 16S rRNA, bootstrap values listed at nodes (stopped at 550 bootstrap pseudoreplicates based on MRE bootstopping criteria) 75

Figure 2. 50% majority rule tree from the maximum likelihood analysis of 16S rRNA (stopped at 550 bootstrap pseudoreplicates based on MRE bootstopping criteria) 76

Figure 3. Topology inferred from the Bayesian analysis of 16S rRNA, posterior probabilities are listed at the nodes (38,780,000 generations) 77

Figure 4. Most likely tree from the maximum likelihood analysis of 16S rRNA with variable regions removed, bootstrap values listed at nodes (stopped at 450 bootstrap pseudoreplicates based on MRE bootstopping criteria)..... 78

Figure 5. 50% majority rule tree from the maximum likelihood analysis of 16S rRNA with variable regions removed (stopped at 450 bootstrap pseudoreplicates based on MRE bootstopping criteria) 79

Figure 6. Topology inferred from the Bayesian analysis of 16S rRNA with variable regions removed, posterior probabilities are listed at the nodes (6,650,000 generations)..... 80

Figure 7. Consensus network based on the most likely trees for the 16S rRNA and 16S RRNA with variable regions removed datasets (Figures 1 and 4), calculated using mean edge weights and a threshold of 0.33 81

Figure 8. Most likely tree from the maximum likelihood analysis of 28S rRNA, bootstrap values listed at nodes (stopped at 450 bootstrap pseudoreplicates based on MRE bootstopping criteria) 82

Figure 9. 50% majority rule tree from the maximum likelihood analysis of 28S rRNA (stopped at 450 bootstrap pseudoreplicates based on MRE bootstopping criteria).... 83

Figure 10. Topology inferred from the Bayesian analysis of 28S rRNA, posterior probabilities are listed at the nodes (4,360,000 generations)..... 84

Figure 11. Supernetwork based on the most likely trees from the 16S rRNA and 28S rRNA datasets (Figures 1 and 8), calculated using the Z-closure method with TreeSizeWeightedMean edge weights..... 85

Figure 12. Most likely tree from the maximum likelihood analysis of COI mitochondrial DNA, bootstrap values listed at nodes (1000 bootstrap pseudoreplicates)..... 85

Figure 13. 50% majority rule tree from the maximum likelihood analysis of COI mitochondrial DNA (1000 bootstrap pseudoreplicates) 86

Figure 14. Topology inferred from the Bayesian analysis of COI mitochondrial DNA, posterior probabilities are listed at the nodes (12,210,000 generations)..... 87

Figure 15. Most likely tree from the maximum likelihood analysis of exonic regions of RPS23 nuclear protein-encoding gene, bootstrap values listed at nodes (1000 bootstrap pseudoreplicates)..... 87

Figure 16. 50% majority rule tree from the maximum likelihood analysis of exonic regions of RPS23 nuclear protein-encoding gene (1000 bootstrap pseudoreplicates) 88

Figure 17. Topology inferred from the Bayesian analysis of exonic regions of RPS23 nuclear protein-encoding gene, posterior probabilities are listed at the nodes (11,090,000 generations) 89

Figure 18. Most likely tree from the maximum likelihood analysis of intronic region of RPS23 nuclear protein-encoding gene, bootstrap values listed at nodes (1000 bootstrap pseudoreplicates)..... 90

Figure 19. 50% majority rule tree from the maximum likelihood analysis of intronic regions of RPS23 nuclear protein-encoding gene (1000 bootstrap pseudoreplicates) 91

Figure 20. Topology inferred from the Bayesian analysis of intronic regions of RPS23 nuclear protein-encoding gene, posterior probabilities are listed at the nodes (11,040,000 generations) 92

Figure 21. Most likely tree from the maximum likelihood analysis of the concatenated dataset of 16S rRNA, 28S rRNA, COI mitochondrial protein-encoding DNA and RPS23 nuclear protein-encoding gene including intron and exons, bootstrap values listed at nodes (stopped at 800 bootstrap pseudoreplicates based on MRE bootstopping criteria) 93

Figure 22. 50% majority rule tree from the maximum likelihood analysis of the concatenated dataset of 16S rRNA, 28S rRNA, COI mitochondrial protein-encoding DNA and RPS23 nuclear protein-encoding gene including intron and exons (stopped at 800 bootstrap pseudoreplicates based on MRE bootstopping criteria) 94

Figure 23. Topology inferred from the Bayesian analysis of the concatenated dataset of 16S rRNA, 28S rRNA, COI mitochondrial protein-encoding DNA and RPS23 nuclear protein-encoding gene including intron and exons, posterior probabilities are listed at the nodes (5,631,000 generations) 95

CHAPTER 1

Chapter 1: Morphology and function of the ovipositor mechanism in Ceraphronoidea (Hymenoptera)

Introduction

Ceraphronoidea are one of the most understudied groups of parasitic Hymenoptera despite their ubiquity in the environment and fascinating life history strategies which span from primary to quaternary parasitism (Hyper- hyper- hyper parasitism)(Haviland 1920). Records of parasitism by ceraphronoids cover a wide range of hosts from eight different insect orders; Hemiptera, Thysanoptera, Hymenoptera, Neuroptera, Coleoptera, Trichoptera, Diptera and Mecoptera (Austin 1984, Chiu et al. 1981, Cooper and Dessart 1975, Dessart 1967, 1992, Dessart and Bournier 1971, Evans et al. 2005, Fergusson 1980, Ghesquiere 1960, Ishii 1937, Luhman et al. 1999, Muesebeck 1979, Priesner 1936, Sinacori et al. 1992). At least two species, *Dendrocerus carpenteri* (Curtis), and *Dendrocerus aphidum* (Rondani), serve as models for research concerning: resource use and allocation by parasitoids (Araj et al. 2006), mate location (Schwoerer et al., 1999), development and host interactions (Marris et al. 2000), sex determination of offspring (Chow and Mackauer 1996), host discrimination (Chow and Mackauer 1999), and behavioral evolution in bio-control systems (Muller et al. 1997).

The phylogenetic placement of Ceraphronoidea remains uncertain. Using expressed sequence tag (EST) data, Sharanowski et al. (2010) placed Ceraphronoidea as sister to Evanioidea, but with low support statistics and limited exemplars. Heraty et al. (2011) using

sequence data from four genetic loci, placed Ceraphronoidea as sister to Stephanidae or Stephanidae + Orussidae. Vilhelmsen et al. (2010) found Ceraphronoidea to be sister to Megalyroidea in the Evaniomorpha based on morphological data. Sharkey et al. (2011) using a morphological data set based largely on Vilhelmsen et al. (2010) also suggested a sister relationship between Ceraphronoidea and Megalyroidea. More data are clearly needed to robustly estimate these evolutionary relationships. Untapped character systems, such as the ovipositor complex may contain phylogenetically informative data that can help us surmount this problem.

Despite the extensive work done on both functional morphology and phylogenetic implications of the Hymenoptera ovipositor system (Austin and Field 1997, Copland 1971, King and Copland 1969, Oeser 1961, Quick et al. 1992, Quicke et al. 1994, Quick and Fitton 1995, Quick et al. 1999, Smith 1970, Vilhelmsen 2000, Vilhelmsen et al. 2001), the ceraphronoid ovipositor has never been formally described.

Our goal is to describe the skeletal and muscular anatomy of the ovipositor complex in Ceraphronoidea using representatives from across the superfamily, especially to discover phylogenetically-relevant variation between major lineages within Ceraphronoidea.

Materials and methods

Taxa examined

Megaspilinae was represented by *Megaspilus armatus* (Say), *Conostigmus abdominalis* (Boheman) and *Trassedia luapi* (Cancemi). Lagynodinae (Megaspilidae) is represented here by *Lagynodes* AFEsp1. Ceraphronidae is represented by *Ceraphron*

AFEsp4 and *Aphanogmus* AFEsp1. Several specimens of each species were used with the exception of *Trassedia luapi* where only one specimen was available for dissection. The single specimen of *Trassedia luapi*, was treated with proteinase K for DNA extraction, which macerated soft tissues, and therefore only the skeletal structures were examined for this taxon. Specimen information is given in Table 1.

Specimen preparations

Dry preparations were used for the initial visualization of muscles and sclerites. Specimens were immersed in absolute ethanol for one hour to dehydrate them. They were then critical point dried. The abdomen was then dissected and the ovipositor complex and terminal segments were removed and imaged. Images were made throughout the process of dissection of the ovipositor structure itself to view the position of muscles and sclerites. For wet preparations, specimens were taken from 95% ethanol where they were stored and transferred to glycerin on a concave microscope slide. The apex of the abdomen was removed, dissected and prepared for imaging in much the same process as the dry preparations. Some specimens were macerated in KOH before observations and images were made. Treatment of specimens is given in Table 1.

Since these are relatively small structures on very small insects (the ovipositor of *Aphanogmus* AFEsp1 <0.2mm), it was necessary to use multiple visualization techniques to appreciate the three dimensional complexity and relationships of structures in the ovipositor system. Dissections and observations were made using an Olympus SZX16 stereo microscope and an Olympus CX41 compound microscope.

Imaging

Images were taken under both bright field and laser scanning confocal microscopy (LSM). Bright field images were taken using an Olympus CX41 compound microscope with an Olympus DP71 microscope digital camera. Image stacks were taken for all of the bright field images. Stacks were combined using the CombineZP (Hadley 2010). LSM images were taken using the Zeiss 710 Laser Scanning Microscope. LSM images were created and edited using the Zeiss ZEN software. Adobe Photoshop was used in the final editing of the images. Imaging methods used for specimens is given in Table 1.

Terminology used for descriptions

Traditionally, morphological descriptions have been done as free text and do not link labels to logical, explicitly defined concepts. Vogt et al. 2010 described problems with the lack of uniform terminology which can lead to misunderstanding of morphology. An example of this kind of problem would be the use of the term stylet by Lacaze-Duthiers (1849) in reference to the first valvula, and the use of the term stylet by André (1879) in reference to the anatomical cluster of the first valvula and the first valvifer. The morphological descriptions here are made using terms taken from biomedical ontologies. The benefit of using ontologies is that the terms are associated with anatomical, phenotypic and spatial concepts that are explicitly defined. This removes any ambiguity concerning the structures to which the terms are referring. Descriptions are written as free text and as characters and character states,which employ anatomical terminology from the newly develpoed Hymenoptera Anatomy Ontology (HAO) (5/8/2011, 10:25, Yoder et al. 2010).

Characters and states are written using the same anatomical terminology as well as phenotypic terms from the Phenotypic Quality Ontology 1.2 (PATO) (21/2/2012, 12:34, Gkoutos et al. 2004), and the bio-spatial ontology (BSPO)(10/09/2009, 9:32, http://www.berkeleybop.org/ontologies/bspo.owl) Concepts used from the HAO, PATO and the bio-spatial ontology are listed in Table 1.

Results

First valvifer

The lateral surface of the first valvifer in *Ceraphron* AFEsp4, *Aphanogmus* AFEsp1, *Lagynodes* AFEsp1, *Conostigmus abdominalis* and *Megaspilus armatus* is D-shaped, with the anterior margin curved (Figure 1). In *Trassedia luapi* there are two sclerites in this position, the dorsal sclerite of the first valvifer and the ventral sclerite of the first valvifer. The dorsal sclerite of the first valvifer and the ventral sclerite of the first valvifer articulate with one another at the anterior end of the margin between the two sclerites. The dorsal sclerite of the first valviferal condyle of the ventral sclerite of the first valvifer is located anteriorly on the ventral sclerite of the first valvifer. The ventral sclerite of the first valviferal fossa of the dorsal sclerite of the first valvifer is located on the antero-ventral area of the dorsal sclerite of the first valvifer. The ventral margin of the dorsal sclerite of the first valvifer is thickened. The antero-dorsal margin of the dorsal sclerite of the first valvifer is thickened.

In *Megaspilus armatus*, *Conostigmus abdominalis* and *Lagynodes* AFEsp1the anterior flange of the first valvifer projects in an anterior direction off the first valvifer and

overlaps with the posterior margin of the anterior area of the second valvifer. The conjunctiva connecting the anterior margin of the first valvifer with the posterior margin of the anterior area of the second valvifer attaches at the base of the anterior flange of the first valvifer. In Ceraphronidae and *Trassedia luapi* the anterior flange of the first valvifer is absent. The posteroventral corner of the first valvifer bears the second valviferal condyle of the first valvifer. The posterior margin bears the ninth tergal condyle of the first valvifer.

The position of the ninth tergal condyle of the first valvifer along the posterior margin of the first valvifer varies across Ceraphronoidea. The location of the ninth tergal condyle of the first valvifer is symmetric to the ventral and dorsal margins of the first valvifer in *Conostigmus abdominalis* and *Lagynodes* AFEsp1. In *Ceraphron* AFEsp4 the distance to the dorsal margin is greater than the distance to the ventral margin. In *Megaspilus armatus* the distance to the dorsal margin is less than the distance to the ventral margin. In *Aphanogmus* AFEsp1, the articulation is adjacent to the dorsal margin of the first valvifer. In *Trassedia luapi* the ninth tergal condyle is on the ventral area of the dorsal sclerite of the first valvifer. The first valvifer, when at rest, is oriented dorso-ventraly for the most part in Ceraphronoidea. However, in *Ceraphron* AFEsp4 the dorsal end is oriented posteriorly, creating a 45 degree angle with the long axis of the ovipositor. In Ceraphronidae, the anterior margin is sharply defined, and uniformly sclerotized.

1: Shape of the lateral surface of the first valvifer

(0) D-shaped (Figure 1A)

(1) L-shaped (Figure 1B)

2: Presence of the dorsal sclerite of the first valvifer

(0) present (Figure 1B)

(1) absent

3: Presence of the ventral sclerite of the first valvifer

(0) present (Figure 1B)

(1) absent

4: Presence of the dorsal sclerite of the first valviferal condyle of the ventral sclerite of the first valvifer

(0) present

5: Presence of the ventral sclerite of the first valviferal fossa of the dorsal sclerite of the first valvifer

(0) present

6: Location of the ventral sclerite of the first valviferal fossa of the dorsal sclerite of the first valvifer

(0) on the antero-ventral area of the dorsal sclerite of the first valvifer (Figure 1B)

7: Location of the dorsal sclerite of the first valviferal condyle of the ventral sclerite of the first valvifer

(0) on the anterior area of the ventral sclerite of the first valvifer (Figure 1B)

8: Thickness of the ventral margin of the dorsal sclerite of the first valvifer

(0) increased thickness (Figure 2E)

9: Thickness of the antero-dorsal margin of the ventral sclerite of the first valvifer

(0) increased thickness (Figure 2E)

10: Presence of the anterior flange of the first valvifer

(0) present (Figure 3C, 2F)

(1) absent (Figure 4E)

11: Location of the second valviferal condyle of the first valvifer

(0) posteroventral corner of the first valvifer (Figure 1C)

12: Location of the ninth tergal condyle of the first valvifer

(0) posterior margin of the first valvifer (Figure 2B)

13: Location of the ninth tergal condyle of the first valvifer on the posterior margin of the first valvifer

(0) equidistant to the ventral margin of the first valvifer and the dorsal margin of the first valvifer (Figure 1A)

(1) distance to the ventral margin of the first valvifer less than the distance to the dorsal margin of the first valvifer (Figure 2B)

(2) distance to the ventral margin of the first valvifer greater than the distance to the dorsal margin of the first valvifer (Figure 1C)

(3) adjacent to the dorsal margin of the first valvifer (Figure 1F)

(4) ventrally on the dorsal sclerite of the first valvifer (Figure 2E)

14: Orientation of the posterior margin of the first valvifer

(0) at a right angle to the dorsal flange of the second valvifer (Figure 1A)

(1) at an acute angle to the dorsal flange of the second valvifer (Figure 1D)

Second valvifer

The area anterior of the first valviferal fossa of the second valvifer is expanded dorsally into a broad, flat, laterally directed surface that is located anterior to the first valvifer. The pars articularis is located antero-ventrally on the second valvifer. In *Ceraphron* AFEsp4, and *Trassedia luapi* the basal line of the second valvifer is present as a sharply defined ridge, while in *Aphanogmus* AFEsp1 and Megaspilidae as a diffuse thickening of the cuticle. In *Trassedia luapi*, anterior to the first valviferal fossa of the second valvifer, there is a lateral depression which accommodates the ventral sclerite of the first valvifer. The dorsal projection of the second valvifer in *Ceraphron* AFEsp4 and *Trassedia luapi*, projects a distance greater than the shortest distance from the anterior margin of the anterior area of the second valvifer to the posterior margin of the anterior area of the second valvifer. The posterior margin of the anterior area of the second valvifer is a sharply defined ridge in *Ceraphron* AFEsp4 and *Trassedia luapi*.

The posterior area of the second valvifer is elongate and convex laterally. The ventral margin of the second valvifer curves medially and dorsally, and accommodates the posterior second valvifer-second valvula muscle. The genital membrane is invaginated between the second valvifers along its entire length, creating an elongate depression which accomodates the first and second valvulae.

15: Shape of the anterior area of the second valvifer

(0) broad flat area anterior to the intervalvifer articulation (Figure 4B)

16: Shape of the anterior and dorsal margins of the anterior area of the second valvifer

(0) curving (Figure 2E)

17: Location of the pars articularis

(0) located on the antero-ventral area of the second valvifer (Figure 4C)

18: Presence of the basal line of the second valvifer

(0) present

19: Conspicuousness of the basal line of the second valvifer

(0) ridge like (Figure 3B)

(1) increased thickness (Figure 4C)

20: Location of depression that accommodates the ventral sclerite of the first valvifer

(0) anterior to the first valviferal fossa of the second valvifer (Figure 2E)

21: Depression that accommodates the ventral sclerite of the first valvifer

(0) present

(1) absent

22: Dorsal projection of the second valvifer projecting a distance greater than the shortest distance from the anterior margin of the anterior area of the second valvifer to the posterior margin of the anterior area of the second valvifer

(0) present (Figure 2E)

(1) absent (Figure 4D)

23: Shape of the posterior margin of the anterior area of the second valvifer

(0) ridge-like (Figure 3A)

(1) not ridge-like (Figure 4B)

24: Shape of the posterior area of the second valvifer

(0) elongated (Figure 3A)

25: Shape of the ventral margin of the second valvifer

(0) curved medially and dorsally (Figure 2F)

26: Shape of the genital membrane

(0) invaginated between the second valvifers (Figure 2F)

First valvula

The distal area of the first valvula in *Ceraphron* AFEsp4 and *Trassedia luapi* is linear, and in *Megaspilus armatus*, *Conostigmus abdominalis*, *Lagynodes* AFEsp1 and *Aphanogmus* AFEsp1 is spatulate. In Ceraphronidae, *Trassedia luapi* the first valvula is straight and tapered distally, in *Conostigmus abdominalis* the first valvula is curving dorsally. In *Conostigmus abdominalis* the median side of the ventral margin of the first valvula bears a row of stout setae that are directed distally.

27: Shape of the distal area of the first valvula

(0) linear (Figure 1D)

(1) spatulate (Figure 4B)

28: Shape of the distal area of the first valvula

(0) straight (Figure 3E)

(1) curving dorsally (Figure 4B)

29: Shape of the apex of the first valvula

(0) tapered (Figure 1D)

Second valvula

The distal area of the second valvula is located medial to the posterior area of the second valvifer and the third valvula. The bulb bears the processus articularis ventro-laterally, the processus muscularis antero-dorsally, and the anterior notch of the second valvula accomodating first valvula and the ventral ramus of the second valvula. The dorsal rami of the second valvulae are continuous with one another distal to the bulb. The dorsal valve distal to the bulb gradually tapers. The anterior margin of the bulb is curved dorsally. In *Aphanogmus* AFEsp1, the height of the bulb is equal to half the height of the anterior area of the second valvifer. In *Ceraphron* AFEsp4 and Megaspilidae, the height of the bulb is less than half the height of the anterior area of the second valvifer. Annuli are present in *Megaspilus armatus*, *Conostigmus abdominalis* and *Lagynodes* AFEsp1, and absent in Ceraphronidae and *Trassedia luapi*. In *Conostigmus abdominalis* and *Lagynodes* AFEsp1, there are four annuli, and in *Megaspilus armatus* there are six.

30: Location of the processus articularis

(0) laterally on the bulb (Figure 4C)

31: Location of the processus muscularis

(0) antero-dorsally on the bulb (Figure 4C)

32: Location of the anterior notch of the second valvula

(0) anteriorly on the bulb (Figure 1C)

33: Attatchment quality of distal region of second valvulae

(0) continuous (Figure 2D)

34: Shape of the distal area of the dorsal valve

(0) tapered gradually (Figure 2C)

35: Shape of the dorsal margin of the bulb anteriorly

(0) curved (Figure 2A)

36: Height of the proximal area of the dorsal ramus of the second valvula

(0) half the height of the anterior area of the second valvifer (Figure 2C)

(1) less than the height of the anterior area of the second valvifer (Figure 2A)

37: Presence of annuli

(0) present (Figure 1A)

(1) absent (Figure 2D)

38: Number of annuli

(0) four (Figure 1A)

(1) six (Figure 1C)

Third valvula

Anteriorly, the ventral margin of the third valvula curved dorsally. The dorsal margin reaching the median bridge. The third valvula is convex laterally and tapers distally. The median surface is concave and membranous.

39: Shape of the anterior region of the third valvula

(0) ventral margin curved dorsally and reaching the median bridge (Figure 1B)

40: Shape of the lateral surface of the third valvula

(0) convex

41: Shape of the distal region of the third valvula

(0) tapered (Figure 1B)

Abdominal tergum 9

The anterior margin of abdominal tergum 9 is U-shaped. The dorsal area of abdominal tergum 9 is narrow and strap-like, broadening laterally. The lateral surface of abdominal tergum 9 is quadrangular. The first valviferal fossa of abdominal tergum 9 is located on the anterior-most margin of abdominal tergum 9. The anterior flange is adjacent to the antero-lateral margin of abdominal tergum 9 proximally, while posteriorly the distance from the anterior flange to the margin gradually increases.

42: Shape of anterior margin of abdominal tergum 9

(0) U-shaped

43: Shape of the dorsal area of abdominal tergum 9

(0) slender (Figure 1F)

44: Shape of the lateral area of abdominal tergum 9

(0) quadrangular (Figure 4B)

45: Location of the first valviferal fossa of abdominal tergum 9

(0) on the anterior-most margin of abdominal tergum 9 (Figure 3C)

46: Location of the anterior flange

(0) adjacent to the anterior margin of abdominal tergum 9 anteriorly and the distance from the margin gradually increasing posteriorly (Figure 4B)

47: Presence of gland median to second valvifer

(0) present (Figure 1B, 1E, 3A)

(1) absent

Muscles

S7-first valvula muscle (M1): Arises adjacent to the anterior margin of abdominal sternum 7 and inserts on the ventral ramus of the first valvula adjacent to the fusion of the first valvula to the dorsal end of the first valvifer (Figure 2A, 3E, 3f).

48: Location of the S7-first valvula muscle insertion on abdominal sternum 7

(0) adjacent to the anterior margin

49: Location of the S7-first valvula muscle insertion on the first valvula

(0) on the proximal side of the ventral ramus of the first valvula

Dorsal T8-T9 muscle (M2): Arises adjacent to the anterior margin of the dorsal area of abdominal tergum 8 and inserts on the anterior margin of the dorsal area of abdominal tergum 9 (Figure 1E, 2A, 3B, 3D, 4A).

50: Location of the dorsal T8-T9 muscle insertion on abdominal tergum 8

(0) adjacent to the anterior margin of abdominal tergum 8

51: Location of the dorsal T8-T9 muscle insertion on abdominal tergum 9

(0) on the anterior margin of the dorsal region of abdominal tergum 9

Lateral T8-T9 muscle (M3): Arises postero-dorsal to the dorsal T8-T9 muscle on abdominal tergum 8, and inserts on the anterior flange of abdominal tergum 9(Figure 1E, 2B, 3B, 3D, 4A).

52: Location of the Lateral T8-T9 muscle insertion on abdominal tergum 8

(0) postero-dorsal to the insertion of the dorsal T8-T9 muscle

53: Location of the Lateral T8-T9 muscle insertion on abdominal tergum 9

(0) on the anterior flange of abdominal tergum 9

T8-first valvifer muscle (M4): Arises dorsal to the lateral T8-T9 muscle on abdominal tergum 8, and inserts on the first valvifer adjacent to the ninth tergal condyle of the first valvifer (Figure 3C, 3D, 4A).

54: Location of the T8-first valvifer muscle insertion on abdominal tergum 8

(0) dorsal to the insertion of the lateral T8-T9 muscle on abdominal tergum 8

55: Location of the T8-first valvifer muscle insertion on the first valvifer

(0) adjacent to the ninth tergal condyle of the first valvifer

Dorsal T9-second valvifer muscle (M5): Subdivided into two bundles arising from the anterior flange of abdominal tergum 9 and the dorsal and ventral surfaces surrounding the anterior flange of abdominal tergum 9, and inserts along the posterior margin of the anterior area of the second valvifer (Figure 1D, 3F, 4A, 4D, 4F).

56: Shape of the dorsal T9-second valvifer muscle

(0) split into two bundles

57: Location of the dorsal T9-second valvifer muscle insertion on abdominal tergum 9

(0) on and adjacent to the anterior flange of abdominal tergum 9

58: Location of the dorsal T9-second valvifer muscle insertion on the second valvifer

(0) on the posterior margin of the anterior area of the second valvifer

Second valvifer-anterior T9 muscle (M6): Arises broadly from the medial side of the posterior area of the second valvifer, and inserts on the cordate apodeme of abdominal tergum 9 (Figure 1E, 2B, 3B, 3F, 4A).

59: Location of the second valvifer-anterior T9 muscle insertion on the second valvifer

(0) on the medial side of the posterior area of the second valvifer

60: Location of the second valvifer-anterior T9 muscle insertion on abdominal tergum 9

(0) on the cordate apodeme of abdominal tergum 9

Posterior T9-second valvifer muscle (M7): Arises from the strap-like dorsal area of abdominal tergum 9 and inserts on the median bridge of the second vlavifers (Figure 3D, 3F, 4A, 4D).

61: Location of the posterior T9-second valvifer muscle insertion on abdominal tergum 9

(0) on the dorsal region of abdominal tergum 9

62: Location of the posterior T9-second valvifer muscle insertion on the second valvifer

(0) on the median bridge of the second valvifer

First valvifer-genital membrane muscle (M8): Arises from the medial side of the first valvifer near the intervalvifer articulation, extends posterio-medially where it inserts medially on the genital membrane (Figure 2A, 3F, 4D, 4E).

63: Location of the first valvifer-genital membrane muscle insertion on the first valvifer

(0) on the median side of the first valvifer adjacent to the intervalvifer articulation

64: Location of the first valvifer-genital membrane muscle insertion on the genital membrane

(0) on the medial region of the genital membrane

Posterior second valvifer-second valvula muscle (M9): Arises broadly from the medial side of the posterior area of the second valvifer, and inserts on the processus musculares. In *Ceraphron* AFEsp4 fewer than half of the bands of the muscle arise anterior of the intervalvifer articulation on the anterior area of the second valvifer (Figure 2F3B, 3F, 4A, 4E, 4F).

65: Location of the posterior second valvifer-second valvula muscle insertion on the second valvifer

(0) on the median side of the posterior area of the second valvifer

(1) on the median side of the anterior area of the second valvifer and the posterior area of the second valvifer

66: Location of the posterior second valvifer-second valvula muscle insertion on the second valula

(0) on the processus musculares

Discussion

Functional Morphology

To understand complex ecological interactions such as those between a parasitoid and its host we need to know the structure and function of anatomical entities involved in the interaction. In non-aculeate Hymenoptera, the ovipositor is used to penetrate the host and/or the substrate surrounding the host in order to deposit an egg. Substrates such as the puparium of a fly, wood where a wood boring larva might be found, or in the case of a hyperparasitoid, the remains of the primary host might present various obstacles for the wasp to overcome.

Ican easily imagine that it would require the evolution of various specialized morphologies to cope with these obstacles, and potentially more than one method may have been utilized to overcome the same obstacle (Quick et al. 1999, Vincent and King 1996).

The first valvifer is continuous with the first valvula, and the condition is the same for the second valvifer and second valvula. The reason it is beneficial to refer to the valvifers and valvulae as separate structures is because, functionally, they serve different roles. The distinction we use to differentiate the valvula from the valvifer is the presence of the olistheters. The olistheters are an interlocking "tongue and groove" mechanism that bind the first and second valvulae together while allowing them to slide back and forth, along one another. This indicates that the first valvula extends along the first valvifer where the aulax is present and the second valvula along the second valvifer where the rachis is present. The rachis, and therefore the second valvula, extends from the anterior margin of the anterior area of the second valvifer to the apex of the dorsal projection of the second valvifer. This margin is curved and creates a stable anchor along which the first valvula can slide.

The initial movement of the ovipositor, in preparation for oviposition is to extend the valvulae from their resting position between the paired second valvifers and paired third valvulae. This movement exposes the apex of the ovipositor so that it can access the host. From observation it seems that this movement is accomplished by the posterior second valvifer-second valvula muscles. When these muscles contract they cause the bulb to pivot at the basal articulation, which moves the distal end of the second valvulae, and subsequently the first valvulae, in a ventral direction.

To move the valvulae from the active position to the resting position I hypothesize that ceraphronoids contract the S7-first valvula muscle. Abdominal sternum 7 extends posteriorly, and lies ventral to the valvulae. The muscle attachment to the first valvula is located proximally, adjacent to the first valvifer. When this long slender muscle contracts, abdominal sternum 7 will pull the valvulae back into the resting position between the paired second valvifers and third valvulae.

The first valvifers, second valvifers and abdominal tergum 9 form the machinery that drives the movement which causes the first valvulae to slide longitudinally along the second valvulae. The muscles driving this movement are the dorsal T9-second valvifer muscles and the ventral T9-second valvifer muscles. As the dorsal T9-second valvifer muscles contract, abdominal tergum 9 pushes the first valvifer in an anterior direction. The first valvifer will pivot on the intervalvifer articulation which slides the first valvula in a distal direction. When the ventral T9-second valvifer muscles contract, abdominal tergum 9 pulls the first valvifer in the opposite direction which results in the first valvula moving in a proximal direction. Since the paired first valvifers and the proximal areas of the first valvulae are separated by a region of conjunctiva, we hypothesize that the structures can move independently from one another; however the range of independent motion would be greatly reduced.

Variation in Ceraphronoidea

Differences in morphology usually reflect differences in life history. The presence or absence of annuli at the tip of the ovipositor, for example, may depend on the substrate into which the wasp is ovipositing, as well as the circumstances under which oviposition is taking

place (Quick et al. 1999). Of the species examined, ceraphronids and *Trassedia luapi* lack annuli, while the rest of Megaspilidae all bear annuli on the second valvulae. Since the presence and density of these serrations are associated with different substrate consistencies (Quick et al. 1999), it might be possible to predict trends in host location and substrate texture.

Another phenotypically variable feature we see in Ceraphronoidea is the location of the tergo-valvifer articulation along the posterior margin of the first valvifer. The closer the tergovalvifer articulation is to the intervalvifer articulation, and consequently the further it is from the dorsal end of the first valvifer, the further the dorsal end of the first valvifer will move relative to the distance that abdominal tergum 9 moves. As this movement is what slides the first valvula along the second valvula, the distance the first valvifer moves determines the distance the first valvula moves. With a larger range of movement, the substrate can be penetrated more quickly since the first valvulae will be thrust further into the substrate with each cycle of movement as opposed to a slower drilling that we would see with a shorter range of movement. The same can be said for the egg moving down the length of the ovipositor, a larger range of movement will move the egg further with each cycle of movement which will allow the wasp to oviposit more quickly.

The distance of the processus musculares from the basal articulation is another mechanical variation in Ceraphronoidea. The greater this distance is, the easier it is for the posterior second valvifer-second valvula muscle to extend the valvulae. Consequently, the greater this distance is, the further the muscle must contract to fully extend the valvulae.

I observed in *Trassedia luapi* that there are two sclerites that perform the role of the first valvifer. I hypothesize that the first valvifer has become divided into the dorsal sclerite of the first valvifer and the ventral sclerite of the first valvifer. The ventral sclerite is oriented horizontally, with the posterior end forming the intervalvifer articulation with the second valvifer. There is a depression in the lateral face of the second valvifer which accommodates the anterior end of the ventral sclerite of the first valvifer. The dorsal sclerite of the first valvifer is continuous with the first valvula dorsally, and forms the tergovalvifer articulation with abdominal tergum 9 posteriorly. The dorsal and ventral sclerites of the first valvifer articulate at the anterior end of this division between them. At the posterior end of the division between the two sclerites, they are thickened so that they abut against one another. This articulation point allows the dorsal sclerite to pivot anteriorly when the ventral sclerite is at rest in the depression on the second valvifer. When the dorsal sclerite pivots posteriorly so that the posterior end of the division between the sclerites comes together, the two sclerites will then continue posteriorly together as a unit, as the ventral sclerite pivots on the intervalvifer articulation. This movement using two points of articulation allows for a very large range of movement, and allows the first valvulae to slide a very long distance along the second valvulae. This large range of movement may be necessary to move the egg very quickly down the length of the ovipositor. The lack of annuli on the apex of the valvulae indicates that this wasp may oviposit into a soft substrate. We hypothesize that the host of *Trassedia luapi* will be found in the open or within a soft substrate and there will be reason for the female to deposit an egg quickly. Across all of Hymenoptera, there is no record of ovipositor morphology comparable to this double hinge.

Additional features unique to Ceraphronoidea

The method that Ceraphronoidea use to move the valvulae into the resting position is different than many other hymenopteran groups. Most hymenopterans have a muscle called the anterior second valvifer-second valvula muscle. This muscle arises from the antero-dorsal margin of the second valvifer and inserts on the distal area of the bulb (King and Copland 1969, Vilhelmsen 2000). The absence of this muscle in Ceraphronoidea could be due to the fact that abdominal sternum 7 extends posteriorly, protecting the ventral side of the ovipositor. Because of this, the S7-first valvula muscle can very easily and efficiently pull the valvulae into the resting position and because of the redundant system, the anterior second valvifer-second valvula muscle is absent. Another reason could be the enlarged gland located medial to the second valvifers found in Ceraphronidae and *Lagynodes* AFEsp1. This large gland is positioned between the second valvifers and leaves little room for the anterior second valvifer-second valvula muscle.

Conclusion

The general function of the ovipositor regarding the interaction of muscles and sclerites follows a common pattern throughout Hymenoptera, however, crucial differences have been identified including the unique method ceraphronids use to retract the ovipositor into its resting position, and the fascinating morphology of the first valvifer in *Trassedia luapi*. In the future, other taxa within Hymenoptera will be coded for these characters in an effort to provide evidence to help determine the sister group to Ceraphronoidea. It is important that further studies of the Hymenoptera ovipositor be done using explicitly defined

morphological classes so that the data can be combined and confidently compared to and combined with other datasets.

REFERENCES

André, E., 1879. Species des Hyménoptères d'Europe et d'Algérie. First edition. Beaune, France.

Araj, S.A., Wratten, S.D., Lister, A.J., Buckley, H.L., 2006. Floral nectar affects longevity of the aphid parasitoid *Aphidius ervi* and its hyperparasitoid *Dendrocerus aphidum*. New Zealand Plant Protection 59, 178-183.

Austin, A.D. 1984. New species of Platygastridae (Hymenoptera) from India which parasitise pests of mango, particularly Procontarinia spp. (Diptera: Cecidomyiidae). Bulletin of Entomological Research 74, 549-557.

Austin, A.D., Field, S.A., 1997. The Ovipositor system of scelionid and platygastrid wasps (Hymenoptera: Platygastroidea): comparative morphology and phylogenetic implications. Invertebrate Taxonomy 11, 1-87.

Chiu, S.C., Chou, L.J., Chou, K.C. 1981. A preliminary survey on the natural enemies of Kerria lacca (Kerr) in Taiwan. Journal of Agricultural Research of China 30, 420–425.

Chow, A., Mackauer, M., 1996. Sequential allocation of offspring sexes in the hyperparasitoid wasp, *Dendrocerus carpenteri*. Animal Behaviour 51(4), 859-870.

Chow, A., Mackauer, M., 1999. Marking the package or its contents: Host discrimination and acceptance in the ectoparasitoid *Dendrocerus carpenteri* (Hymenoptera: Megaspilidae). Canadian Entomologist 131(4), 495-505.

Copland, M.J.W., King, P.E., 1971. The structure and possible function of the reproductive system in some Eulophidae and Tetracampidae. The Entomologist 104, 4-28.

Cooper, K.W., Dessart, P., 1975. Adult, larva and biology of *Conostigmus quadratogenalis* Dessart and Cooper, sp.n., (Hym. Ceraphronoidea), parasite of *Boreus* (Mecoptera) in California. Bulletin et Annales de la Societe Royale Belge d'Entomologie 111, 37-53.

Dessart, P. 1967. Description de Dendrocerus (Macrostigma) noumeae sp. nov. de Nouvelle Caledonie (Ceraphronoidea Megaspilidae). Entomophaga 12, 343–349.

Dessart, P. 1992. Revision d'Aphanogmus fulmeki Szelenyi, 1940 (Hymenoptera, Ceraphronoidea, Ceraphronidae) avec remarques biologiques. Bulletin de l'Institute Royal des Sciences Naturelles de Belgique 62, 83–91.

Dessart P, Bournier A (1971) *Thrips tabaci* Lindman (Thysanoptera), hôte inattendu d'Aphanogmus fumipennis (Thomson) (Hym. Ceraphronidae). Bulletin et Annales de la Societe Royale Entomologique de Belgique 107, 116–118.

Evans, G.A., Dessart, P. & Glenn, H. 2005. Two new species of *Aphanogmus* (Hymenoptera: Ceraphronidae) of economic importance reared from *Cybocephalus nipponicus* (Coleoptera: Cybocephalidae). Zootaxa 1018, 47–54.

Fergusson, N. D. M., 1980. A revision of the British species of *Dendrocerus* Ratzeburg (Hymenoptera: Ceraphronoidea) with a review of their biology as aphid hyperparasites. Bulletin of the British Museum (Natural History), 41(4), 255-314.

Ghesquiere, J. 1960. Le genre Atritomellus Kieffer en Afrique du Nord (Hymenoptera Proctotrupoidea Ceraphronidae). Bulletin et Annales de la Societe Royale Belge d'Entomologie 96, 205–215.

Gkoutos, G.V., Green, E.C.J., MallonA.-M., Blake, A., Greenaway, S., Hancock, J.M., Davidson, D. 2004. Ontologies for the description of mouse phenotypes. Comparative and Functional Genomics 5(6-7), 545-551.

Hadley, A., 2010. CombineZP. Available from: http://www.hadleyweb.pwp.blueyonder.co.uk/

Haviland, M.D., 1920. On the mionimics and development of *Lygocerus testaceimanus* Kieffer, and Lygocerus cameroni Kieffer (Proctotrypoidea-Ceraphronidae), parasites of Aphidius (Braconidae). Quarterly Journal of Microscopical Science 65, 361-372.

Heraty, J., Ronquist, F., Carpenter, J.M., Hawks, D., Schulmeister, S., Dowling, A.P., Murray, D., Munro, J., Wheeler, W.C., Schiff, N., Sharkey, M., 2011. Evolution of the Hymenopteran megaradiation. Molecular Phylogenetics and Evolution 60(1), 73-88.

Ishii, T. 1937.On the natural enemies of *Prontaspis yanonensis* Kuw. Agriculture & Horticulture, Tokyo 12(1), 60–70.

King, P.E., Copland, M.J.W., 1969. The structure of the female reproductive system in the Mymaridae (Chalcidoidea: Hymenoptera). Journal of Natural History, 3(3), 349-365.

Lacaze-Duthiers, H., 1849. Recherches sur l'armure genital des Insectes. Annales Des Sciences Naturelles Zoologie 12, 353-374

Luhman, J.C., Holzenthal, R.W., Kjaerandsen, J.K. 1999. New host record of a ceraphronoid (Hymenoptera) in Trichoptera pupae. Journal of Hymenoptera Research 8(1), 126.

Marris, G. C., Weaver, R. J., & Edwards, J. P., 2000. Endocrine interactions of ectoparasitoid wasps with their hosts: An overview. Comparative Biochemistry and Physiology Part B Biochemistry and Molecular Biology 126B(Supplement 1), S64.

Muesebeck, C.F.W. 1979. Superfamily Ceraphronoidea. *in* Krombein, K.V., Hurd, P.D. Smith, D.R. and Burks, B.D. (ed.): Catalog of Hymenoptera in America north of Mexico. Smithsonian Institution Press, Washington, DC. 1187–1198.

Muller, C. B., Voelkl, W., & Godfray, H. C. J., 1997. Are behavioural changes in parasitised aphids a protection against hyperparasitism? European Journal of Entomology 94(2), 221-234.

Oeser, R., 1961. Vergleichend-morphologische untersuchungen über den ovipositor der Hymenopteren. Mitteilungen Aus Dem Zoologischen Museum In Berlin 37(1), 1-119.

Priesner, H. 1936. Aphanogmus steinitzi spec. nov., ein Coniopterygiden-Parasit (Hymenoptera-Proctotrupoidea). Bull. Soc. ent. Egypte 20, 248–251.

Quicke, D.L.J., Fitton, M.G., Ingram, S., 1992. Phylogenetic implications of the structure and distribution of ovipositor valvilli in the Hymenoptera (Insecta). Journal of Natural History. 26(3), 587-608.

Quicke, D.L.J., Fitton, M.G., Tunstead, J.R., Ingram, S.N., Gaitens, P.V, 1994. Ovipositor structure and relationships within the Hymenoptera, with special reference to the Ichneumonoidea. Journal of Natural History, 28(3), 635-682.

Quick, D.L.J., Fitton, M.G., 1995. Ovipositor steering mechanisms in parasitic wasps of the families Gasteruptiidae and Aulacidae (Hymenoptera). Proceedings of the Royal Society of London B Biological Sciences 261, 99-103.

Quick, D., Leralec, A., Vilhelmsen, L., 1999. Ovipositor structure and function in the parasitic Hymenoptera with an exploration of new hypotheses. Atti dell'Accademia Nazionale Italiana de Entomologia 47, 197-239

Schwoerer, U., Voelkl, W., Hoffmann, K. H., 1999. Foraging for mates in the hyperparasitic wasp, *Dendrocerus carpenteri*: Impact of unfavourable weather conditions and parasitoid age. Oecologia (Berlin) 119(1), 73-80.

Sharanowski, B.J., Robbertse, B., Walker, J., Randal, V., Yoder, R., Spatafora, J., Sharkey, M.J., 2010. Expressed sequence tags reveal Proctotrupomorpha (minus Chalcidoidea) as sister to Aculeata (Hymenoptera: Insecta). Molecular Phylogenetics and Evolution 57, 101-112.

Sinacori, A., Mineo, G., Lo Verde, G. 1992. Osservazioni su Aphanogmus steinitzi Priesner (Hym. Ceraphronidae) parassitoide di Conwentzia psociformis (Curtis) (Neur. Coniopterygidae). Phytophaga 4, 29–48.

Sharkey, M.J., Carpenter, J.M., Vilhelmsen, L., Heraty, J., Liljeblad, J., Dowling, A.P.G., Schulmeister, S., Murray, D., Deans, A.R., Ronquist, F., Krogmann, L., Wheeler, W.C., 2011. Phylogenetic relationships among superfamilies of Hymenoptera. Cladistics 27, 1-33.

Smith, E.L., 1970. Evolutionary morphology of external insect genitalia. 2. Hymenoptera. Annals of the Entomological Society of America 63(1), 1-27.

Vilhelmsen, L. 2000. The ovipositor apparatus of basal Hymenoptera (Insecta): phylogenetic implications and functional morphology. Zoologica Scripta, 29(4), 319-345.

Vilhelmsen, L., Isidoro, N., Romani, R., Basibuyuk, H.H., Quicke, D.L.J., 2001. Host location and oviposition in a basal group of parasitic wasps: the subgenual organ, ovipositor apparatus and associated structures in the Orussidae (Hymenoptera, Insecta). Zoomorphology 121, 63-84.

Vilhelmsen, L., Mikó, I., Krogmann, L., 2010. Beyond the wasp-waist: structural diversity and phylogenetic significance of the mesosoma in apocritan wasps (Insecta: Hymenoptera). Zoological Journal of the Linnean Society 159, 22-194.

Vincent, J.F.V., King, M.J., 1996. The mechanism of drilling by wood wasp ovipositors. Biomimetics 3, 187-201.

Vogt, L., Bartolomaeus, T., Giribet, G., 2010. Linguistic problem of morphology: structure versus homology and the standardization of morphological data. Cladistics 26, 301-325.

Yoder, M.J., Mikó, I., Seltmann, K.C., Bertone, M.A., Deans, A.R., 2010. A gross anatomy ontology for Hymenoptera. PLoS ONE, 5(12), e15991.doi:10.1371/journal.pone.0015991.

Table 1. Specimens observed for morphological description including specimen identifiers, preparation techniques, imaging method and collecting locality.

Taxon	Specimen identifier	preparation	study techniques	Collecting event
Megaspilus armatus	NCSU 0071199	KOH, glycerine	brightfield	USA: VA: Essex co, 1mi SE Dunnsville, 37˚52'N 76˚48'W, 29.v-9.vi.1995, D R Smith, MT
	NCSU 0055645	glycerine	brightfield, CLSM 20x	USA: Kentucky: Turkey Run, 18-30.v.2007
	NCSU 0056307	glycerine	CLSM 40x water imersion	USA: Kentucky: Turkey Run, 18-30.v.2007
Conostigmus abdominalis	NCSU 0056302	KOH, glycerine	brightfield	SWEDEN, Dr, Saterdalen, Nasakerspussen, alder wood ravine N 60º22' E 15º43' (=TrapID 10) 08.vii-21.vii.2003 (=coll. event ID 397) Leg. Swedish Malaise Trap Project (Swedish Museum of Natural History)
	NCSU 0056301	KOH, glycerine	brightfield	SWEDEN, Dr, Saterdalen, Nasakerspussen, alder wood ravine N 60º22' E 15º43' (=TrapID 10) 08.vii-21.vii.2003 (=coll. event ID 397) Leg. Swedish Malaise Trap Project (Swedish Museum of Natural History)
	NCSU 0055647	glycerine	brightfield, CLSM 20x	SWEDEN, Dr, Saterdalen, Nasakerspussen, alder wood ravine N 60º22' E 15º43' (=TrapID 10) 08.vii-21.vii.2003 (=coll. event ID 397) Leg. Swedish Malaise Trap Project (Swedish Museum of Natural History)
Lagynodes AFEsp1	NCSU 0055643	glycerine	brightfield	USA: NC: Eno river, sifted litter, 29.vii.2010
	NCSU 0055306	glycerine	CLSM 20x, 40x water imersion	USA: NC: Eno river, sifted litter, 25.vii.2010
Ceraphron AFEsp4	NCSU 0071198	CPD	brightfield	MADG'R: Prov.Antsiranana R.S. Manongarivo 20.4 km 219ºSW Antanambo 1860m 14º02.8'S 48º24.1'E 3.xi.1998 B.L.Fisher#1990 sifted litter (leaf mold, rotten wood) rainforest
	IM1418, NCSU 0071197	glycerine	brightfield, CLSM 20x	MADAGASCAR: Province Fianarantsoa, Parc National Ranomafana, Belle Vue at Talatakely, elev 1020 m 16-26 February 2003 12º15.99'S, 47º25.21'E Collector: R. Harin'Hala California Acad of Sciences malaise, secondary tropical forest MA-02-09C-54
Aphanogmus AFEsp1	NCSU 0055648	glycerine	brightfield	Hungary Szolnok 25.vi.2002 Komlosi
	NCSU 0002419	glycerine	CLSM 40x water imersion	Hungary Szolnok 25.vi.2002 Komlosi
Trassedia AFEsp1	NCSU 0071196	Proteinase K, glycerine	brightfield, CLSM 20x	MADAGASCAR: Tianwara Prov, MA-02-09B-59 CASLOT 016656

Table 2. Labels linked to anatomical concepts including URI links to ontologies.

label	Concept	URI
abdomen	The tagma that is located posterior to the thorax.	http://purl.obolibrary.org/obo/HAO_0000015
abdominal sternum	The sternum that is located on the abdominal segment.	http://purl.obolibrary.org/obo/HAO_0001425
abdominal sternum 7	The abdominal sternum that is located on abdominal segment 7.	http://purl.obolibrary.org/obo/HAO_0000044
abdominal tergum	The tergum that is located in the abdomen.	http://purl.obolibrary.org/obo/HAO_0001426
abdominal tergum 8	The tergum that is located on abdominal segment 8.	http://purl.obolibrary.org/obo/HAO_0000061
abdominal tergum 9	The tergum that is located on abdominal segment 9. In females, accommodates the origins of the muscles that are the primary protractors and retractors of the first valvulae.	http://purl.obolibrary.org/obo/HAO_0000075
acute angle	An angle which is less than 90 degrees.	http://purl.obolibrary.org/obo/PATO_0001051
adjacent to	A spatial quality inhering in a bearer by virtue of the bearer's being located near in space in relation to another entity.	http://purl.obolibrary.org/obo/PATO_0002259
anatomical cluster	The anatomical group that has its parts adjacent to one another.	http://purl.obolibrary.org/obo/HAO_0000041
anatomical entities	Biological entity that is either an individual member of a biological species or constitutes the structural organization of an individual member of a biological species.	http://purl.obolibrary.org/obo/HAO_0000000
angle	A shape that is formed by two lines or rays diverging from a common point (the vertex).	
annuli	The carina that is transverse and extends across the lateral wall of the first valvula or the second valvula.	http://purl.obolibrary.org/obo/HAO_0001173
anterior	anterior to	
anterior	Toward or at the head (front) end of the body or structure.	
anterior area of the second valvifer	The area of the second valvifer which is anterior to the first valviferal fossa of the second valvifer.	
anterior flange	The flange that extends along the anterolateral margin of the abdominal tergum 9.	http://purl.obolibrary.org/obo/HAO_0001171
anterior flange of abdominal tergum 9	The flange that extends along the anterolateral margin of the abdominal tergum 9.	http://purl.obolibrary.org/obo/HAO_0001171
anterior flange of the first valvifer	The flange that extends anteriorly on the first valvifer and overlaps with the posterior margin of the anterior area of the second valvifer.	
anterior margin	no definition	http://purl.obolibrary.org/obo/BSPO_0000671
anterior notch of the second valvula	The notch that is located anteriorly on the dorsal ramus of the second valvula that accommodates that ventral ramus of the second valvula and the first valvula.	

Table 2. (Continued)

Label	Concept	URI
anterior notch of the second valvula	The notch that is located anteriorly on the dorsal ramus of the second valvula that accommodates that ventral ramus of the second valvula and the first valvula.	
anterior second valvifer-second valvula muscle	The ovipositor muscle that arises from the anterodorsal part of the second valvifer and inserts subapically on the processus articulares.	http://purl.obolibrary.org/obo/HAO_0001166
anterior to	A spatial quality inhering in a bearer by virtue of the bearer's being located toward the front of an organism relative to another entity.	http://purl.obolibrary.org/obo/PATO_0001632
anteriorly	anterior region	
anterior-most	no definition	http://purl.obolibrary.org/obo/BSPO_0000036
anterodorsally	anterodorsal to	
anteroventral	anteroventral to	
apex	The anatomical point that is distal to all other anatomical points of an anatomical entity.	
apodeme	The process that is internal.	http://purl.obolibrary.org/obo/HAO_0000142
area	The anatomical structure that is delimited by material or immaterial anatomical entities.	http://purl.obolibrary.org/obo/HAO_0000146
articulation	The anatomical cluster that is composed of the fossa and the condyle inserting into the fossa.	http://purl.obolibrary.org/obo/HAO_0000151
attaches	attachment quality	
attachment quality	A structural quality inhering in a bearer by virtue of the bearer's having connection or association with another entity.	http://purl.obolibrary.org/obo/PATO_0001435
aulax	The impression that extends along the dorsal surface of the dorsal ramus of the first valvula and articulates with the rhachis.	http://purl.obolibrary.org/obo/HAO_0000152
bands	The area that is oblong and differs from surrounding areas in coloration, surface sculpture and setae.	http://purl.obolibrary.org/obo/HAO_0000163
basal articulation	The articulation that is located between the proximal region of the second valvula and the second valvifer.	http://purl.obolibrary.org/obo/HAO_0001177
basal line of the second valvifer	The anatomical line on the second valvifer that extends from the pars articularis to the posterior margin of the anterior area of the second valvifer.	
broad	increased width	
bulb	The anterior area of the dorsal ramus of the second valvula that is bulbous.	
condyle	The articular surface that is convex and is inserted into the fossa of an adjacent sclerite.	http://purl.obolibrary.org/obo/HAO_0000220
conjunctiva	The area of the integument that is weakly sclerotized, with thin exocuticle.	http://purl.obolibrary.org/obo/HAO_0000221
conspicuousness	A quality inhering in a bearer by virtue of its visibility.	http://purl.obolibrary.org/obo/PATO_0001998

Table 2. (Continued)

Label	Concept	URI
continuous	A quality of a single process inhering in a bearer by virtue of the bearer's being uninterrupted in time, sequence, substance, or extent.	http://purl.obolibrary.org/obo/PATO_0000689
convex	A shape quality that obtains by virtue of the bearer having inward facing edges; having a surface or boundary that curves or bulges outward, as the exterior of a sphere.	http://purl.obolibrary.org/obo/PATO_0001355
cordate apodeme	The apodeme on the anterior margin of the abdominal tergum 9. The ventral T9-second valvifer muscle attaches partly on the apodeme.	http://purl.obolibrary.org/obo/HAO_0001585
corner	The projection that is located at the intersection of two or more edges.	http://purl.obolibrary.org/obo/HAO_0000223
curved	A curvature quality inhering in a bearer by virtue of the bearer's having or being marked by a curve or smoothly rounded bend.	http://purl.obolibrary.org/obo/PATO_0000406
curved dorsal	A curvature quality inhering in a bearer by virtue of the bearer's being curved towards the back or upper surface of an organism.	http://purl.obolibrary.org/obo/PATO_0001468
cuticle	The acellular anatomical structure that is the external layer of the integument (covers the entire body surface as well as lines ectodermal invaginations such as the stomodeum, proctodeum and tracheae) and produced by the epidermal cells.	http://purl.obolibrary.org/obo/HAO_0000240
depression	The area that is external, concave, and does not correspond to an apodeme.	http://purl.obolibrary.org/obo/HAO_0000241
distal	distal to	
distal to	A spatial quality inhering in a bearer by virtue of the bearer's being located further from a more centrally located entity.	http://purl.obolibrary.org/obo/PATO_0001234
distance	A quality that is the extent of space between two entities.	http://purl.obolibrary.org/obo/PATO_0000040
dorsal	At or toward the top or upper surface of the body or structure (above).	
dorsal area	dorsal region	
dorsal flange of the second valvifer	The flange that extends on the dorsal margin of the second valvifer. Part of the ventral T9-second valvifer muscle attaches to the flange.	http://purl.obolibrary.org/obo/HAO_0001577
dorsal margin	anatomical margin and (overlaps some dorsal side)	http://purl.obolibrary.org/obo/BSPO_0000679
dorsal ramus of the second valvula	The area that extends along the dorsal margin of the second valvula, and bears the processus articularis anteriorly and bears the processus muscularis on the antero-dorsal region and articulates anteriorly with the second valvifer via the basal articulation.	
dorsal region	anatomical region and (overlaps some dorsal side)	http://purl.obolibrary.org/obo/BSPO_0000079

Table 2. (Continued)

Label	Concept	URI
dorsal T8-T9 muscle	The abdominal muscle that arises from the anteromedian margin of the abdominal tergum 8 and inserts on the anteromedian margin of the abdominal tergum 9.	http://purl.obolibrary.org/obo/HAO_0001571
dorsal T9-second valvifer muscle	The ovipositor muscle that arises along the posterodorsal part of the anterior margin and from the anterior flange of abdominal tergum 9 and inserts on the anterior part of the dorsal flanges of the second valvifer.	http://purl.obolibrary.org/obo/HAO_0001569
dorsal valve	The anatomical cluster that is composed of the second valvulae.	http://purl.obolibrary.org/obo/HAO_0001658
dorsal to	A spatial quality inhering in a bearer by virtue of the bearer's being located toward the back or upper surface of an organism relative to another entity.	http://purl.obolibrary.org/obo/PATO_0001233
dorsally	dorsal to	
D-shaped	A concave 2-D shape quality inhering in a bearer by virtue of the bearer's being shaped in the form of the letter D.	http://purl.obolibrary.org/obo/PATO_0002357
elongated	A quality inhering in a bearer by virtue of the bearer's length being notably higher than its width.	http://purl.obolibrary.org/obo/PATO_0001154
first valvifer	The area that is proximal to and is connected with the first valvula via the dorsal ramus of the first valvula. The first valvifer articulates with the abdominal tergum 9 via the tergo-valvifer articulation and with the second valvifer via the intervalvifer articulation.	http://purl.obolibrary.org/obo/HAO_0000338
first valviferal fossa of the second valvifer	The fossa that is located on the second valvifer and articulates with the second valviferal condyle of the first valvifer.	
first valvifer-genital membrane muscle	The ovipositor muscle that arises from the posterior part of the first valvifer and inserts anteriorly on the genital membrane anetrior to the T9-genital membrane muscle.	http://purl.obolibrary.org/obo/HAO_0001746
first valvula, first valvulae	The sclerite that is distal to the first valvifer and articulates with the second valvula via the aulax.	http://purl.obolibrary.org/obo/HAO_0000339
flange	The projection that is lamella-like and is located on a rim, carina, apodeme or edge.	http://purl.obolibrary.org/obo/HAO_0000344
flat	A quality inhering in a bearer by virtue of the bearer's having a horizontal surface without a slope, tilt, or curvature.	http://purl.obolibrary.org/obo/PATO_0000407
fossa	The articular surface that is concave and accomodates the condyle of another sclerite.	http://purl.obolibrary.org/obo/HAO_0000353
genital membrane	The conjunctiva that connects the ventral margins of the second valvifers arching above the second valvula.	http://purl.obolibrary.org/obo/HAO_0001757
genitalia	The anatomical system that is involved in copulation, fertilization and/or oviposition.	http://purl.obolibrary.org/obo/HAO_0000374
gland	The anatomical cluster that is composed of epithelial cell(s) that secrete or excrete materials not related to their ordinary metabolic needs.	http://purl.obolibrary.org/obo/HAO_0000375

Table 2. (Continued)

Label	Concept	URI
gradually	A quality inhering in a bearer by virtue of the bearer's progressing by regular or continuous degrees.	requested
height	A 1-D extent quality inhering in a bearer by virtue of the bearer's vertical dimension of extension.	http://purl.obolibrary.org/obo/PATO_0000119
increased thickness	A thickness which is relatively high.	http://purl.obolibrary.org/obo/PATO_0000591
increasing	increased quality	
integument	The anatomical system that forms the covering layer of the animal, ectodermal in origin and composed of epidermal cells producing the cuticle.	http://purl.obolibrary.org/obo/HAO_0000421
intervalvifer articulation	The articulation between the first valvifer and second valvifer.	http://purl.obolibrary.org/obo/HAO_0001558
invaginated	A shape quality in which a portion of the outermost boundary of an entity folds in space such that a portion that was originally convex is now concave.	http://purl.obolibrary.org/obo/PATO_0001748
lateral	lateral to	
lateral surface	intersection_of: BSPO:0000005 ! anatomical surface	http://purl.obolibrary.org/obo/BSPO_0000382
lateral T8-T9 muscle	The ninth abdominal tergal muscle that arises from the anterolateral margin of the abdominal tergum 8 and inserts on the anterolateral margin of the abdominal tergum 9.	http://purl.obolibrary.org/obo/HAO_0001776
laterally	lateral to	
lateral to	A spatial quality inhering in a bearer by virtue of the bearer's being located toward the side relative to another entity.	http://purl.obolibrary.org/obo/PATO_0001193
line	The anatomical structure that is linear.	http://purl.obolibrary.org/obo/HAO_0001586
linear	A shape quality inhering in a bearer by virtue of the bearer's being narrow, with the two opposite margins parallel.	http://purl.obolibrary.org/obo/PATO_0001199
L-shaped	An angular shape quality inhering in a bearer by virtue of the bearer's having a single angle in its length giving the bearer the form of the letter L.	http://purl.obolibrary.org/obo/PATO_0002225
margin	The line that delimits the periphery of an area.	http://purl.obolibrary.org/obo/HAO_0000510
medial	medial to	
medial region	medial side	
medial side	a point in the centre of the organism (where the left-right axis intersects the midsagittal plane)	http://purl.obolibrary.org/obo/BSPO_0000067
medial to	A spatial quality inhering in a bearer by virtue of the bearer's being located toward the middle relative to another entity.	http://purl.obolibrary.org/obo/PATO_0001191
medially	medial to	
mesosoma	The anatomical cluster that is composed of the prothorax, mesothorax and the metapectal-propodeal	http://purl.obolibrary.org/obo/HAO_0000576

Table 2. (Continued)

Label	Concept	URI
	complex.	
muscle	The portion of tissue that is composed of contractile fibers.	http://purl.obolibrary.org/obo/HAO_0000641
ninth tergal condyle of the first valvifer	The condyle that is located on the first valvifer and articulates with the first valviferal fossa of abdominal tergum 9.	
notch	The depression that is located on a margin, edge or carina.	http://purl.obolibrary.org/obo/HAO_0000648
olistheters	The anatomical cluster that is composed of the rhachis of the second valvula and the aulax of the first valvula.	http://purl.obolibrary.org/obo/HAO_0001103
ovipositor	The anatomical cluster that is composed of the first valvulae, second valvulae, third valvulae, first valvifers and second valvifers .	http://purl.obolibrary.org/obo/HAO_0000679
ovipositor apparatus	The anatomical cluster that is composed of the ovipositor, abdominal terga 8-10, abdominal sternum 7 and muscles connecting them.	http://purl.obolibrary.org/obo/HAO_0001600
pars articularis	The area that is situated on the anteriorly on the ventral margin of the second valvifer and forms the lateral part of the basal articulation.	http://purl.obolibrary.org/obo/HAO_0001606
posterior	posterior to	
posterior area of the second valvifer	the area of the second valvifer that is posterior to the first valviferal fossa of the second valvifer	
posterior margin	anatomical margin and (overlaps some posterior side)	http://purl.obolibrary.org/obo/BSPO_0000672
posterior second valvifer-second valvula muscle	The ovipositor muscle that arises posteroventrally from the second valvifer and inserts on the processus musculares of the second valvula.	http://purl.obolibrary.org/obo/HAO_0001815
posterior T9-second valvifer muscle	The ovipositor muscle that arises medially from the posterodorsal part of abdominal tergum 9 and inserts on the median bridge of the second valvifers.	http://purl.obolibrary.org/obo/HAO_0001813
posterodorsal to	A spatial quality inhering in a bearer by virtue of the bearer's being located toward the rear and upper surface of an organism relative to another entity.	http://purl.obolibrary.org/obo/PATO_0001916
postero-medially	postero-medial region	
posteroventral	posteroventral to	
posteroventral to	A spatial quality inhering in a bearer by virtue of the bearer's being located toward the rear and abdomen of an organism relative to another entity.	http://purl.obolibrary.org/obo/PATO_0001918
processus articularis	The process that extends laterally from the proximal part of the second valvula and forms the median part of the basal articulation, and corresponds to the site of attachment for the anterior second valvifer-second valvula muscle.	http://purl.obolibrary.org/obo/HAO_0001704

Table 2. (Continued)

Label	Concept	URI
processus musculares	The process that extends dorsally from the proximal part of the second valvula to the genital membrane. The posterior second valvifer-second valvula muscle attaches on the process.	http://purl.obolibrary.org/obo/HAO_0001703
projection	The process that is located on an edge.	http://purl.obolibrary.org/obo/HAO_0000829
protruding	A shape quality inhering in a bearer by virtue of the bearer's extending out above or beyond a surface or boundary.	http://purl.obolibrary.org/obo/PATO_0001598
proximal	proximal to	
proximal	The point closest to the body, at to toward the base of an appendage; synonymous with proximal.	
proximal side	no definition	http://purl.obolibrary.org/obo/BSPO_0000061
quadrangular	A shape quality inhering in a bearer by virtue of the bearer's having four angles and four sides.	http://purl.obolibrary.org/obo/PATO_0001988
ramus	The process that is located on the funicular segment.	http://purl.obolibrary.org/obo/HAO_0001688
region	The anatomical structure that is delimited by at least one immaterial anatomical entity.	http://purl.obolibrary.org/obo/HAO_0000893
reproductive system	The anatomical system that is involved in reproduction.	http://purl.obolibrary.org/obo/HAO_0000895
ridge	The apodeme that is elongate.	http://purl.obolibrary.org/obo/HAO_0000899
ridge-like	requested	
right angle to	An angle which is 90 degrees to another entity.	http://purl.obolibrary.org/obo/PATO_0001321
S7-first valvula muscle	The muscle that originates from the abdominal sternum 7 and inserts on ventral ramus of the first valvula.	http://purl.obolibrary.org/obo/HAO_0001668
sclerite	The area of the integument where the cuticle is well sclerotised with thick exocuticle.	http://purl.obolibrary.org/obo/HAO_0000909
second valvifer	The area that is proximal to the second valvula and is connected to the second valvula via the ventral ramus of the second valvula and the basal articulation.	http://purl.obolibrary.org/obo/HAO_0000927
second valviferal condyle of the first valvifer	The condyle that is located on the first valvifer and articulates with the first valviferal fossa of the second valvifer.	
second valvula	The area that is continuous proximally with the second valvifer via the ventral ramus of the second valvula, articulates with the second valvifer via the basal articulation and with the first valvula via the olistheters and is delimited posteromedially by the median longitudinal line of the ovipositor.	http://purl.obolibrary.org/obo/HAO_0000928
segments	The anatomical cluster that is connected to other segments via conjunctivae and muscles and is delimited by its sclerites.	http://purl.obolibrary.org/obo/HAO_0000929

Table 2. (Continued)

Label	Concept	URI
setae	The sensillum that is multicellular and consists of trichogen, tormogen, and sense cells.	http://purl.obolibrary.org/obo/HAO_0000935
slender	A shape quality inhering in a bearer by virtue of the bearer's being small or narrow in circumference or width in proportion to length or height.	http://purl.obolibrary.org/obo/PATO_0002212
spatulate	A shape quality inhering in a bearer by virtue of the bearer's being oblong, with the lower end very much attenuated.	http://purl.obolibrary.org/obo/PATO_0001937
sternum	The sclerite that is located on the sternum.	http://purl.obolibrary.org/obo/HAO_0000955
straight	A shape quality inhering in a bearer by virtue of the bearer's being free of curves, bends, or angles.	http://purl.obolibrary.org/obo/PATO_0002180
T8-first valvifer muscle	The ovipositor muscle that originates from the lateral part of the abdominal tergum 8 and inserts on the dorsal margin of the first valvifer.	http://purl.obolibrary.org/obo/HAO_0001640
tapered	A shape quality inhering in a bearer by virtue of the bearer's being gradually narrower or thinner toward one end.	http://purl.obolibrary.org/obo/PATO_0001500
tergo-valvifer articulation	The articulation that is located between the abdominal tergum 9 and the first valvifer.	http://purl.obolibrary.org/obo/HAO_0001636
tergum	The area that is located on the integument and is dorsal of the ventral diaphragm.	http://purl.obolibrary.org/obo/HAO_0001006
third valvula	The area that is located posterior to the second valvifer and is connected to the second valvifer via conjuntiva.	http://purl.obolibrary.org/obo/HAO_0001012
U-shaped	A concave 3-D shape quality inhering in a bearer by virtue of the bearer's being shaped in the form of the letter U.	http://purl.obolibrary.org/obo/PATO_0001879
ventral margin	no definition	http://purl.obolibrary.org/obo/BSPO_0000684
ventral ramus of the first valvula	The process that extends along the ventral margin of the first valvula.	http://purl.obolibrary.org/obo/HAO_0000891
ventral ramus of the second valvula	The area that is proximally fused with the anterior margin of the second valvifer and bears the rhachis.	http://purl.obolibrary.org/obo/HAO_0001107

Figure 1. Photos of the ovipositor structure; images taken using bright field microscopy; all specimens bisected along the sagittal plane except (B) and (D); LV = lateral view, MV = median view; numbers indicate character number and state; muscles are indicated with muscle numbers; triangles mark location of associated states; anterior to left except (B) anterior is to upper left corner and (C) anterior is to lower left corner; (A) *Conostigmus abdominalis* (Megaspilidae: Megaspilinae), MV, soft tissues removed, note approximate right angle formed by the first valvifer and the dorsal flange of the second valvifer. (B) *Trassedia luapi* (Megaspilidae: Megaspilinae), LV, soft tissues removed, note the division of the first valvifer into dorsal and ventral sclerites. (C) *Megaspilus armatus* (Megaspilidae: Megaspilinae), MV, soft tissues removed. (D) *Ceraphron* AFEsp4 (Ceraphronidae) critical point dried, LV, note sharp angle formed by the first valvifer and the dorsal flange of second valvifer. (E) *Lagynodes* AFEsp1 (Megaspilidae: Lagynodinae), MV, distal area of first and second valvulae removed. (F) *Aphanogmus* AFEsp1 (Ceraphronidae), MV, note the location of the tergo-valvifer articulation adjacent to the dorsal end of the first valvifer.

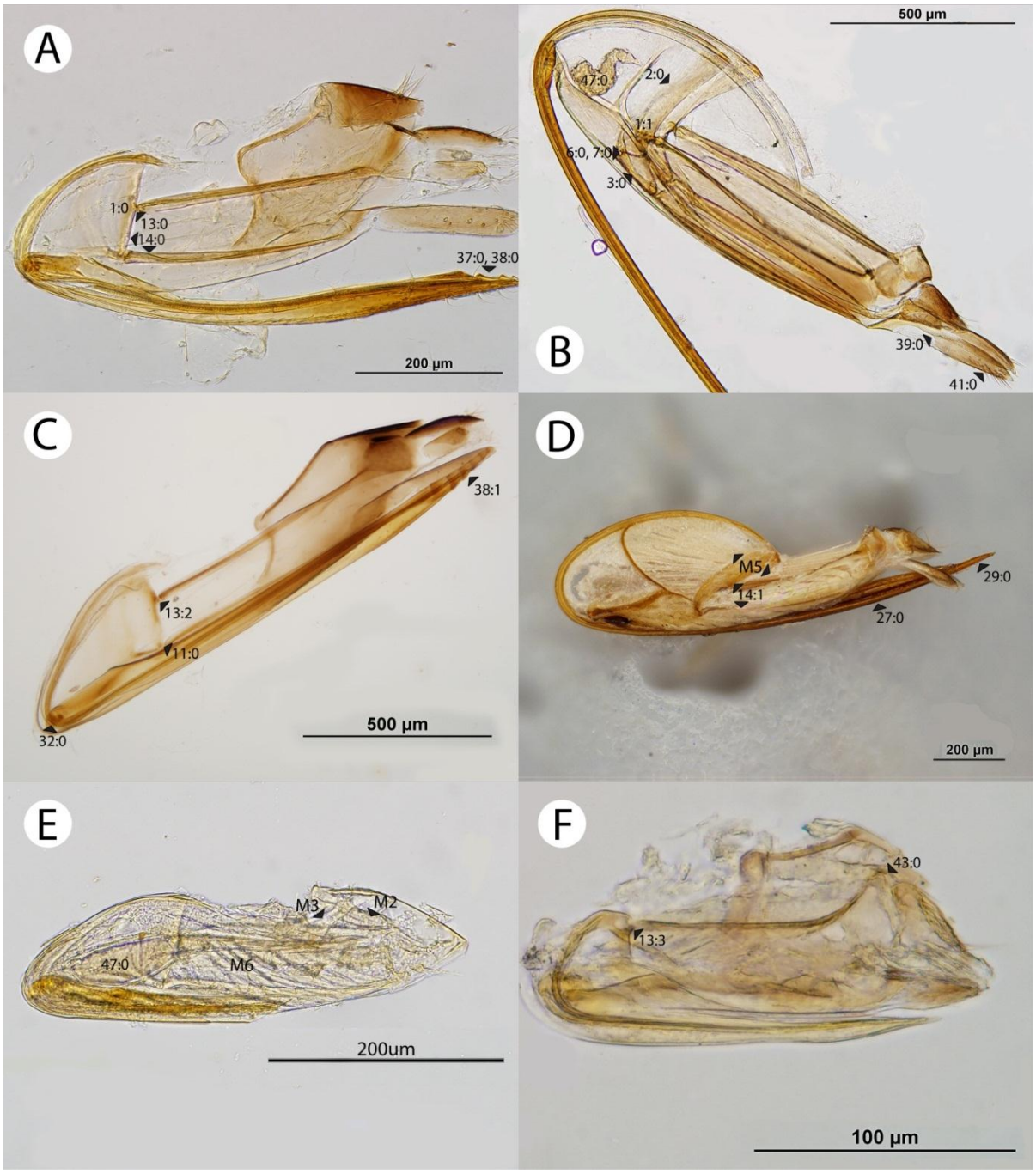
A
1:0
13:0
14:0
37:0, 38:0
200 µm
500 µm
47:0
2:0
1:1
5:0, 7:0
3:0
B
39:0
41:0
C
38:1
13:2
11:0
32:0
500 µm
D
M5
14:1
29:0
27:0
200 µm
E
M3
M2
47:0
M6
200um
F
43:0
13:3
100 µm

Figure 2. Photos of the ovipositor structure; images taken using laser scanning confocal microscopy; all specimens bisected along the sagittal plane except (E) and (F); LV = lateral view, MV = median view; numbers indicate character number and state; muscles are indicated with muscle numbers; triangles mark location of associated states;(A) *Conostigmus abdominalis* (Megaspilidae: Megaspilinae),MV, anterior to lower left corner; (B) *Conostigmus abdominalis* (Megaspilidae: Megaspilinae), LV, anterior to lower left corner; (C) *Aphanogmus* AFEsp1 (Ceraphronidae), MV, anterior to left; (D) *Aphanogmus* AFEsp1 (Ceraphronidae), LV, anterior to lower left corner; (E) *Trassedia luapi* (Megaspilidae: Megaspilinae), LV, anterior to upper left corner; *Megaspilus armatus* (Megaspilidae: Megaspilinae), cross setion through anterior area of the second valvifer; anterior facing out; note anterior flange of the first valvifer.

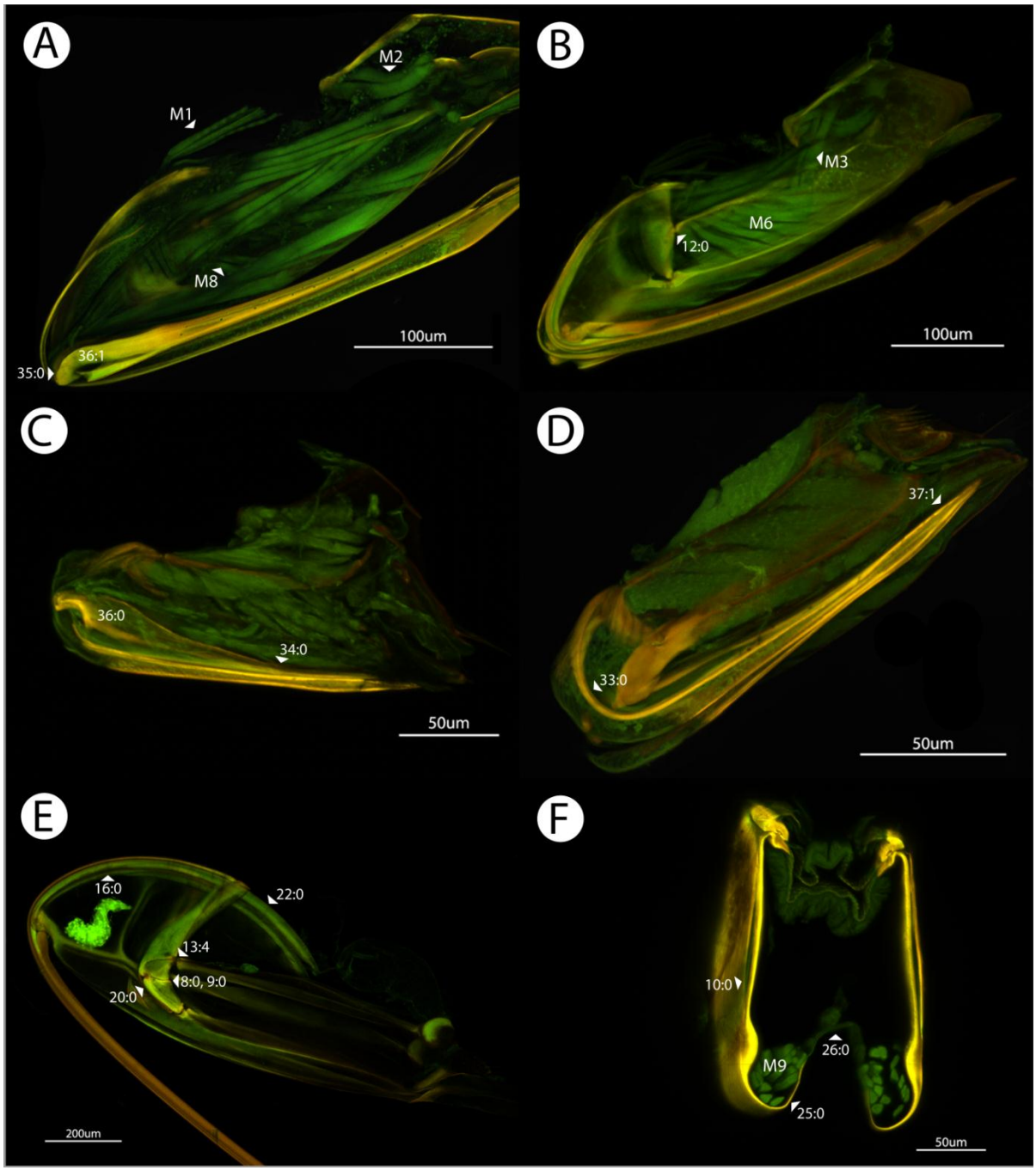
A
M2
M1
M8
100um
36:1
35:0
B
M3
M6
12:0
100um
C
36:0
34:0
50um
D
37:1
33:0
50um
E
16:0
22:0
13:4
8:0, 9:0
20:0
200um
F
10:0
26:0
M9
25:0
50um

Figure 3. Photos of the ovipositor structure; images taken using laser scanning confocal microscopy except (A) taken using bright field microscopy; all specimens bisected along the sagittal plane; LV = lateral view, MV = median view; numbers indicate character number and state; muscles are indicated with muscle numbers; triangles mark location of associated states; anterior to left except (F) anterior is to lower left corner; (A) *Ceraphron* AFEsp4 (Ceraphronidae), LV, distal end of first and second valvulae removed; (B) *Ceraphron* AFEsp4 (Ceraphronidae), LV, note large and brightly fluorescing gland, apex of first and second valvulae removed; (C) *Conostigmus abdominalis* (Megaspilidae: Megaspilinae), LV; (D) *Conostigmus abdominalis* (Megaspilidae: Megaspilinae), MV; (E) *Megaspilus armatus* (Megaspilidae: Megaspilinae), LV, valvulae moved ventral of abdominal sternum 7, note muscle M1 extending from the first valvula to abdominal sternum 7;(F) *Megaspilus armatus* (Megaspilidae: Megaspilinae), MV, valvulae moved ventral of abdominal sternum 7.

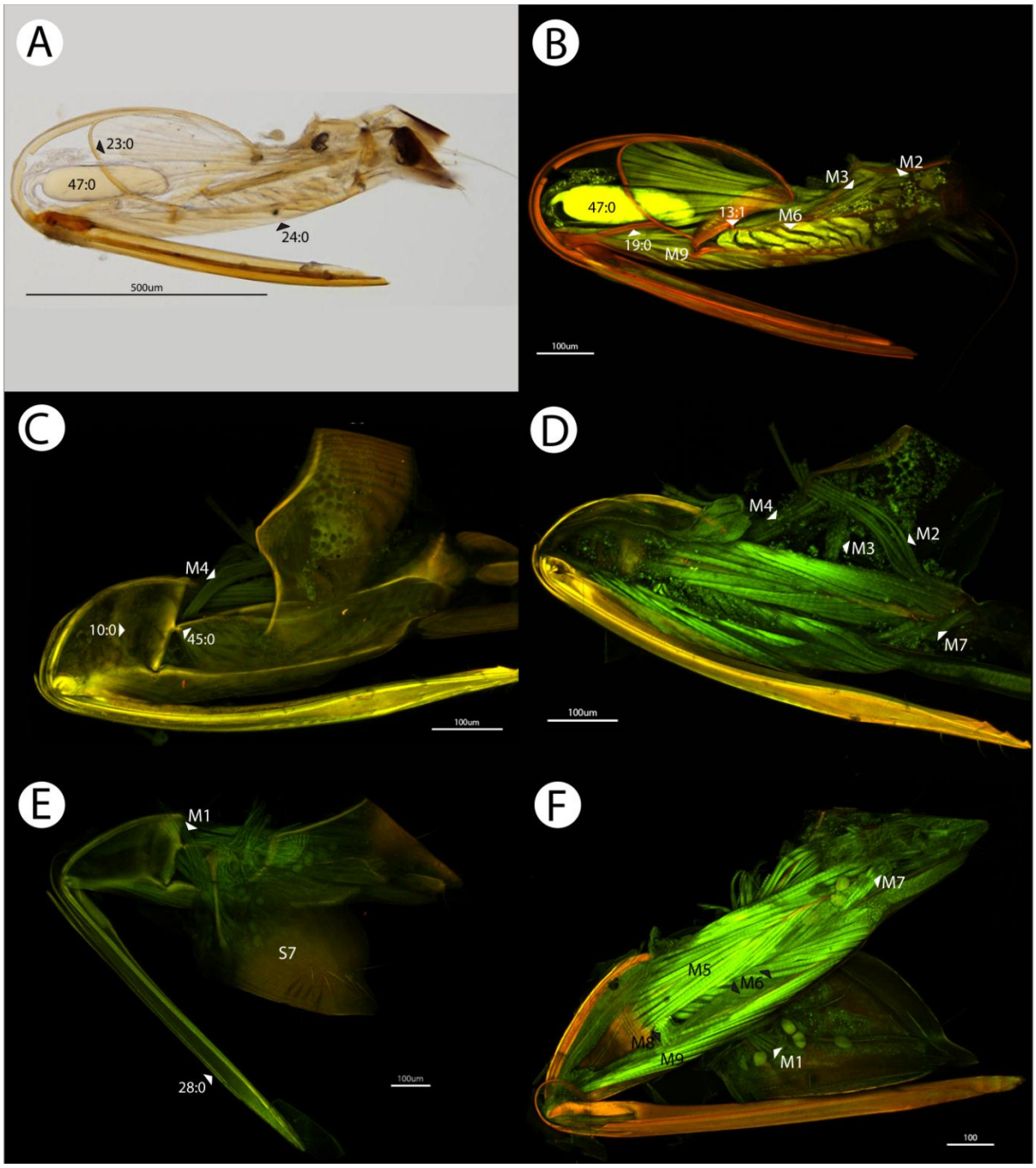
A
23:0
47:0
24:0
500um
B
47:0
M3
M2
13:1
M6
19:0
M9
100um
C
M4
10:0
45:0
100um
D
M4
M2
M3
M7
100um
E
M1
S7
28:0
100um
F
M7
M5
M6
M8
M9
M1
100

Figure 4. Photos of the ovipositor; images taken using bright field microscopy; all specimens bisected along the sagittal plane; all specimens in median view except (C); numbers indicate character number and state; muscles are indicated with muscle numbers; triangles mark location of associated states; anterior to left except (A) and (C); (A) *Conostigmus abdominalis* (Megaspilidae: Megaspilinae), anterior to lower left corner; (B) *Conostigmus abdominalis* (Megaspilidae: Megaspilinae), soft tissues removed, the first valvifer and abdominal tergum 9 are separated from the second valvifer, area of second valvula distal to bulb removed, note curvature and expanded distal area of the first valvula; (C) *Conostigmus abdominalis* (Megaspilidae: Megaspilinae), basal articulation separated showing median side of second valvifer (left) and lateral side of second valvula (right); (D) *Megaspilus armatus* (Megaspilidae: Megaspilinae), valvulae moved ventral of abdominal sternum 7, note length of dorsal projection of the second valvifer; (E) *Ceraphron* AFEsp4 (Ceraphronidae), note the unsclerotized area between the posterior margin of the anterior area of the second valvifer and the first valvifer; (F) *Ceraphron* AFEsp4 (Ceraphronidae), note the site of insertion of muscle M5 along the posterior margin of the anterior area of the second valvifer and the dorsal projection of the second valvifer.

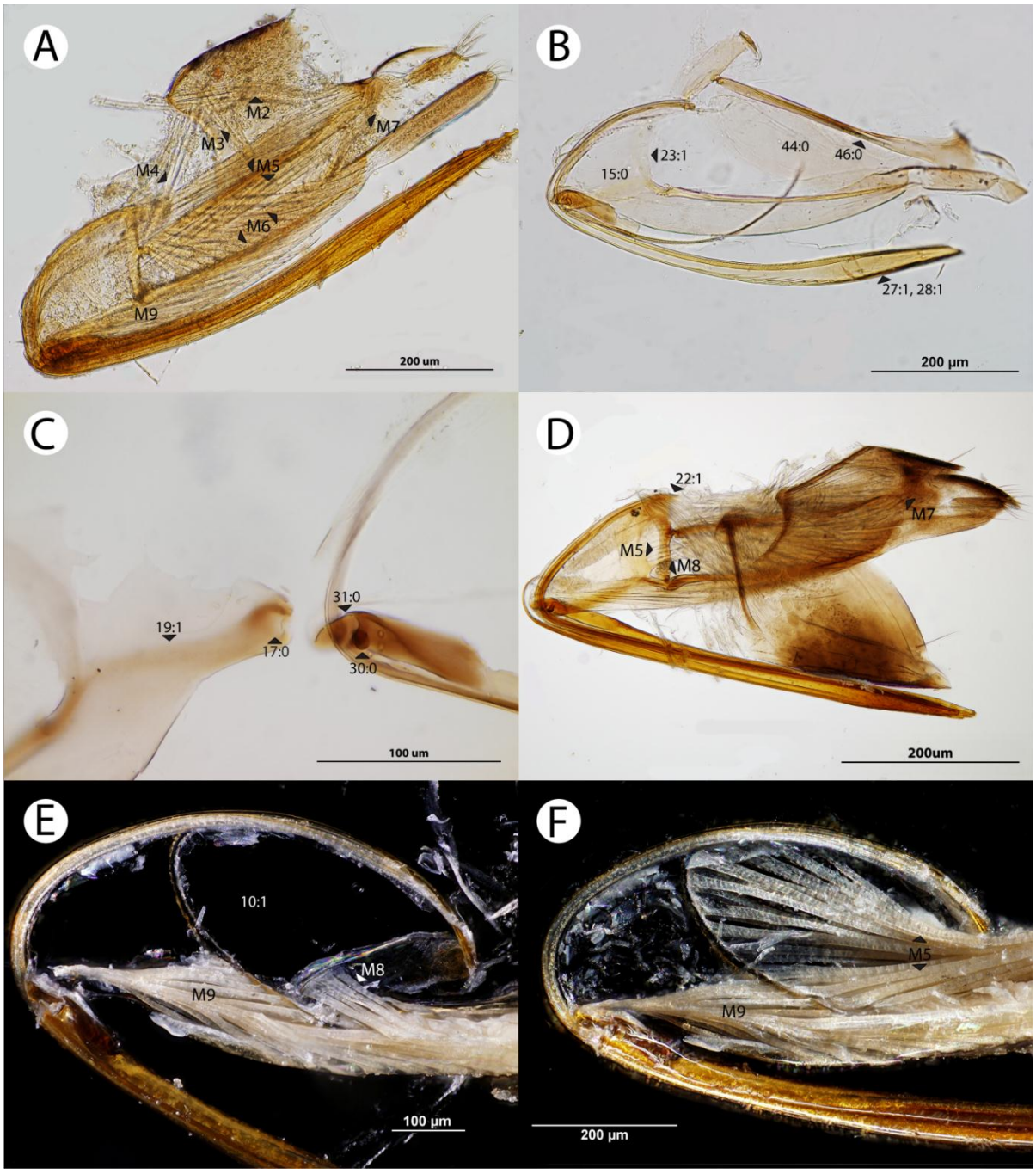
A
M2
M3
M4
M5
M6
M7
M9
200 um
B
15:0
23:1
44:0
46:0
27:1, 28:1
200 µm
C
19:1
17:0
31:0
30:0
100 um
D
22:1
M5
M8
M7
200um
E
10:1
M8
M9
100 µm
F
M5
M9
200 µm

CHAPTER 2

Phylogeny of the Megaspilinae (Hymenoptera: Ceraphronoidea: Megaspilidae) Based on Molecular Data.

Introduction

The group we now recognize as Ceraphronoidea had traditionally been classified as a lineage within Proctotrupoidea, until it was formally elevated as its own superfamily by Masner and Dessart (1967). Rasnitsyn (1980) placed Ceraphronoidea in the Evaniomorpha based on morphology of extant species and fossil specimens. The known diversity and a brief overview of the taxonomic history of Ceraphronoidea was recently published by Johnson and Musetti (2004). Masner and Dessart (1967) provide the most detailed history of the taxonomy of Ceraphronoidea. The superfamily is robustly monophyletic (Dowton and Austin 2001, Heraty et al. 2011, Ronquist et al. 1999, Sharkey et al. 2011), however the placement of Ceraphronoidea within Hymenoptera remains elusive (Dowton and Austin 2001, Heraty et al. 2011, Ronquist et al. 1999, Sharkey et al. 2011, Sharanowski et al. 2010).

Taxonomic History

Ceraphronoidea is comprised of four families; Ceraphronidae, Megaspilidae, Stigmaphronidae† and Radiophronidae†. The recent description of *Masner lubomirus* Mikó and Deans (2009) brings the species composition of Ceraphronidae to 302, in 15 genera. Megaspilidae is divided into two subfamilies: Lagynodinae, with 25 valid species in 6 genera; and Megaspilinae, with 275 valid species in 7 genera (Mikó and Deans 2009, Mikó et

al. 2011). Along with the current accepted generic concepts, there are 28 generic concepts which are now regarded as junior synonyms.

Megaspilidae was first recognized as a taxonomic group by Ashmead (1893), who described the group at the tribe level. He later raised the group to the level of subfamily (Ashmead 1903). The first use of the family name Megaspilidae was by Rodendorf (1963), where he described fossil specimens. Masner and Dessart (1967) more formally described the group at the family level where they also established the subfamilies Lagynodinae and Megaspilinae.

Despite substantial rivionary efforts (Dessart 1966, Dessart and Cancemi 1987, Masner and Dessart 1967), there is yet no clear consensus on how to classify taxa within Megaspilinae. There are currently seven valid genera in Megaspilinae; *Conostigmus* Dahlbom, *Creator* Alekseev, *Dendrocerus* Ratzeburg, *Megaspilus* Westwood, *Platyceraphron* Kieffer, *Trassedia* Cancemi, and *Trichosteresis* Förster. The diversity of Megaspilinae is largely dominated by two genera; *Dendrocerus* with 98 valid species, and *Conostigmus* with 163 valid species. The remaining genera comprise only 11 valid species. Megaspilinae has been demonstrated as monophyletic (Deans and Murray unpublished) however, the genus *Trassedia* is not included in that dataset. Mikó and Deans (2009) predict, based on morphological evidence, that *Trassedia* is sister to Ceraphronidae.

Due largely to the efforts of Paul Dessart (active 1962-2001, deceased 2001) the taxonomy of Ceraphronoidea has received a great deal of revisionary work. Dessart (1966) synonymized *Lygocerus* Förster, *Macrostigma* Rodani, *Prodendrocerus* Kieffer and *Neolygocerus* Ishii with *Dendrocerus*. He also synonymized *Dichogmus* Thomson with

Conostigmus (Dessart 1973) and in a paper co-authored with Cancemi synonymized *Ecnomothorax* Dessart and Masner with *Conostigmus* (Dessart and Cancemi 1987). Other past generic concepts include: *Eumegaspilus* Ashmead, synonymized with *Conostigmus* by Ashmead (1893); *Conostigmoides* Dodd synonymized with *Conostigmus* by Masner (1964); *Atritomus* Förster synonymized with *Dendrocerus* by Kieffer (1907); *Basoko* Risbec synonymized with *Dendrocerus* by Fergusson (1980); *Habropelte* Thomson synonymized with *Megaspilus* by Kieffer (1907); and *Thibloneura* Thomson synonymized with *Trichosteresis* by Kirchner (1867). *Thiblonura* is the only objective synonymy, the type species being the same as *Trichosteresis*. Although Fergusson (1980) didn't provide any morphological evidence to justify these synonymies, Dessart and Cancemi (1987) observed the morphological similarity between the two concepts declared "Il nous rendait la un grand service, car depuis plusieurs annees nous etions confrontes au probleme de la delimitation de ce taxon… (He [Fergusson] did us a great service, because for several years we were confronted with the problem of the delimitation of this taxon…)" (page 318). The lack of surety expressed by taxonomists and the difficulties in defining diagnostic characteristics at the generic level reveal the necessity to collect molecular data that will help define monophyletic groups.

Thanks to the extensive taxonomic work done by these dedicated taxonomists, there is a framework in place that has yet to be phylogenetically tested. The goal of my study is to test the phylogenetic integrity of the current generic concepts by examining the monophyly of *Dendrocerus* and *Conostigmus*, as well as the validity of the other genera with respect to the evolutionary history of these wasps.

Materials and Methods

Taxon sampling

The genus-, and family-level taxonomic concepts followed throughout this study were catalogued by Johnson and Musetti (2004), with the addition of the genus *Masner* Mikó and Deans, described in 2009. The 42 ingroup taxa were chosen to represent generic and species group concepts across Megaspilidae (Table 1); all seven currently recognized megaspiline genera are represented by at least one taxon in the analysis. Of past generic concepts, *Lygocerus* and *Basoko* are represented (Table1).

The outgroups include six exemplars of Lagynodinae and ten of Ceraphronidae (Table 1). Determinations for 23 of the ingroup and outgroup taxa were done by István Mikó while I was the determiner for the remaining specimens. Voucher specimens are deposited in the Frost Entomological Museum.

Nucleotide Sampling and Laboratory Protocols

Males lend themselves to unambiguous identification since the male genitalia bear the most reliable diagnostic characters, therefore male specimens were used for DNA extraction whenever possible. Male genitalia were removed from specimens for identification prior to DNA extraction. Subsequent dissection of extracted specimens revealed that soft tissues had remained intact indicating that the proteinase K may not been have able to permeate the exoskeleton to access the soft tissues. With that in mind, the prothorax was separated from the rest of the thorax to expose the tender bits of the specimen. Total genomic extractions were done using the Qiagen DNeasy® Tissue Kit (Qiagen Sciences, Germantown, Maryland)

with some modifications to the standard protocol; a) I used 40µl of proteinase K rather than 20µl, b) After the second wash of buffer solution, instead of a single centrifuge of 3 minutes, an initial centrifuge of 1 minute, the flow-through was discarded and the spin column was re-centrifuged for 3 minutes to dry the membrane. These protocol adjustments helped to prevent accidental re-wetting of the membrane when removing the collection tube as the final wash was discarded. In order to increase the concentration of genomic DNA for specimens smaller than the recommended amount of tissue to be used for extraction (25mg = 4-6mm of rat tail), the final elution volume was 100µl of the elution buffer rather than 200µl. Final genomic templates were stored at -20°C.

PCR amplification protocols varied based on need. Standard amplifications were done in 10-25 µl solutions, if the resulting gel electrophoresis indicated the need for gel excision, 50 µl solutions were used. Concentration of $MgSO_4$ varied as they were optimized for the locus to be amplified. In a 10 µl reaction, the amounts of reagents used was 0.2 µl of 10 mM dNTP, 1 µl PCR buffer (New England Biolabs, Ipswich, MA), 0.8-2.1 µl of 50mM $MgSO_4$, 0.4 µl of forward primer, 0.4 µl of reverse primer, 0.1 µl of Taq polymerase (New England Biolabs, Ipswich, MA), and 0.6-1.5 µl of genomic template. For different reaction volumes, amount of each reagent was modified to maintain concentrations. Reactions were done in batches, each batch done with one negative control.

Loci sampled included a ~572bp fragment of mitochondrial 16S rRNA, a ~448bp fragment of nuclear 28S rRNA, a section of the nuclear ribosomal protein S23 coding region (RPS23), and a region of mitochondrial cytochrome c oxidase subunit I (COI). All primers used as well as the aligned length of the sequences are listed in table 2. Final optimized

thermal cycler protocols are listed in table 3. RPS23 required the use of a "step down" protocol, starting with three cycles using the annealing temperature of 61°C, followed by five cycles with annealing temperature of 58°C, then finishing with twenty five cycles with annealing temperature of 54°C. Amplification of RPS23 also required the use of a nested reverse primer. After the initial amplification using the RPS23-21aF forward and RPS23-21bR reverse primers, the product was re-amplified using the same forward and the RPS23-21aR reverse primer (Table 2). The same thermal cycler protocol was used for both amplifications of RPS23. In the early stages of the project, there was a great amount of difficulty in amplifying 28S using the 28SD2D3_BJS_F and 28SD2D3_BJS_R primers (Table 2). After examining the few sequences attained using these primers, the forward was modified creating the 28SD2D3_AFE_F forward primer was designed which was more effective (Table 2).

The amplified PCR product and controls were confirmed using a 1% GenePure 3:1 agarose gel (ISC Bio Express, Kaysville, UT) run at 95 volts. The PCR product was marked with 5X sample loading buffer (Bio-Rad Laboratories, Hercules, CA). If gel excision was required, a 1% low melt agarose gel (Fisher Scientific, Fair Lawn, NJ) was used with 5x sample loading buffer (Qiagen Sciences, Germantown, Maryland) and run at 70 volts for an extended period of time to allow the bands of desired length to be identified and removed. In the case of gel excision, genetic material was extracted from the agarose using the QIAquick® Gel Extraction Kit (Qiagen Sciences, Germantown, Maryland) with minor modifications to the protocol. Rather than centrifuging immediately after the wash buffer was

added, the buffer was allowed to sit in the column for 2-5 minutes before centrifuging. For elution, 30 µl rather than 50 µl of elution buffer was used to increase the final concentration.

In preparation for the sequencing reaction, PCR product was purified. In the case of gel excisions, the product is already purified from the gel extraction procedure. Raw PCR products were purified using ExoSAP-IT (Affymetrix inc. USB® products, Cleveland, Ohio). The ExoSAP-IT neutralizes the remnants of the PCR reagents so that they will not interfere with the sequencing reaction. The protocol for the purification was modified by using a 1:5 dilution of the ExoSAP-IT solution. 2 µl of the PCR product was combined with 1 µl of the diluted ExoSAP-IT. The thermal cycler protocol was; 37°C for 15 minutes, followed by 80°C for 15 minutes.

Sequence Alignment and Phylogenetic Analyses

Contigs were assembled and sequences edited using Geneious Pro 5.1.5 (Biomatters Ltd., Auckland, New Zealand). Each locus was aligned independently using MAFFT v6 alignment software (Katoh et al. 2002) under default settings; alignment method set on auto to allow the program to choose the best method for the number of alignments, gap opening penalty set at 1.53, JTT PAM number set to 200/k=2, threshold score = 39, alignment initiated with the first sequence. I compiled datasets for each locus, RPS23 was divided into two sets; one composed of the intron and the other of the exons. After visual examination of the aligned 16S dataset, I determined that there was a great deal of highly variable regions. For this reason 16S was run in the program Gblocks 0.91b (Castresana 2000) under default settings, which removes potentially ambiguously aligned regions. As a result, I compiled two

16S datasets; one containing the originally aligned 16S, and one with the variable blocks removed. A concatenated dataset with all of the loci was also compiled. Using BioEdit 7.0.9 (Hall 1999) I translated the protein-encoding regions into amino acid sequences to examine the alignment, manual adjustments were made to correct for the reading frame. Using jModeltest 0.1 (Posada 2008) I calculated likelihood scores and in turn used them to determine the best model for each gene via Bayesian information criteria (Table 4).I performed an analysis of each dataset independently. I used MEGA 5.05 (Tamura et al. 2011) to determine the number of parsimony informative sites.

I accessed RAxML 7.2.8 (Stamatakis 2006) through the CIPRES Science Gateway (Miller et al. 2010) to perform the maximum likelihood analyses. Each dataset is analyzed using GTRCAT model for the bootstrapping phase and GTRGAMMA for the final tree inference. I set each dataset to run for 1000 rapid bootstrap pseudoreplicates using the MRE bootstopping criterion which stops the analysis when convergence criteria are met. The rapid bootstrap algorithm (Felsenstein 1985) is faster than the standard bootstrap algorithm and is comparable to the standard bootstrapping algorithm. I performed the Bayesian inference analyses using MrBayes 3.1.2 (Huelsenbeck and Ronquist 2001, Ronquist and Huelsenbeck 2003). Using the CIPRES Science Gateway, I analyzed the individual gene datasets. I ran the Bayesian analysis for the concatenated dataset on the Duke cluster. I set parameters to accommodate the models chosen for the number of substitution types, among-site rate variation, and the substitution rate matrix (Table 5). Each of the Bayesian analyses ended when the average standard deviation of split frequencies was lower than 0.01. I set the burninfrac to 25%. To ensure that the effective sample size (ESS) was >200 for each

analysis, I loaded the trace files from the MrBayes analyses were into the program Tracer 1.5.0 (Rambaut and Drummond 2007).

To visualize the differences between tree topologies, I used Splitstree 4.11.3 (Huson and Bryant 2006) to construct phylogenetic networks. To show the difference in signal between 16S and 16S with variable regions removed, the most likely trees from the single gene maximum likelihood analyses were combined into a consensus network. The consensus network computes the consensus splits of trees that have complete sampling (trees with identical taxon representation). Mean edge weights were used and the threshold was set at 0.33. The super-network method using the Z-Closure method (Huson et al. 2004) was used to compare the differences in topology between the most likely 16S and 28S trees from the maximum likelihood analyses. For the super-network method edge weights were set at TreeSizeWeightedMean. The super-network method was used because it allows partial trees (trees with only partially overlapping taxon representation) to be combined into a network.

Results

The final concatenated dataset of 58 taxa included 2887 characters, 1176 of which were parsimony informative (Table 4). The base composition for 28S and the RPS23 exons were fairly balanced (A+T% of 28S = 40.91% and RPS23 exons = 49.11%) with the RPS23 intron being A-T rich (78.17%). High A-T richness in the mitochondrial genome is expected for hymenopterans. Whitfield and Cameron (1998) list the mean A-T composition of 16S across Hymenoptera varying from 77.4% (Tenthredinoidea) to 85.9% (Platygastroidea). They also list Ceraphronoidea with only two representatives with a mean of 81.4% A-T composition.

The base composition of my 16S, and COI are A-T rich (A+T% of 16S = 91.30%, and COI = 73.57%) (Table 5). The degree of A-T richness is unexpected for 16S since it is much higher than the previously recorded values for Ceraphronoidea. The ESS for the Bayesian analyses was >200 (Table 6).

In the concatenated analyses, *Trassedia luapi* is placed with high support as sister to Ceraphronidae. In order to more accurately represent its evolutionary history, all references to Megaspilidae here and below will refer to Megaspilidae minus *Trassedia*.

Model based Analyses

The bootstrap pseudoreplicates run in RAxML were stopped based on MRE-based Bootstopping criterion. The number of replicates run for each bootstrap analysis was as follows: 16S – 550 pseudoreplicates; 16S with variable blocks removed – 450 pseudoreplicates; 28S – 450 pseudoreplicates; COI – 1000 pseudoreplicates; RPS23 exons – 1000 pseudoreplicates; RPS23 intron – 1000 pseudoreplicates; concatenated dataset – 800 pseudoreplicates. Two statistics were used to ensure that the MrBayes runs had reached convergence: the Average standard deviation of split frequencies (ASDSF) which is a measure of the similarity between the tree samples of the two independent runs; and the potential scale reduction factor (PSRF) which should approach 1.000 for each of the parameters (Gelman and Rubin 1992). The bootstrap values (BV) are mapped onto the most likely trees from the maximum likelihood (ML) analysis, and the posterior probability (PP) values are mapped onto the 50% majority rule tree produced via Bayesian inference (BI).

The trees from the 16S analyses (Figure 1, 2, 3) show a paraphyletic Megaspilinae, with respect to Lagynodinae, and with high support (95% BV; 100% PP). The placement of Lagynodinae within Megaspilinae, however, is not well supported. The ML analysis shows very little resolution within Megaspilinae. *Dendrocerus* AFEsp7 + *Dendrocerus* IMsp29 forming the basal group in *Megaspilinae* (95% BV; 100% PP). The BI tree shows a little more resolution with *Conostigmus* + *Megaspilus* + *Lagynodes* AFEsp1 + *Trichosteresis* comprise a monophyletic clade (75% PP). The remaining Megaspilinae form a clade with some support (66% PP). *Megaspilus* is nested within *Conostigmus* (83% PP), as is *Trichosteresis* (87% PP).

The results for the analyses of the 16S dataset with variable regions removed (Figures 4, 5, 6) are much the same as the results for the dataset with those regions left in, however the removal of variable regions lowered the support values for both ML and BI trees. In the ML analysis, resolution was lost at the base of the Megaspilinae clade. The consensus network of the two 16S ML most likely trees (Figure 7) shows the difference in topology between the trees. The disagreement seen is along the backbone of the tree at the base of Megaspilinae.

The analysis of 28S yielded a high degree of resolution but with long branches at the base of the ML and BI trees (Figures 8, 9, 10). Megaspilinae is monophyletic with high support (100% BV; 100% PP). *Conostigmus* is paraphyletic with respect to the rest of Megaspilinae. *Trichosteresis* is sister to *Conostigmus triangularis* (86% BV; 96% PP) with that group sister to *Conostigmus* sp5 (86% BV; 99% PP). At the base of the remaining Megaspilinae is a clade comprised of *Dendrocerus* IMsp29 + *Dendrocerus* AFEsp7 (100%

BV; 100% PP). Among the remaining *Dendrocerus* there is little resolution, with a few groupings having moderate support.

The supernetwork created from the ML most likely trees of 16S and 28S (Figure 11) shows only a small amount of disagreement between the two topologies. One of the major disagreements is the placement of *Aetholagynodes* AFEsp1 + *Lagynodes* AFEsp1. The rest of the influential disagreement is along the backbone of Megaspilinae.

The trees from the analyses of COI show little resolution and support for any groupings (Figures 12, 13, 14). *Lagynodes* AFEsp1 is maintained as the outgroup in the ML trees; however Megaspilinae is paraphyletic with respect to Lagynodinae in the BI tree.

The resulting topologies from the RPS23 exons incongruent at the base of the tree; the ML trees (Figures 15, 16) show a monophyletic Megaspilinae (72% BV), and the BI tree shows the outgroup nested within Megaspilinae (Figure 17). There is a consistent grouping in all trees comprised of *Dendrocerus marycarveri* + *Dendrocerus* AFEsp5 + *Dendrocerus* AFEsp8 + *Dendrocerus* AFEsp6 + *Dendrocerus carpenter* + *Megaspilus armatus* (100% BV; 100% PP).

None of the trees from the RPS23 intron analyses shows a monophyletic Megaspilinae (Figures 18, 19, 20). The same grouping that was consistent in the analysis of RPS23 exons which included *Megaspilus* is also supported in the RPS23 intron trees (100% BV; 50% PP). There is also a consistent grouping of *Conostigmus* IMsp2 + *Conostigmus Villosus* + *Conostigmus* IMsp9 + *Conostigmus bipunctatus* (63% BV; 96% PP).

From the most likely tree of the concatenated dataset (Figure 21), the 50% majority rule tree from the ML analysis (Figure 22) and the 50% majority rule tree from BI (Figure

23), we see that Megaspilinae is monophyletic (85% BV; 97% PP). *Conostigmus* is paraphyletic with respect to the rest of Megaspilinae with *Trichosteresis* sister to *Conostigmus triangularis* (100% BV; 100% PP). The represented *Conostigmus* are broken into two groups in the ML tree: one containing *Conostigmus* sp5 *Conostigmus triangularis* and *Trichosteresis* AFEsp1 (98% BV); and another containing the rest of *Conostigmus* (52% BV). In the BI tree, the former clade is also represented (100% PP), but the latter is not resolved with *Conostigmus* AFEsp5 forming a polytomy with the rest of *Conostigmus*. The remaining *Conostigmus* form a well-supported clade (96% PP). The remaining genera of Megaspilinae (*Dendrocerus* + *Creator* + *Platyceraphron* + *Megaspilus*) form a monophyletic clade (83% BV; 100%PP). At the base of the clade is a group composed of *Megaspilus armatus*, *Dendrocerus* AFEsp7 and *Dendrocerus* IMsp29 (64% BV; 99% PP). The base of the remaining clade of *Megaspilus* is poorly resolved with low support values in both the ML and BI trees (<50%). Well supported clades include: *Dendrocerus marycarveri* + *Dendrocerus* AFEsp5 (65% BV; 99% PP); *Dendrocerus* AFEsp9 + *Dendrocerus* AFEsp8 (100% BV; 100% PP); and *Dendrocerus cerpenteri* + *Dendrocerus wollastoni* + *Dendrocerus* AFEsp5 (100% BV; 100% PP) with the latter two groups forming clade (76% BV; 87% PP). The remaining taxa form an apical clade (59% BV; 97% PP). Within that clade are the groupings: *Dendrocerus punctipes* + *Dendrocerus laevus/laticeps* + *Dendrocerus nr serricornis* + *Dendrocerus* AFEsp10 + *Dendrocerus nr carpenteri* (50% BV; 96% PP); *Dendrocerus nr serricornis* + *Dendrocerus* AFEsp10 + *Dendrocerus nr carpenteri* (88% BV; 100% PP); and finally *Dendrocerus* AFEsp10 + *Dendrocerus nr carpenteri* (100% BV; 100% PP).

Discussion

The utility of 16S, 28S and COI for determining phylogenetics of hymenopterans is well-documented (Chen et al. 2004, Kuhlmann et al. 2009, Mardulyn and Whitfield 1999), and Lohse et al. (2011) has already proposed RPS23 as a gene that may be useful in determining phylogenetic relationships at this taxonomic level. The paraphyly of Megaspilinae that is observed in many of the single gene analyses may be due to the lack of informative characters or the saturation of base pair changes, both of which make model choice and therefore resulting topology unreliable.

From the branch lengths and support values of the ML and BI trees for 16S (Figures 1, 3), we can see that there is a large amount of information describing the base of the phylogeny as well as along the backbone, however there is little data informing the terminal sub-generic relationships. The same applies to the 28S trees (Figures 8, 10) to an even greater degree, the base of the tree is made up of long branches with highly supported relationships, indicating that there is a great deal of concordant data supporting those relationships. At the sub-generic level, especially within *Dendrocerus*, 28S is unable to confidently determine the relationships. The exonic and intronic regions of RPS23 reveal more about the sub-generic relationships than the basal relationships, each consistently supporting certain sister groupings and species groupings (Figures 15, 17, 18 and 20). The COI trees have little confident resolution of the represented taxa (Figure 12, 14), however, since there are so few taxa represented by this gene there may not be enough closely related taxa to infer any confident relationships. Since COI is a relatively fast evolving gene compared to 16S and 28S (Chen et al. 2004, Mardulyn and Whitfield 1999), taxa that are phylogenetically distant

may be saturated with base changes, which can make it difficult or impossible to confidently infer phylogeny.

Networks are useful for examining the differences in topology by showing the specific nodes where multiple trees disagree. The taxon sampling of 16S and 28S are nearly complete and in confident agreement concerning most of the relationships. This shows that these genes will likely be sufficient to infer basal relationships within Ceraphronoidea, however it might be worthwhile to obtain other sources of information such as a protein-encoding gene that has been shown to be informative at this level. CAD (carbamoyl-phosphate synthetase-aspartate transcarbamoylase-dihydroorotase) has proven useful for other groups within Hymenoptera (Sharanowski et al. 2011) and would likely be an appropriate candidate to pursue in the future.

The utility of RPS23 and COI for this question needs to be further tested by filling in missing data (Table 4) and more extensive and targeted taxon sampling. Concerning the genera that have been found to be nested within *Dendrocerus* (*Megaspilus*, *Platyceraphron*, and *Creator*) or *Conostigmus* (*Megaspilus* and *Trichosteresis*) it is important that those taxa be more extensively sampled to provide support for their placement, and inform future revision.

The concatenated dataset shows the placement of *Trassedia* at the base of Ceraphronidae with high confidence. This corroborates the hypothesis that *Trassedia* does not belong with Megaspilinae based on morphological characters (Mikó and Deans 2009). The highly supported topology, which shows a paraphyletic *Conostigmus*, is an indication that the genus needs revision. The *Conostigmus* spp. that form a clade with *Trichosteresis*

will require further examination of the species concepts and more taxon sampling of both the *Conostigmus* species and *Trichosteresis* to determine if this is a natural group which may be transferred to *Trichosteresis* in the future. Currently *Trichosteresis* contains only two valid species. A similar situation exists for the small clade where *Megaspilus* is sister to two *Dendrocerus* species. More taxon sampling will be needed to clearly determine the bounds of this group and the need for revisionary work. *Platyceraphron* and *Creator* are not as secure in their phylogenetic placement. Despite the lack of support for the sister groupings of these genera, the data indicate that these two genera are derived *Dendrocerus*. A revision of *Dendrocerus* including *Creator* and *Platyceraphron* is clearly necessary.

Basoko represented here by *Dendrocerus africanus* is nested at the base of the *Dendrocerus* clade, but due to the lack of resolution, it is not clear whether or not it forms a monophyletic grouping or not. Neither can we determine the distribution of *Lygocerus* represented by several specimens (Table 1) due to the lack of resolution in the *Dendrocerus* clade

From a few cases, multiple representatives of the same species existed in the data set (Table 1). After preliminary analysis showed very little genetic difference between two specimens such as the two *Dendrocerus penmaricus* specimens and the two *Creator spissicornis* specimens, the morphological concepts were re-examined morphologically, and I was able to reconcile the initial identifications. In the case of *Dendrocerus africanus*, where the two specimens were initially identified as being the same species, were found to actually represent phylogenetically distant species. The analysis combined with the challenge of determining specimens drives home the message that Ceraphronoidea needs revision and

trained taxonomists. In the future, more detailed diagnostic keys and potentially molecular markers will need to be developed to aid in diagnosis.

These data have established a basis for future, more detailed studies. Since both COI and RPS23 provide sub-generic level resolution an informative approach might be to build multiple datasets using these markers and composed of taxa from single genera or closely related genera. Once these datasets have been compiled, the phylogeny of each genus can be more confidently estimated without having to deal with convergence that may occur with data that is saturated with base pair changes. Once this has been done, the backbone of the phylogeny can be established using 16S, 28S and potentially CAD. The generic phylogenies and the subfamily phylogeny can then be combined into a supernetwork employing the Z-closure method which would allow for the incomplete taxon sampling of the smaller trees based on COI and RPS23. Utilizing this method, we can avoid problems associated with saturation of base changes.

REFERENCES

Ashmead, W.H., 1893. Monograph of the North American Proctotrupidae. Bulletin of the United States National Museum 45, 1-472.

Ashmead, W.H., 1903. Classification of the pointed-tailed wasps of the superfamily Proctotrupoidea-II. Journal of the New York Entomological Society 11, 28-34.

Castresana, J., 2000. Selection of conserved blocks from multiple alignments for their use in phylogenetic analysis. Molecular Biology and Evolution 17, 540-552.

Chen, Y., Xiao, H., Fu, J., Huang, D., 2004. A molecular phylogeny of eurytomid wasps inferred from DNA sequence data of 28S, 18S, 16S and COI genes. Molecular Phylogenetics and Evolution 31, 300-307.

Dessart, P., 1966. Contribution a l'étude des Hymenopteres Proctotrupoidea. (XII) A propos des Ceraphronidae Megaspilinae males a antennes rameuses. Bulletin de l'Institute Royal des Sciences Naturelles de Belgique Entomology 42(32), 1-16.

Dessart, P., 1973. *Dichogmus* Thomson, 1868, un genre invalide (Hym. Ceraphronoidea Megaspilidae). Bulletin de l'Institute Royal des Sciences Naturelles de Belgique Entomology 109, 104-130.

Dessart, P., Cancemi, P., 1987. Tableau dichotomique des genres des Ceraphronoidea (Hymenoptera) avec commentaires et nouvelles espèces Frustula Entomologica 7-8,307-372.

Dowton, M., Austin, A.D., 1994. Molecular phylogeny of the insect order Hymenoptera: Apocritan relationships. Proceedings of the National Academy of Sciences 91, 9911-9915.

Dowton, M., Austin, A.D., 2001. Simultaneous analysis of 16S, 28S, COI and morphology in the Hymenoptera: Apocrita – evolutionary transitions among parasitic wasps. Biological Journal of the Linnean Society 74, 87-111.

Fergusson, N.D.M., 1980. A revision of the British species of *Dendrocerus* Ratzeburg (Hymenoptera: Ceraphronoidea) with a review of their biology as aphid hyperparasites. Bulletin of the British museum Natural History Entomology 41, 255-314.

Folmer, O., Black, M., Hoeh, W., Lutz, R., Vrijenhoek, R., 1994. DNA primers for amplification of mitochondrial cytochrome c oxidase subunit I from diverse metazoan invertebrates. Molecular Marine Biology and Biotechnology 3, 294-297.

Gelman, A., Rubin, D., 1992. Inference from iterative simulation using multiple sequences with discussion. Statistical Science 7, 457-511.

Hall, T.A., 1999. BioEdit: a user-friendly biological sequence alignment editor and analysis program for Windows 95/98/NT. Nucleic Acids Symposium Ser. 41, 95-98.

Heraty, J., Ronquist, F., Carpenter, J.M., Hawks, D., Schulmeister, S., Dowling, A.P., Murray, D., Munro, J., Wheeler, W.C., Schiff, N., Sharkey, M.J., 2011. Evolution of the hymenopteran megaradiation. Molecular Phylogenetics and Evolution 60, 73-88.

Huelsenbeck, J.P., Ronquist, F., 2001. MRBAYES: Bayesian inference of phylogenetic trees. Bioinformatics 17, 754-755.

Huson, D.H., Bryant, D., 2006. Application of phylogenetic networks in evolutionary studies. Molecular Biology and Evolution 23(2), 254-267.

Huson, D.H., Dezulian, T., Klöpper, T., Steel, M.A., 2004. Phylogenetic super-networks from partial trees. IEEE/ACM Transitions in Computational Biology and Bioinformatics 1(4), 151-158.

Johnson, N.F., Musetti, L., 2004. Catalog of systematic literature of the superfamily Ceraphronoidea (Hymenoptera). Contributions of the American Entomological Institute 33(2), 1-149.

Katoh, K., Misawa, K., Kuma, K., Miyata, T., 2002. MAFFT: a novel method for rapid multiple sequence alignment based on fast Fourier transform. Nucleic Acids Research 30(14), 3059-3066.

Kieffer, J.J., 1907. Species des Hyménoptères d'Europe et d'Algérie. Volume 10 editor André, E., Librarie Scientifique A. Hermann and Fils, Paris. 1-144.

Kirchner, L., 1867. Catalogus hymenopterorum Europae. C. Ueberreuter, 1-285.

Kuhlmann, M., Almeida, E.A.B., Laurenne, N., Quicke, D.L.J., 2009. Molecular phylogeny and historical biogeography of the bee genus *Colletes* Latreille, 1802 (Hymenoptera: Apiformes: Colletidae), based on mitochondrial COI and nuclear 28S sequence data. Insect Systematics and Evolution 40(3), 291-318.

Lohse, K., Sharanowski, B., Blaxter, M., Nicholls, J.A., Stone, G.N., 2011. Developing EPIC markers for chalcidoid Hymenoptera from EST and genomic data. Molecular Ecology Resources 11, 521-529.

Mardulyn, P., Whitfield J.B., 1999. Phylogenetic signal in the COI, 16S and 28S genes for inferring relationships among genera of Microgastrinae (Hymenoptera; Braconidae):

Evidence of a high diversification rate in this group of parasitoids. Molecular Phyologenetics and Evolution 12(3), 282-294.

Masner, L., 1964. A comparison of some Nearctic and Palearctic genera of Proctotrupoidea (Hymenoptera) with revisional notes. Cas. Csl. Spol. Entomol. 61, 123-155.

Masner, L., Dessart, P., 1967. La reclassification des categories taxonomiques superieures des Ceraphronoidea (Hymenoptera). Bulletin de l'Institute Royal des Sciences Naturelles de Belgique Entomology 43, 1-32.

Mikó, I., Deans, A.R., 2009. *Masner*, a new genus of Ceraphronidae (Hymenoptera, Ceraphronoidea) described using controlled vocabularies. ZooKeys 20, 127-153.

Mikó, I., Yoder, M.J., Deans, A.R., 2011. Order Hymenoptera, family Megaspilidae genus Dendrocerus. Arthropod fauna of the UAE 4, 353-374.

Miller, M.A., Pfeiffer, W., Schwartz, T., 2010. Creating the CIPRES Science Gateway for inference of large phylogenetic trees. Proceedings of the Gateway Computing Environments Workshop (GCE), 14 Nov. 2010, New Orleans, LA, 1-8.

Posada, D., 2008. jModeltest: Phylogenetic modeling averaging. Molecular Biology and Evolution 25, 1253-1256.

Rambaut, A., Drummond, A.J., 2007. Tracer v1.5, available from http://beast.bio.ed.ac.uk/Tracer

Rasnitsyn, A.P., 1980. The origin and evolution of the Hymenoptera. Transactions of the Paleontological Institute AN SSSR 174, 1-190.

Rodendorf, B.B., (1962). Tshlenistonogie traheinie I Helitserovie. Osnovi Paleontolohii, Spravotshnik dlja Paleontologov I Geologov. Moscou, 1-560.

Ronquist, F., Huelsenbeck, J.P., 2003. MrBayes 3: Bayesian phylogenetic inference under mixed models. Bioinformatics 19, 1572-1574.

Ronquist, F., Rasnitsyn, A.P., Roy, A., Eriksson, K., Lindren, M., 1999. Phylogeny of the Hymenoptera: A cladistics reanalysis of Rasnitsyn's (1988) data. Zoological Scripta 28, 13-50.

Sharanowski, B.J., Dowling, A.P., Sharkey, M.J., 2011. Molecular phylogenetics of Braconidae (Hymenoptera: Ichneumonoidea), based on multiple nuclear genes, and implications for classification. Systematic Entomology 36(3), 549-572.

Sharanowski, B.J., Robbertse, B., Walker, J., Voss, S.R., Yoder, R., Spatafora, J., Sharkey, M.J., 2010. Expressed sequence tags reveal Proctotrupomorpha (minus Chalcidoidea) as sister to Aculeata (Hymenoptera: Insecta). Molecular Phylogenetics and Evolution 57, 101-112.

Sharkey, M.J., Carpenter, J.M., Vilhelmsen, L., Heraty, J., Liljeblad, J., Dowling, A.P.G., Schulmeister, S., Murray, D., Deans, A.R., Ronquist, F., Krogmann, L., Wheeler, W., 2011. Phylogenetic relationships among superfamilies of Hymenoptera. Cladistics 28, 80-112.

Stamatakis, A., 2006. RAxML-VI-HPC: Maximumlikelihood-based phylogenetic analysis with thousands of taxa and mixed models. Bioinformatics 22(21), 2688-2690.

Tamura, K., Peterson, D., Peterson, N., Stecher, G., Nei, M., Kumar, S., 2011. MEGA5: Molecular evolutionary genetics analysis using maximum likelihood, evolutionary distance, and maximum parsimony methods. Molecular Biology and Evolution 28, 2731-2739.

Whitfield, J.B., Cameron, S.A., 1998. Hierarchical analysis of variation in the mitochondrial 16S rRNA gene among Hymenoptera. Molecular Biology and Evolution 15(12), 1728-1743.

Table 1. List of taxa including country in which the specimen was collected.

extract ID	O.T.U.	Collection locality	historic taxonomy
315	*Conostigmus* IMsp9	Sweeden	
316	*Dendrocerus halidayi*	Hungary	*Lygocerus*
317	*Dendrocerus carpenteri*	South Africa	*Lygocerus*
319	*Elysoceraphron* IMsp1	Thailand	
320	*Dendrocerus rectangularis*	Sweeden	*Lygocerus*
321	*Dendrocerus marycarveri*	Australia	
322	*Dendrocerus wollastoni*	Australia	
323	*Dendrocerus* IMsp29	Chile	
324	*Dendrocerus penmaricus*	USA	*Megaspilus*
325	*Aphanogmus* AFEsp1	Chile	
326	*Dendrocerus* AFEsp3	Thailand	
327	*Aphanogmus fulmeki*	China	
328	*Conostigmus* sp5	Sweeden	
331	*Conostigmus* IMsp2	Sweeden	
332	*Conostigmus bipunctatus*	Sweeden	
334	*Conostigmus villosus*	Thailand	
335	*Ceraphron* IMsp21	Thailand	
336	*Dendrocerus* IMsp42	Thailand	
337	*Aphanogmus* AFEsp3	Thailand	
338	*Conostigmus abdominalis*	Sweeden	
340	*Conostigmus triangularis*	United Arab Emirates	
460	*Dendrocerus* AFEsp5	Thailand	
462	*Dendrocerus* AEFsp6	Brazil	
463	*Dendrocerus* AFEsp7	Argentina	
464	*Dendrocerus* AFEsp8	Kenya	
467	*Dendrocerus* AFEsp9	Yemen	
468	*Dendrocerus* AFEsp10	Canada	
469	*Dendrocerus* AFEsp11	Mexico	
473	*Conostigmus* AFEsp4	Chile	
481	*Conostigmus* AFEsp5	Australia	
483	*Dendrocerus penmaricus*	Canada	*Megaspilus*
514	*Creator spissicornis*	Sweeden	*Lygocerus*
518	*Trichosteresis* AFEsp1	South Africa	
519	*Megaspilus armatus*	Canada	
563	*Platyceraphron artideterens*	USA	
665	*Creator spissicornis*	Sweeden	*Lygocerus*
666	*Dendrocerus nr carpenteri*	USA	
667	*Dendrocerus ramicornis*	Sweeden	*Lygocerus*
668	*Dendrocerus ramicornis*	Sweeden	*Lygocerus*
669	*Dendrocerus nr serricornis*	Sweeden	
670	*Dendrocerus rectangularis*	Sweeden	*Lygocerus*
672	*Lagynodes* AFEsp1	USA	

Table 1. (Continued)

extract ID	O.T.U.	Collection locality	historic taxonomy
674	*Dendrocerus laevus/laticeps*	Sweeden	
675	*Dendrocerus serricornis*	Sweeden	*Lygocerus*
676	*Dendrocerus punctipes*	Sweeden	
677	*Lagynodes* AFEsp1	USA	
732	*Masner*	Australia	
733	*Masner*	Fiji	
734	*Masner*	Australia	
735	*Aetholagynodes* AFEsp1	Australia	
736	*Aetholagynodes* AFEsp1	Australia	
737	*Aetholagynodes* AFEsp2	USA	
738	*Lagynodes* AFEsp2	Japan	
739	*Trassedia luapi*	French Guyana	
740	*Homoloceraphron*	USA	
741	*Homoloceraphron*	USA	
742	*Dendrocerus africanus*	Kenya	*Basoko*
743	*Dendrocerus africanus*	Kenya	*Basoko*

Table 2. List of primers used for PCR amplification of gene regions including the sequence of the primers (5'-3') and the source where primers were found.

Gene region	Label	Sequence (5' - 3')	Source
16S	16SDAF	CACCTGTTTATCAAAAACAT	Dowton and Austin 1994
	16SDAR	CTGCGATTTGAACTCAAATC	Dowton and Austin 1994
28S	28SD2D3F_BJS_F	CTGRGAAAACCCGAAAGATCG	Sharanowski unpublished
	28SD2D3_AFE_F	CTGRGAAACCCRAAAGATCG	Ernst et al. unpublished
	28SD2D3R_BJS_R	GTCCTGAAAGTACCCAAAGC	Sharanowski unpublished
RPS23	RPS23-21aF	ACVMGVTGGAAGGCYAATCC	Lohse et al. 2011
	RPS23-21aR	ATGACCYTTACGHCCRAATCC	Lohse et al. 2011
	RPS23-21bR	CCDACRGCRTGACCYTTACG	Sharanowski unpublished
COI	CO1-LCO1490-F	GGTCAACAAATCATAAAGATATTGG	Folmer et al. 1994
	CO1-HCO2198-R	TAAACTTCAGGGTGACCAAAAAATCA	Folmer et al. 1994

Table 3. List of gene regions sampled including the PCR thermal cycler protocols used.

Gene Region	Initial denaturation (1 cycle)	Denaturation	Annealing	extension	Replication cycles
16S	94°C - 2 min	94°C - 0:30	50°C - 1:00	72°C - 1:30	35
28S	94°C - 5 min	94°C - 0:30	48°C - 1:00	72°C - 2:00	30
RPS23	94°C - 5 min	94°C - 0:30	61°C - 1:00	72°C - 2:00	3
		94°C - 0:30	58°C - 1:00	72°C - 2:00	5
		94°C - 0:30	54°C - 1:00	72°C - 2:00	25
COI	94°C - 2 min	94°C - 0:30	48°C - 1:00	72°C - 2:00	30

Table 4. List of taxa, including genes representing taxa in the dataset.

extract ID	O.T.U.	16S	28S D2-D3	RPS 23	CO1
315	*Conostigmus* IMsp9	X		X	
316	*Dendrocerus halidayi*	X	X		
317	*Dendrocerus carpenteri*			X	
319	*Elysoceraphron* IMsp1	X	X	X	
320	*Dendrocerus rectangularis*	X	X		
321	*Dendrocerus marycarveri*	X	X	X	X
322	*Dendrocerus wollastoni*	X	X		X
323	*Dendrocerus* IMsp29	X	X		
324	*Dendrocerus penmaricus*	X	X	X	
325	*Aphanogmus* AFEsp1	X	X	X	
326	*Dendrocerus* AFEsp3	X	X		X
327	*Aphanogmus fulmeki*			X	
328	*Conostigmus* sp5	X	X		X
331	*Conostigmus* IMsp2	X	X	X	
332	*Conostigmus bipunctatus*	X		X	X
334	*Conostigmus villosus*	X		X	
335	*Ceraphron* IMsp21	X	X	X	
336	*Dendrocerus* IMsp42	X	X		
337	*Aphanogmus* AFEsp3	X	X	X	
338	*Conostigmus abdominalis*	X		X	X
340	*Conostigmus triangularis*	X	X		X
460	*Dendrocerus* AFEsp5	X	X	X	
462	*Dendrocerus* AEFsp6	X	X		
463	*Dendrocerus* AFEsp7	X	X		
464	*Dendrocerus* AFEsp8	X	X	X	X
467	*Dendrocerus* AFEsp9	X	X		
468	*Dendrocerus* AFEsp10	X	X		
469	*Dendrocerus* AFEsp11	X	X		
473	*Conostigmus* AFEsp4	X		X	
481	*Conostigmus* AFEsp5	X		X	
483	*Dendrocerus penmaricus*	X	X	X	
514	*Creator spissicornis*	X	X		

Table 4. (Continued)

extract ID	O.T.U.	16S	28S D2-D3	RPS 23	CO1
518	*Trichosteresis* AFEsp1	X	X	X	
519	*Megaspilus armatus*	X		X	X
563	*Platyceraphron artideterens*		X		
665	*Creator spissicornis*	X	X		
666	*Dendrocerus nr carpenteri*	X	X		
667	*Dendrocerus ramicornis*	X	X		
668	*Dendrocerus ramicornis*	X	X		
669	*Dendrocerus nr serricornis*	X	X		
670	*Dendrocerus rectangularis*	X	X		
672	*Lagynodes* AFEsp1	X			X
674	*Dendrocerus laevus/laticeps*	X	X		
675	*Dendrocerus serricornis*		X		
676	*Dendrocerus punctipes*	X	X		
677	*Lagynodes* AFEsp1	X			
732	*Masner*		X		
733	*Masner*	X	X		
734	*Masner*	X			
735	*Aetholagynodes* AFEsp1	X	X		
736	*Aetholagynodes* AFEsp1		X		
737	*Aetholagynodes* AFEsp2	X			
738	*Lagynodes* AFEsp2	X			
739	*Trassedia luapi*	X			
740	*Homoloceraphron*	X	X		
741	*Homoloceraphron*	X			
742	*Dendrocerus africanus*		X		
743	*Dendrocerus africanus*		X		

Table 5. List of genes used, including the aligned length in bases, base compositions given in proportions, and models of evolution determined using jModeltest (Posada 2008).

Gene	Aligned length	base composition	Model of evolution	Rate matrix	Model of rate variation
16S	572	A = 0.4143 C = 0.0194, G = 0.0676, T = 0.4987	HKY + Γ		gamma
16S variable regions removed	485	A = 0.4180 C = 0.0207, G = 0.0617, T = 0.4997	TPM1uf + I + Γ	1.0000, 4.0525, 0.6950, 0.6950, 4.0525, 1.0000	gamma
28S	448	A = 0.1513 C = 0.2917, G = 0.2993, T = 0.2578	TVM + Γ	1.2062, 5.4172, 3.8156, 0.5979, 5.4172, 1.0000	gamma
COI	662	A = 0.3514 C = 0.1480, G = 0.1163, T = 0.3843	IM1 + I + Γ	1.0000, 7.8840, 5.1168, 5.1168, 31.9405, 1.0000	gamma
RPS23 exons	188	A = 0.3082 C = 0.2706, G = 0.2384, T = 0.1829	TPM2 + Γ	3.0024, 9.0692, 3.0024, 1.0000, 9.0692, 1.0000	gamma
RPS23 introns	996	A = 0.3785 C = 0.1153, G = 0.1031, T = 0.4032	TPM2uf	0.5177, 2.1953, 0.5177, 1.0000, 2.1953, 1.0000	equal

Table 6. List of datasets including the number of generations to reach an average standard deviation of split frequencies (ASDSF) MrBayes runs, and the effective sample sizes (ESS) calculated from Tracer 1.5.0 (Rambaut and Drummond 2007).

Dataset	Generations	ESS (run 1)	ESS (run 2)
16S	38780000	2970.457	3115.214
16S variable regions removed	6650000	600	600
28S	4360000	394	394
RPS23 exons	11090000	823.7985	1000
RPS23 intron	11040000	961.6266	995
COI	12210000	1043.1115	1051.8595
Concatenated	5631000	903.5754	1282.843

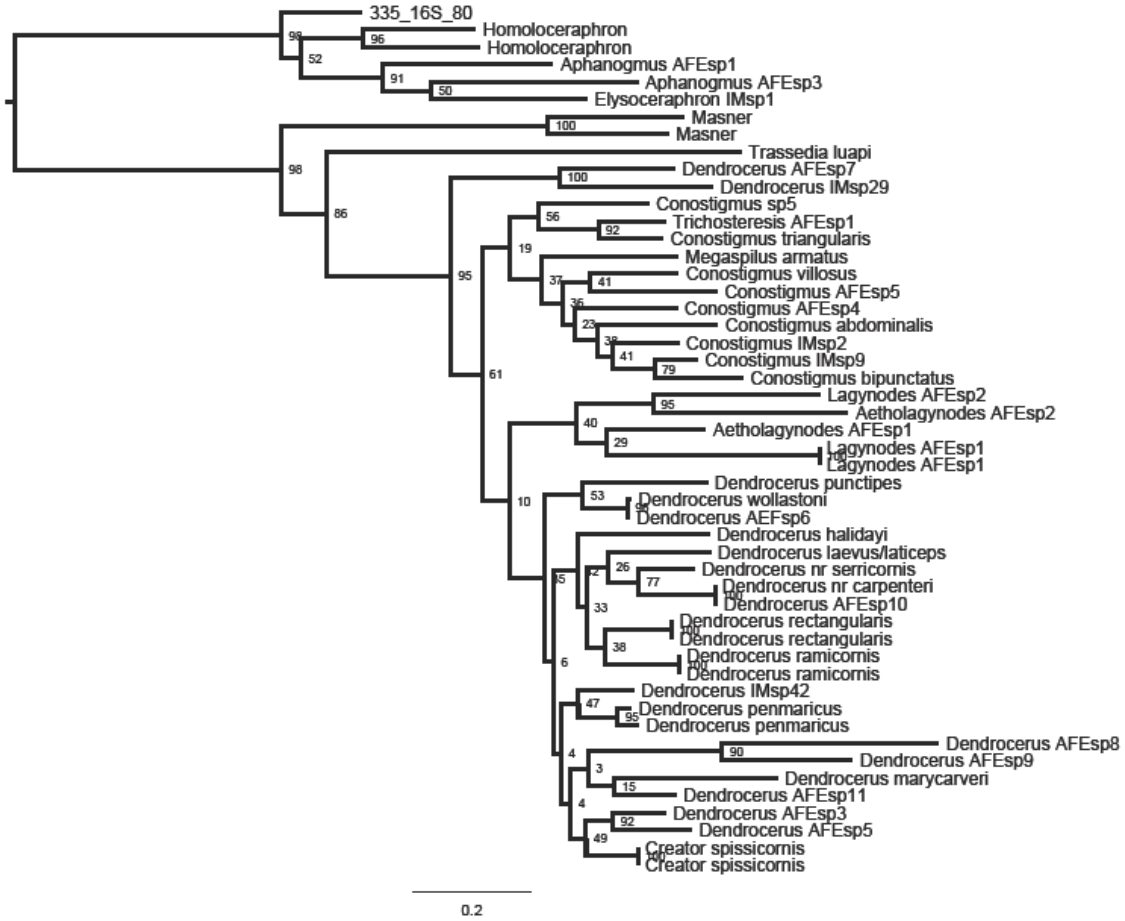

Figure 1. Most likely tree from the maximum likelihood analysis of 16S rRNA, bootstrap values listed at nodes (stopped at 550 bootstrap pseudoreplicates based on MRE bootstopping criteria).

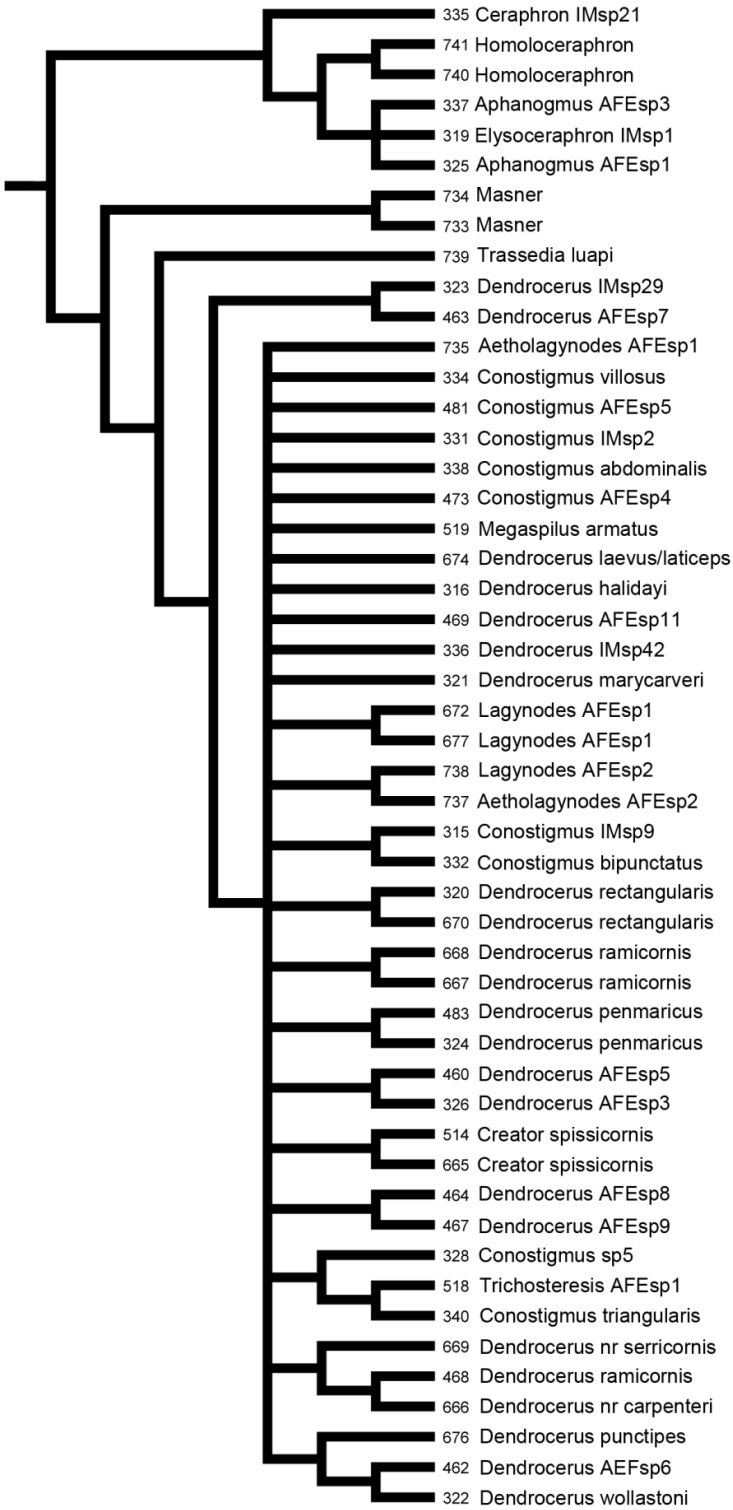

Figure 2. 50% majority rule tree from the maximum likelihood analysis of 16S rRNA (stopped at 550 bootstrap pseudoreplicates based on MRE bootstopping criteria).

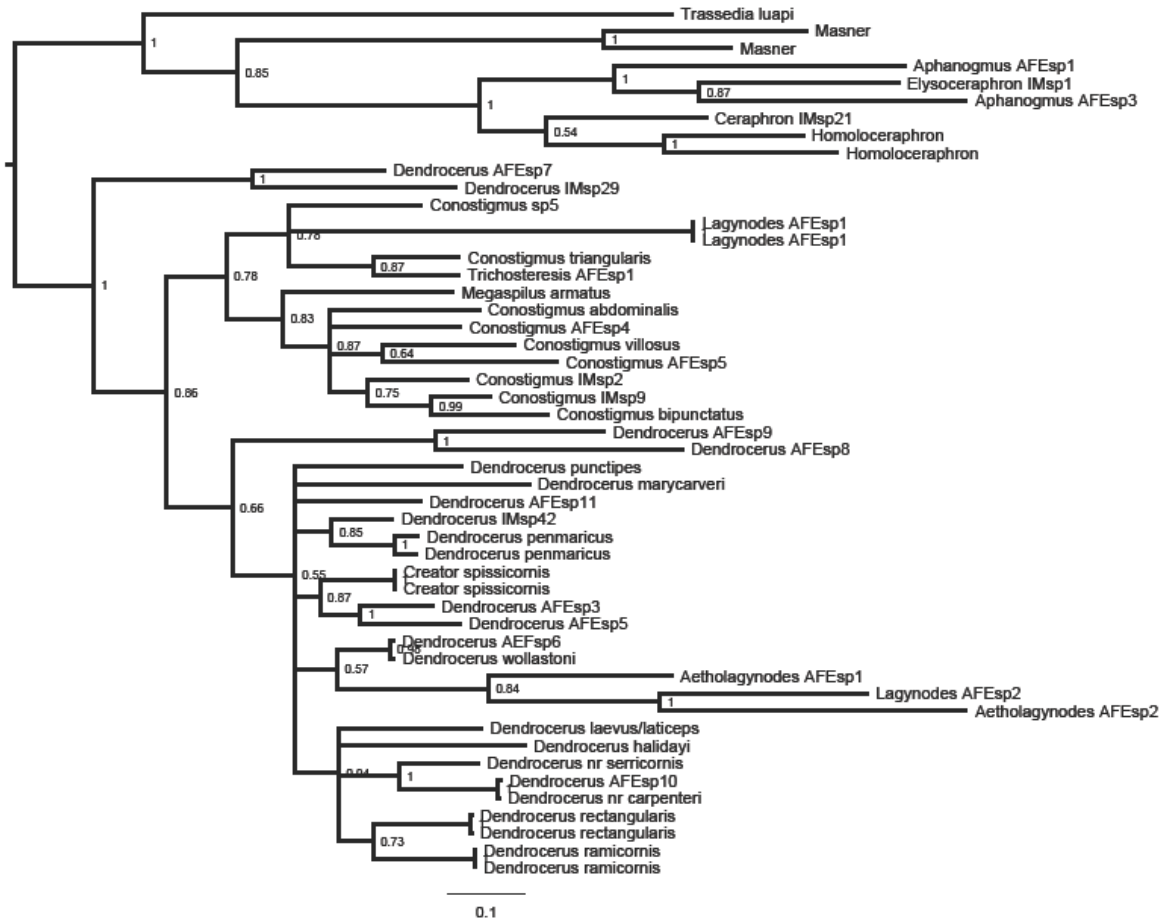

Figure 3. Topology inferred from the Bayesian analysis of 16S rRNA, posterior probabilities are listed at the nodes (38,780,000 generations).

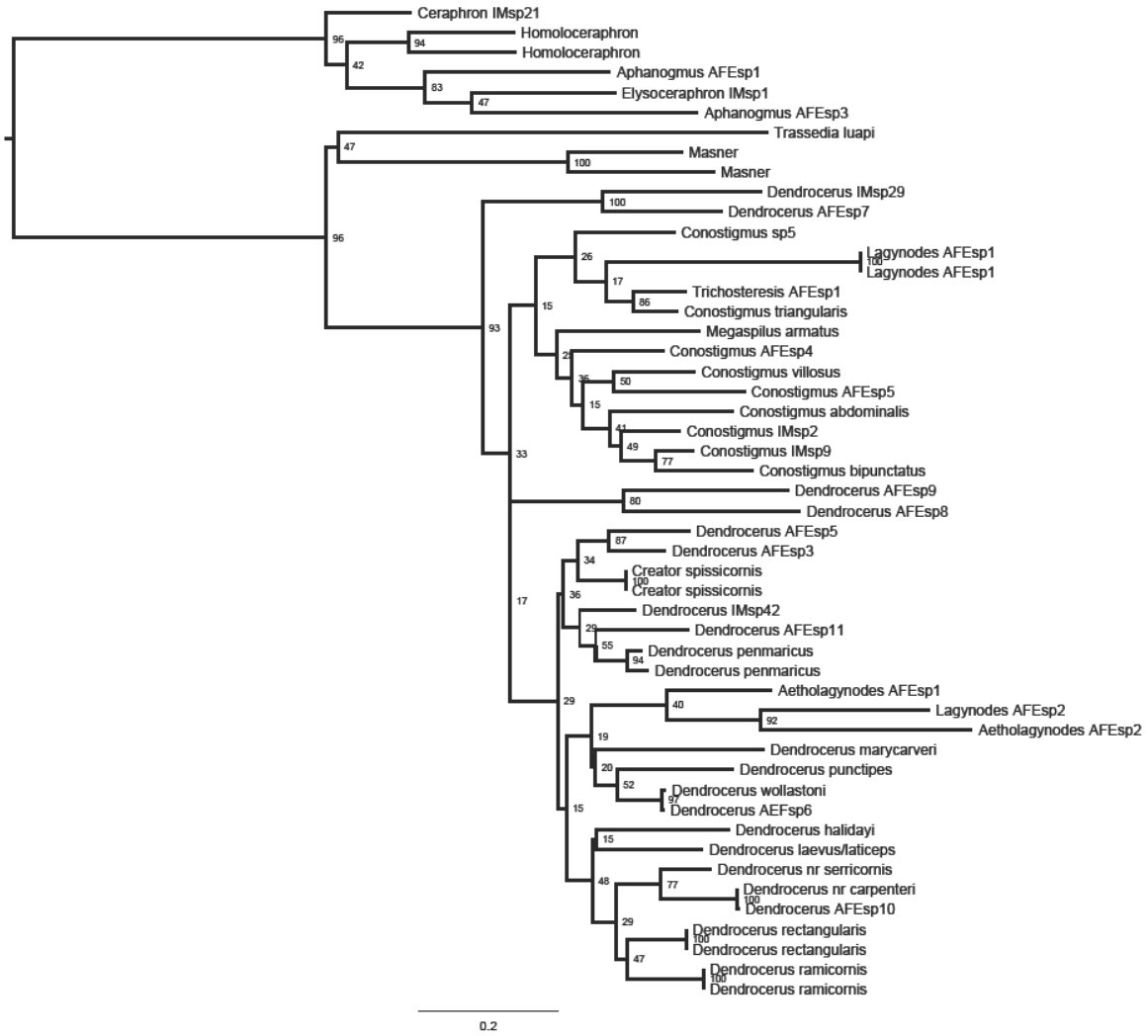

Figure 4. Most likely tree from the maximum likelihood analysis of 16S rRNA with variable regions removed, bootstrap values listed at nodes (stopped at 450 bootstrap pseudoreplicates based on MRE bootstopping criteria).

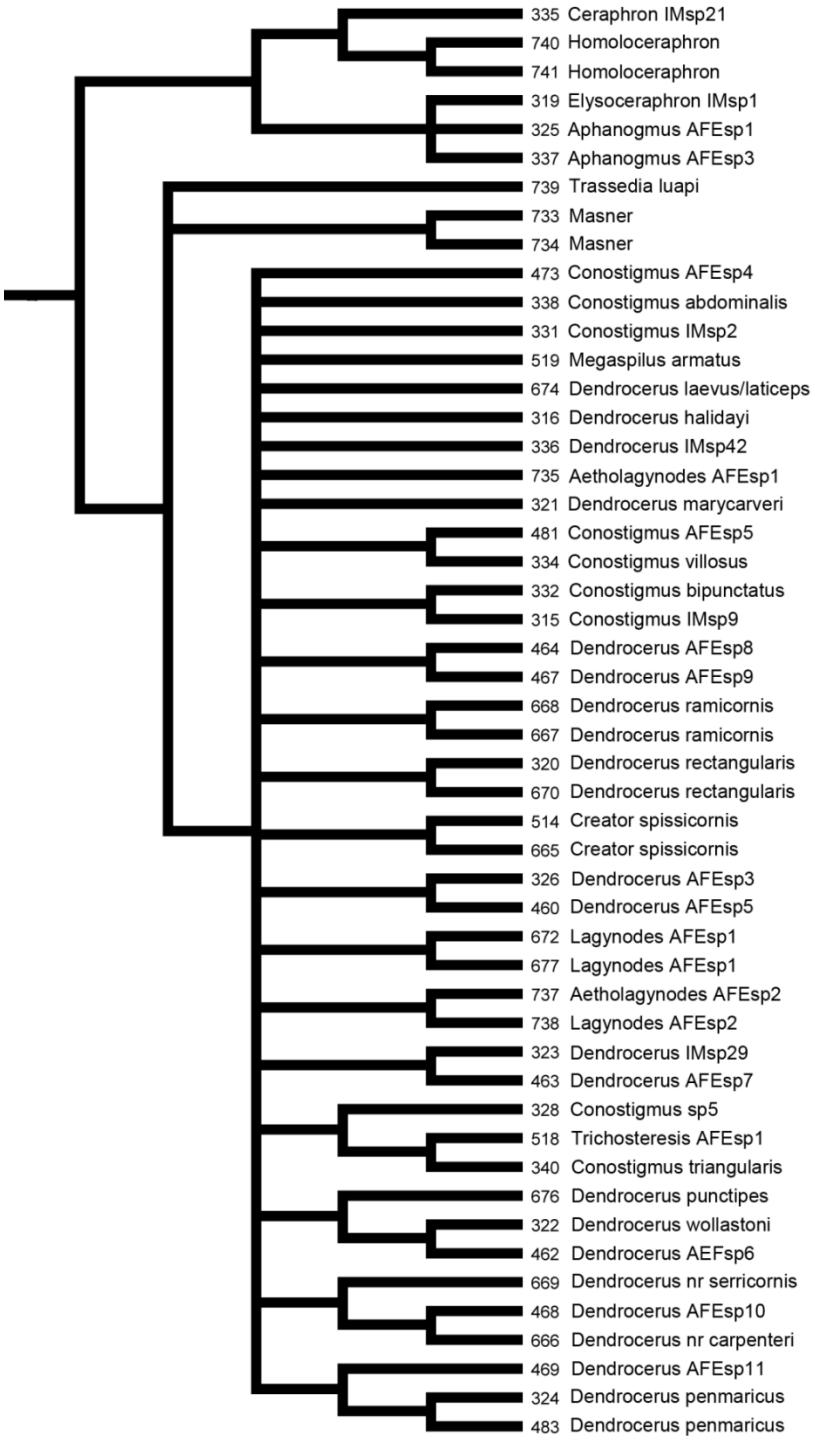

Figure 5. 50% majority rule tree from the maximum likelihood analysis of 16S rRNA with variable regions removed (stopped at 450 bootstrap pseudoreplicates based on MRE bootstopping criteria).

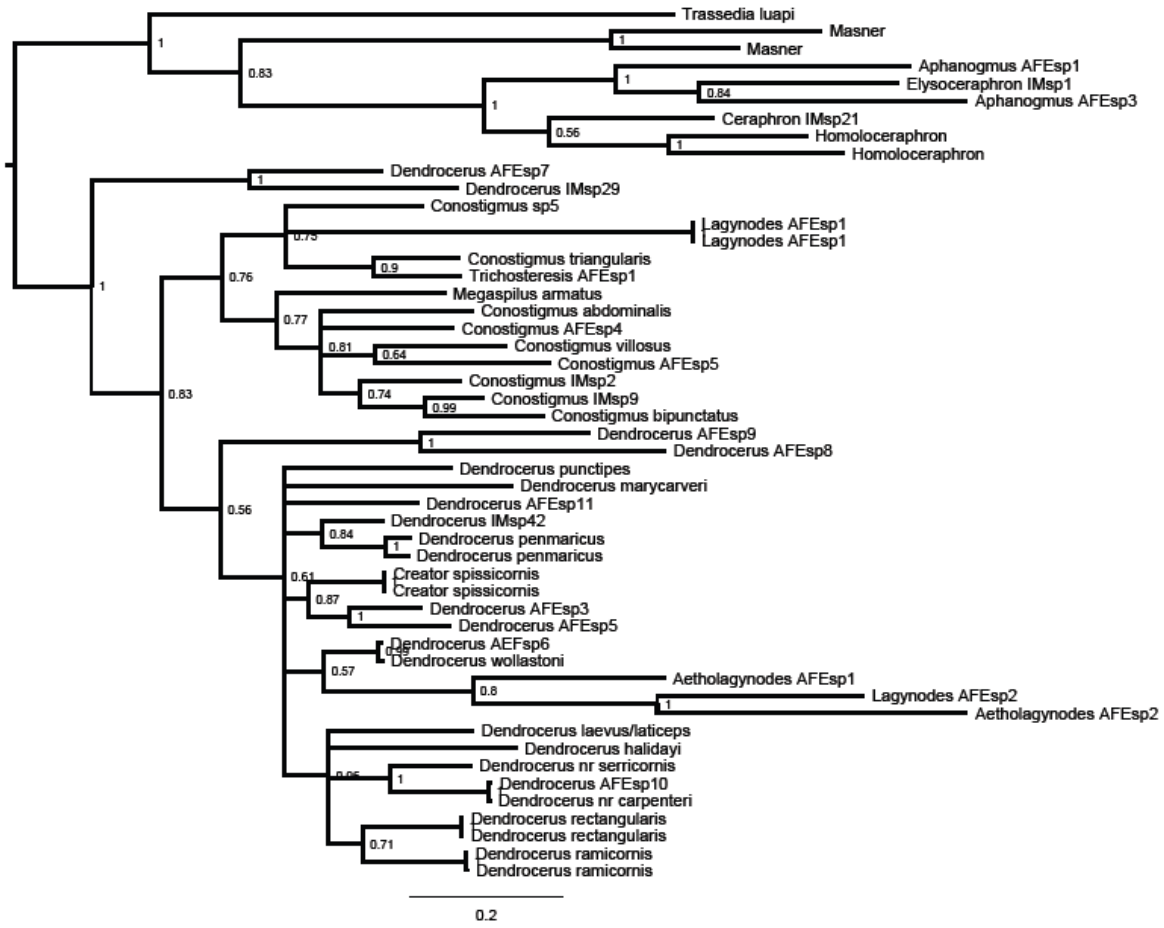

Figure 6. Topology inferred from the Bayesian analysis of 16S rRNA with variable regions removed, posterior probabilities are listed at the nodes (6,650,000 generations).

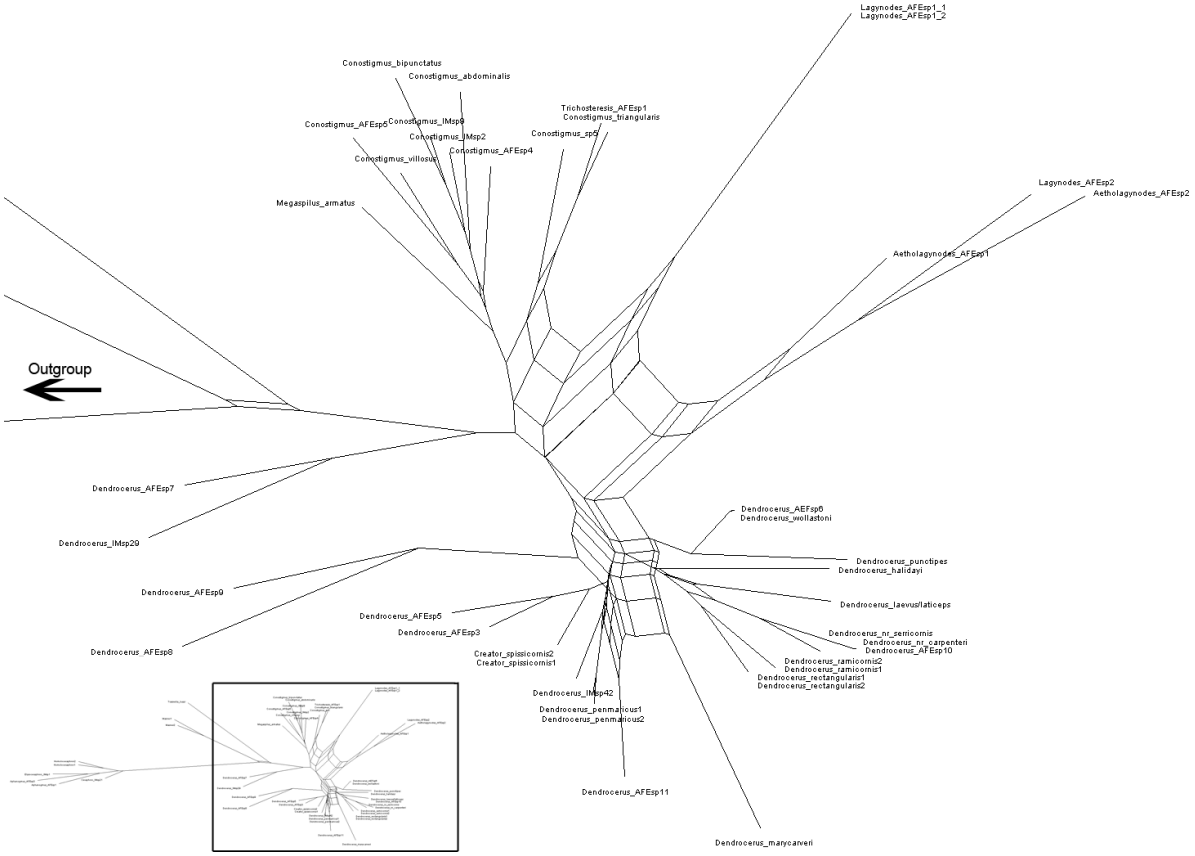

Figure 7. Consensus network based on the most likely trees for the 16S rRNA and 16S RRNA with variable regions removed datasets (Figures 1 and 4), calculated using mean edge weights and a threshold of 0.33.

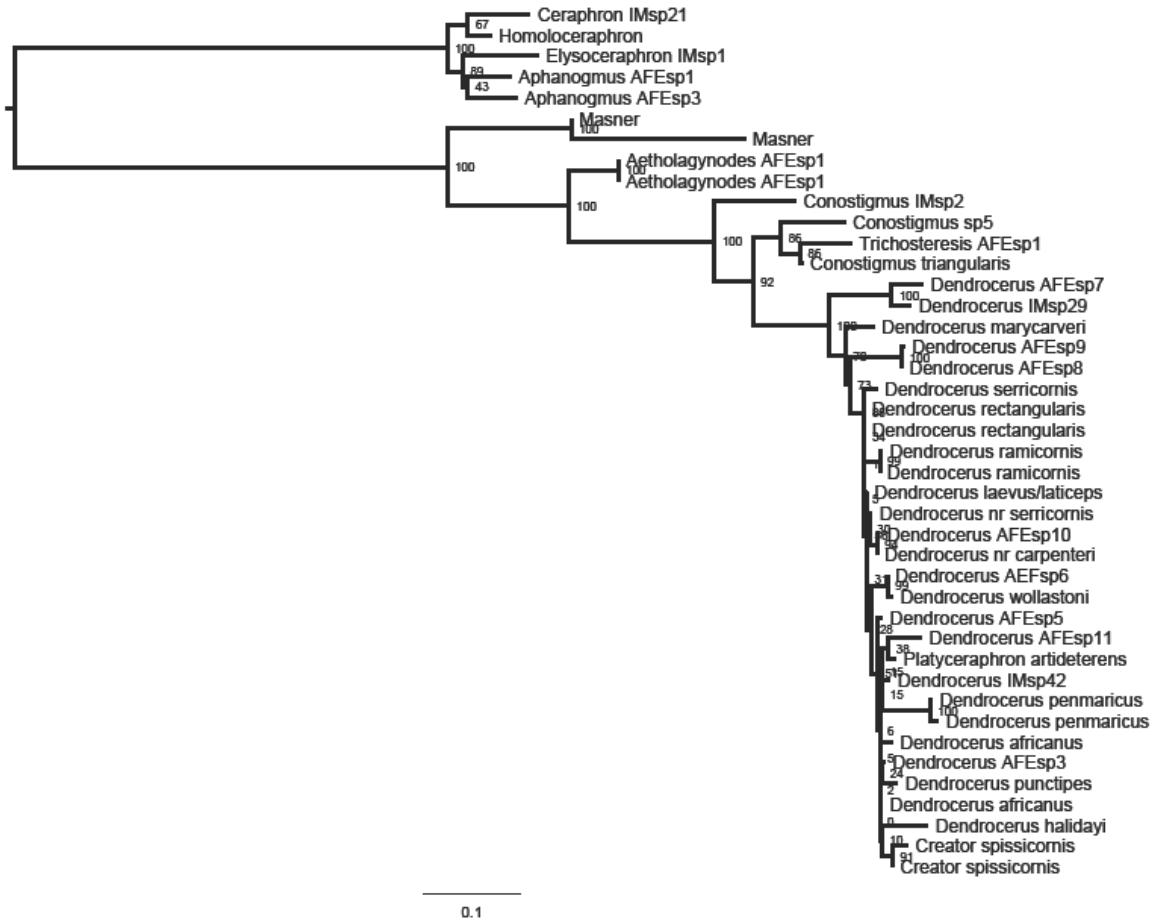

Figure 8. Most likely tree from the maximum likelihood analysis of 28S rRNA, bootstrap values listed at nodes (stopped at 450 bootstrap pseudoreplicates based on MRE bootstopping criteria).

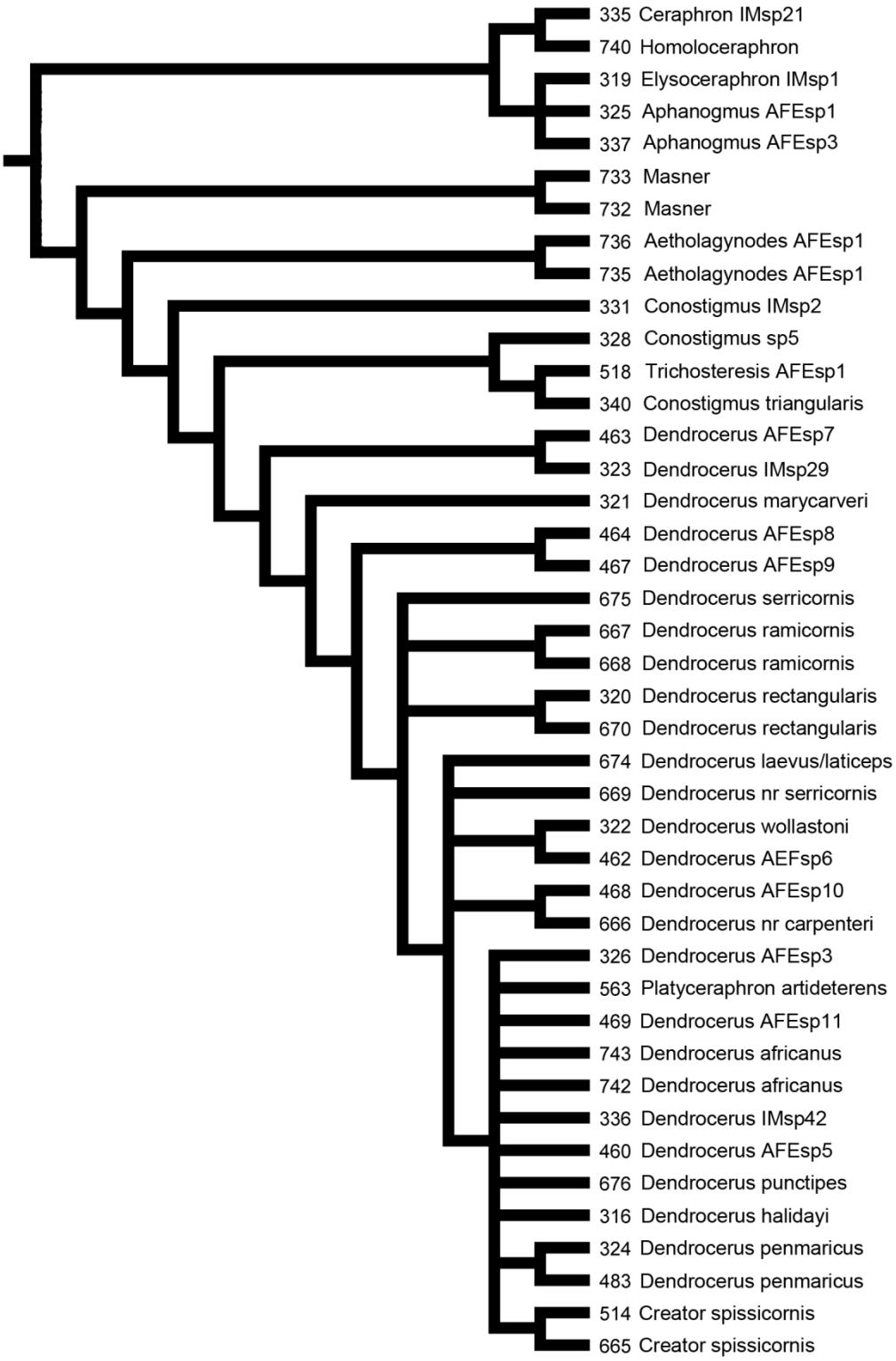
335 Ceraphron IMsp21
740 Homoloceraphron
319 Elysoceraphron IMsp1
325 Aphanogmus AFEsp1
337 Aphanogmus AFEsp3
733 Masner
732 Masner
736 Aetholagynodes AFEsp1
735 Aetholagynodes AFEsp1
331 Conostigmus IMsp2
328 Conostigmus sp5
518 Trichosteresis AFEsp1
340 Conostigmus triangularis
463 Dendrocerus AFEsp7
323 Dendrocerus IMsp29
321 Dendrocerus marycarveri
464 Dendrocerus AFEsp8
467 Dendrocerus AFEsp9
675 Dendrocerus serricornis
667 Dendrocerus ramicornis
668 Dendrocerus ramicornis
320 Dendrocerus rectangularis
670 Dendrocerus rectangularis
674 Dendrocerus laevus/laticeps
669 Dendrocerus nr serricornis
322 Dendrocerus wollastoni
462 Dendrocerus AEFsp6
468 Dendrocerus AFEsp10
666 Dendrocerus nr carpenteri
326 Dendrocerus AFEsp3
563 Platyceraphron artideterens
469 Dendrocerus AFEsp11
743 Dendrocerus africanus
742 Dendrocerus africanus
336 Dendrocerus IMsp42
460 Dendrocerus AFEsp5
676 Dendrocerus punctipes
316 Dendrocerus halidayi
324 Dendrocerus penmaricus
483 Dendrocerus penmaricus
514 Creator spissicornis
665 Creator spissicornis

Figure 9. 50% majority rule tree from the maximum likelihood analysis of 28S rRNA (stopped at 450 bootstrap pseudoreplicates based on MRE bootstopping criteria).

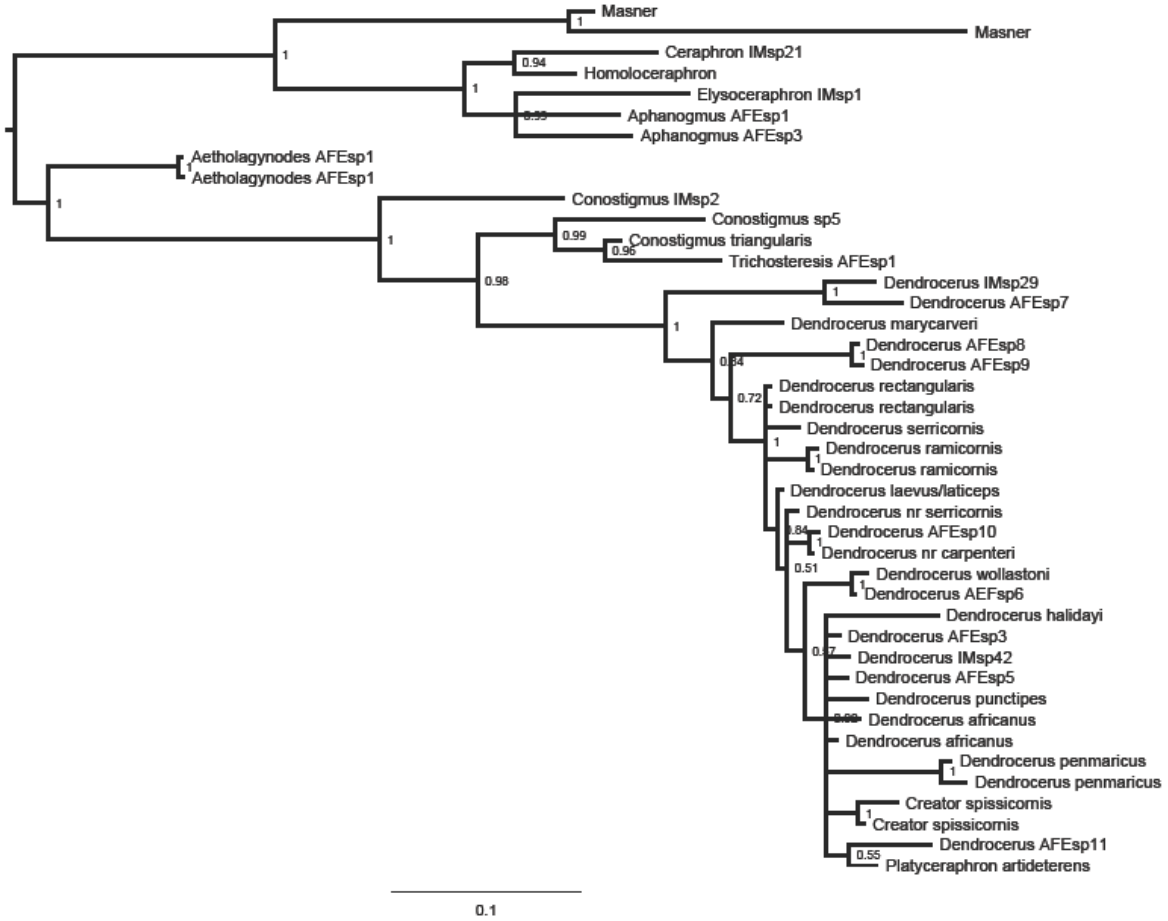

Figure 10. Topology inferred from the Bayesian analysis of 28S rRNA, posterior probabilities are listed at the nodes (4,360,000 generations).

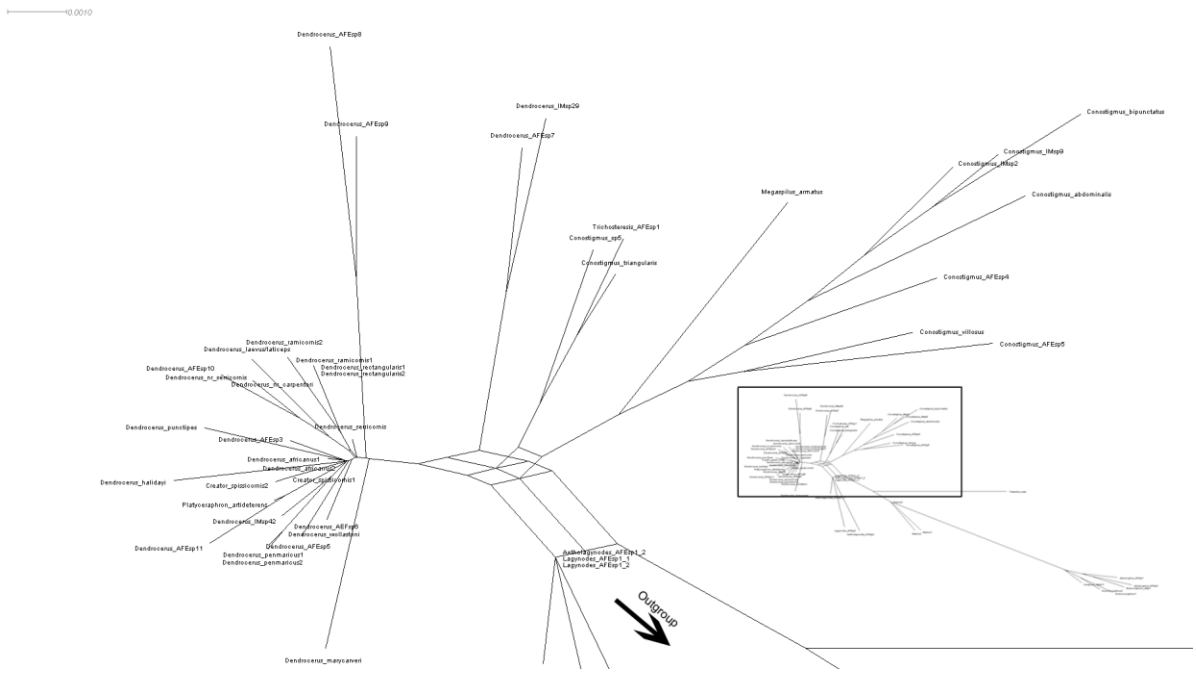

Figure 11. Supernetwork based on the most likely trees from the 16S rRNA and 28S rRNA datasets (Figures 1 and 8), calculated using the Z-closure method with TreeSizeWeightedMean edge weights.

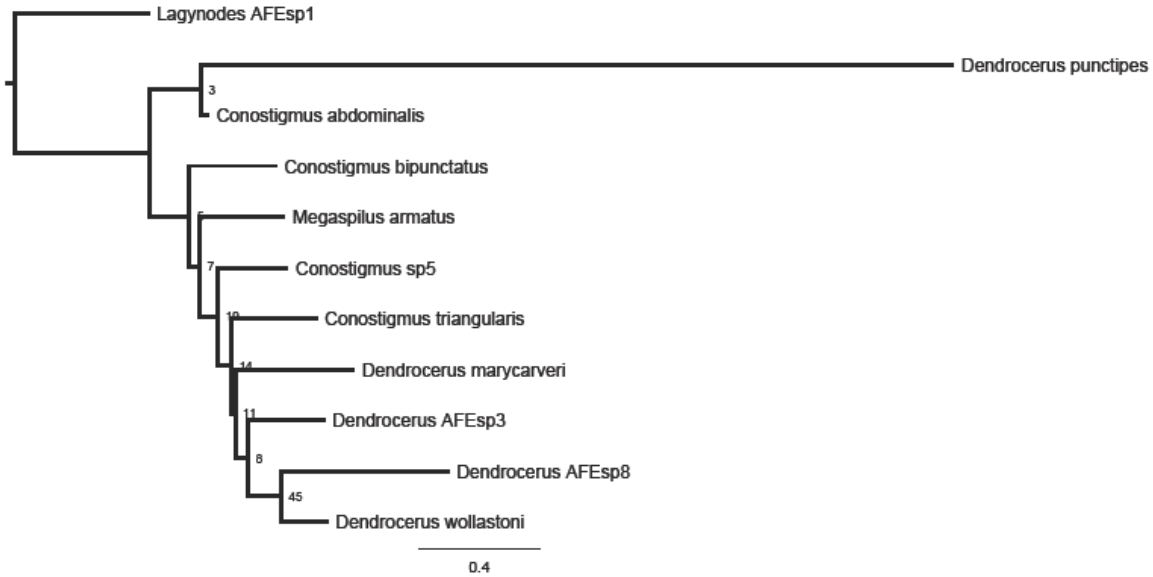

Figure 12. Most likely tree from the maximum likelihood analysis of COI mitochondrial DNA, bootstrap values listed at nodes (1000 bootstrap pseudoreplicates).

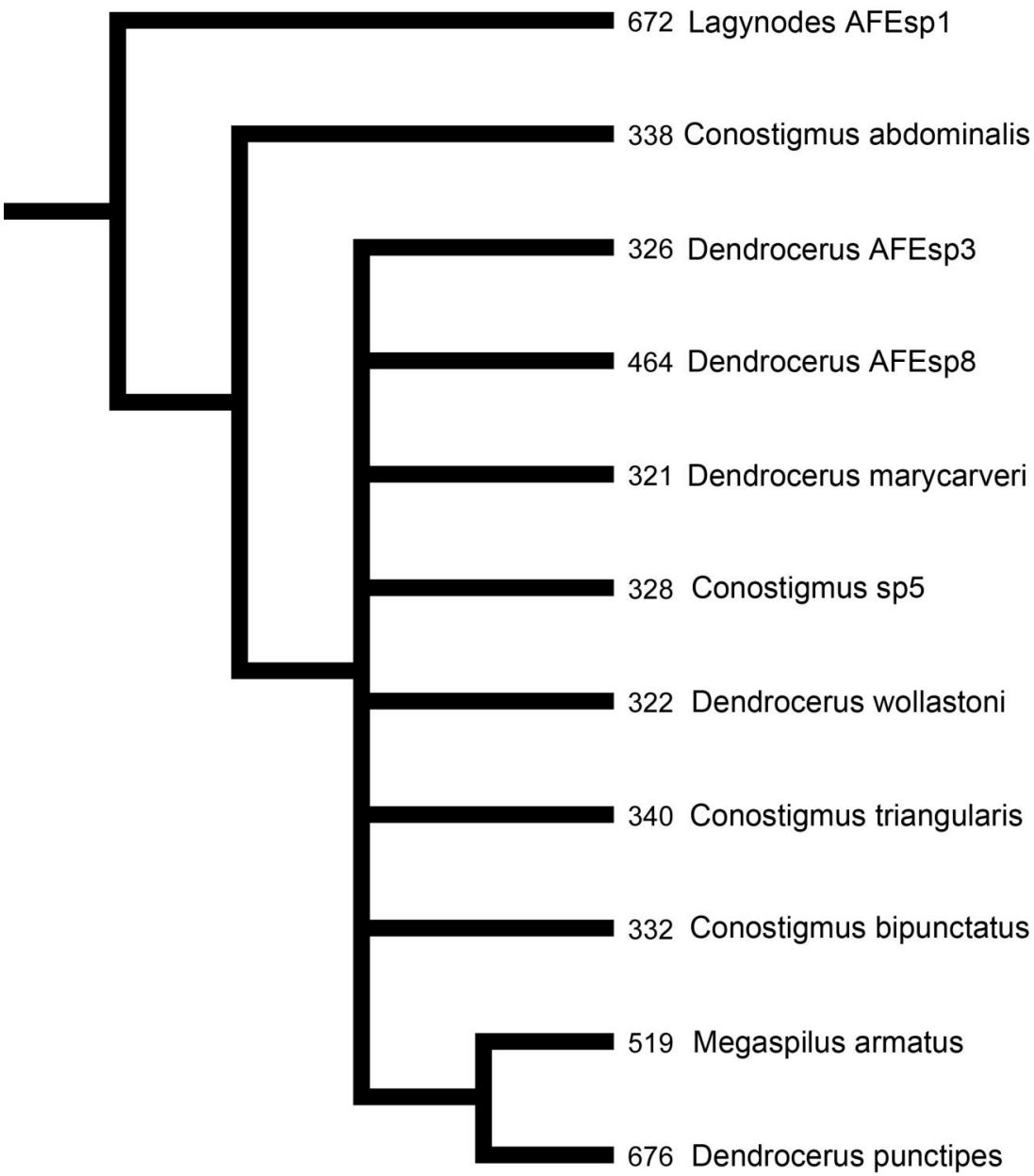

Figure 13. 50% majority rule tree from the maximum likelihood analysis of COI mitochondrial DNA (1000 bootstrap pseudoreplicates).

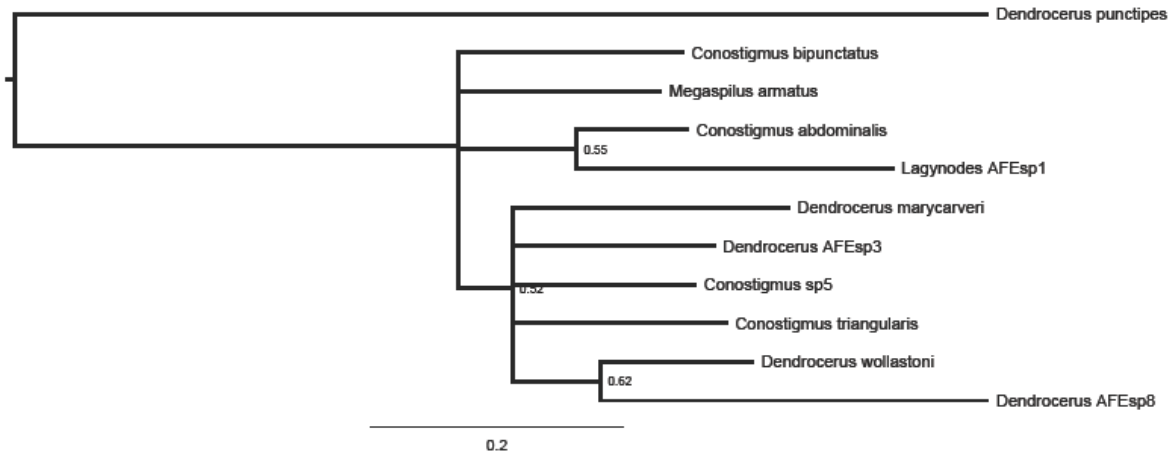

Figure 14. Topology inferred from the Bayesian analysis of COI mitochondrial DNA, posterior probabilities are listed at the nodes (12,210,000 generations).

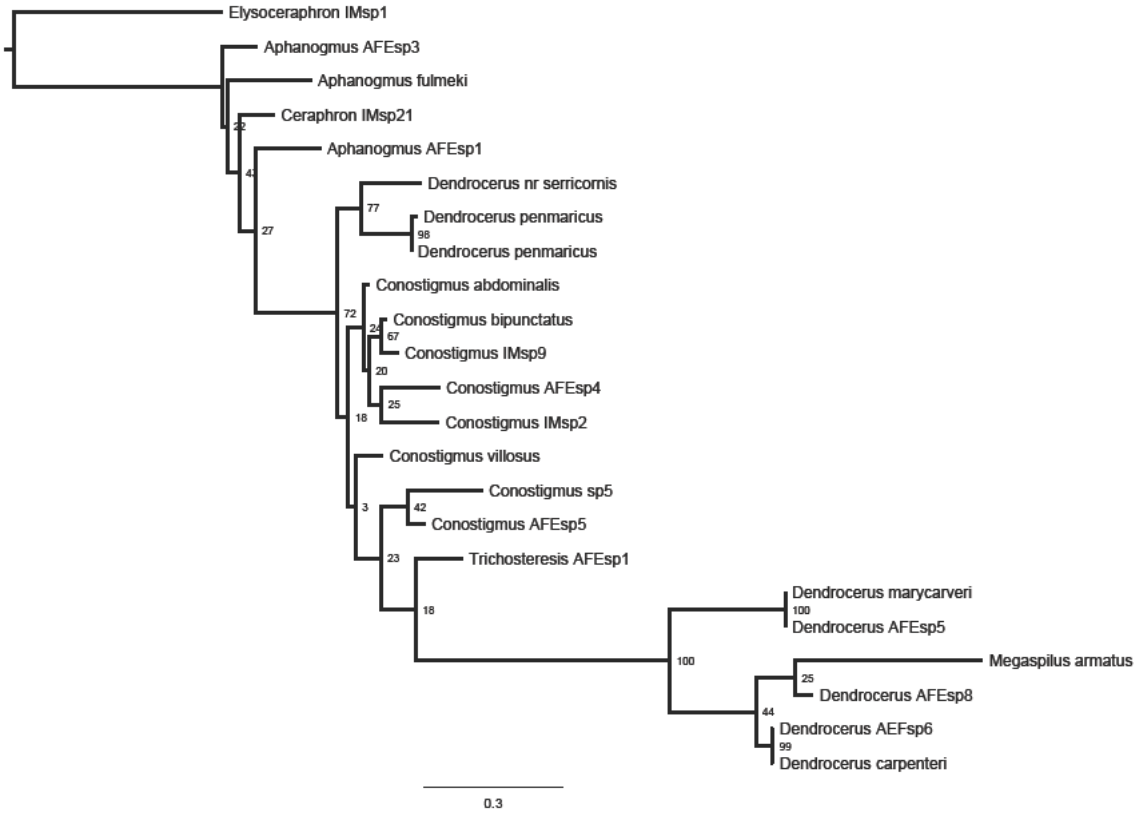

Figure 15. Most likely tree from the maximum likelihood analysis of exonic regions of RPS23 nuclear protein-encoding gene, bootstrap values listed at nodes (1000 bootstrap pseudoreplicates).

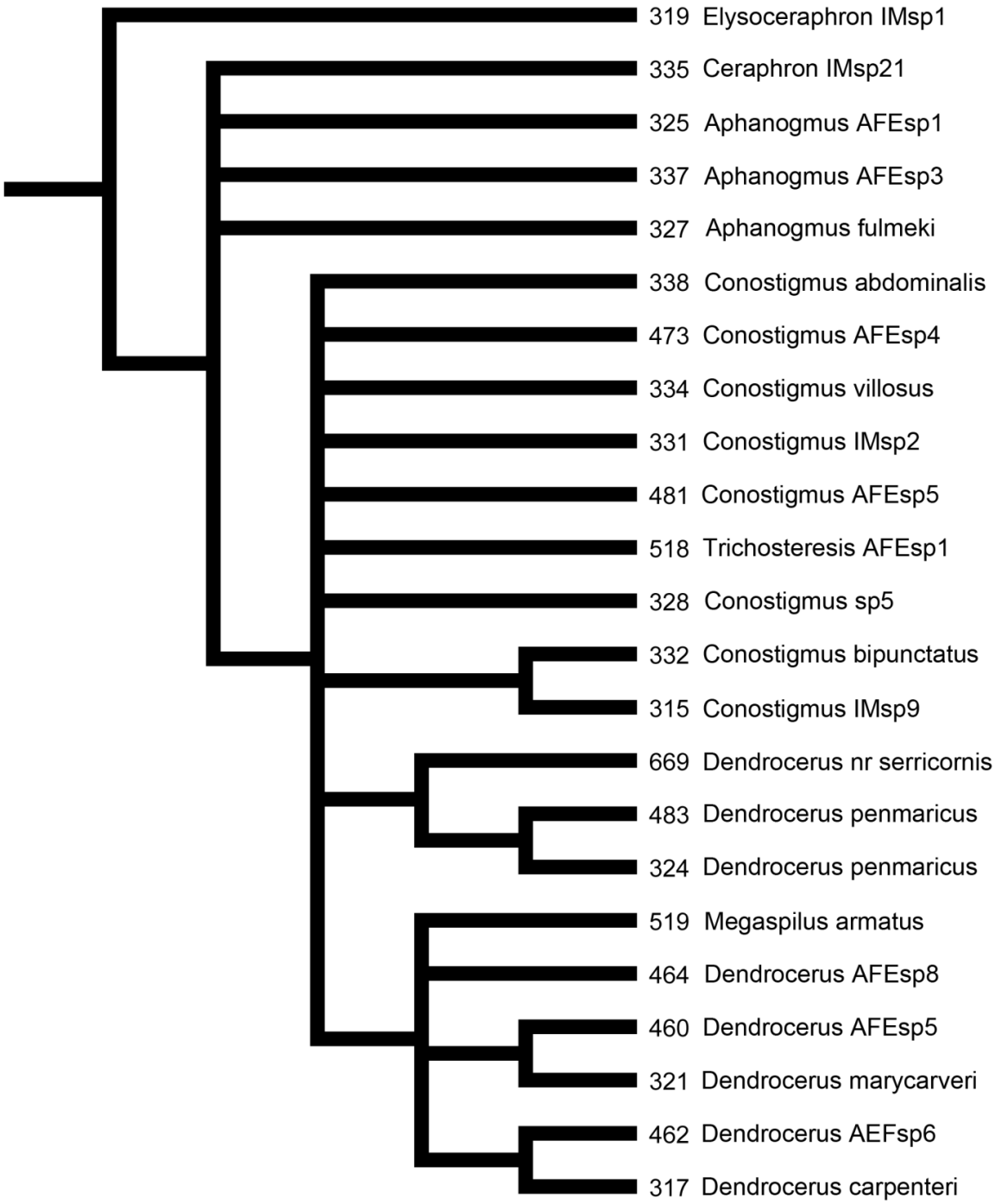
319 Elysoceraphron IMsp1
335 Ceraphron IMsp21
325 Aphanogmus AFEsp1
337 Aphanogmus AFEsp3
327 Aphanogmus fulmeki
338 Conostigmus abdominalis
473 Conostigmus AFEsp4
334 Conostigmus villosus
331 Conostigmus IMsp2
481 Conostigmus AFEsp5
518 Trichosteresis AFEsp1
328 Conostigmus sp5
332 Conostigmus bipunctatus
315 Conostigmus IMsp9
669 Dendrocerus nr serricornis
483 Dendrocerus penmaricus
324 Dendrocerus penmaricus
519 Megaspilus armatus
464 Dendrocerus AFEsp8
460 Dendrocerus AFEsp5
321 Dendrocerus marycarveri
462 Dendrocerus AEFsp6
317 Dendrocerus carpenteri

Figure 16. 50% majority rule tree from the maximum likelihood analysis of exonic regions of RPS23 nuclear protein-encoding gene (1000 bootstrap pseudoreplicates).

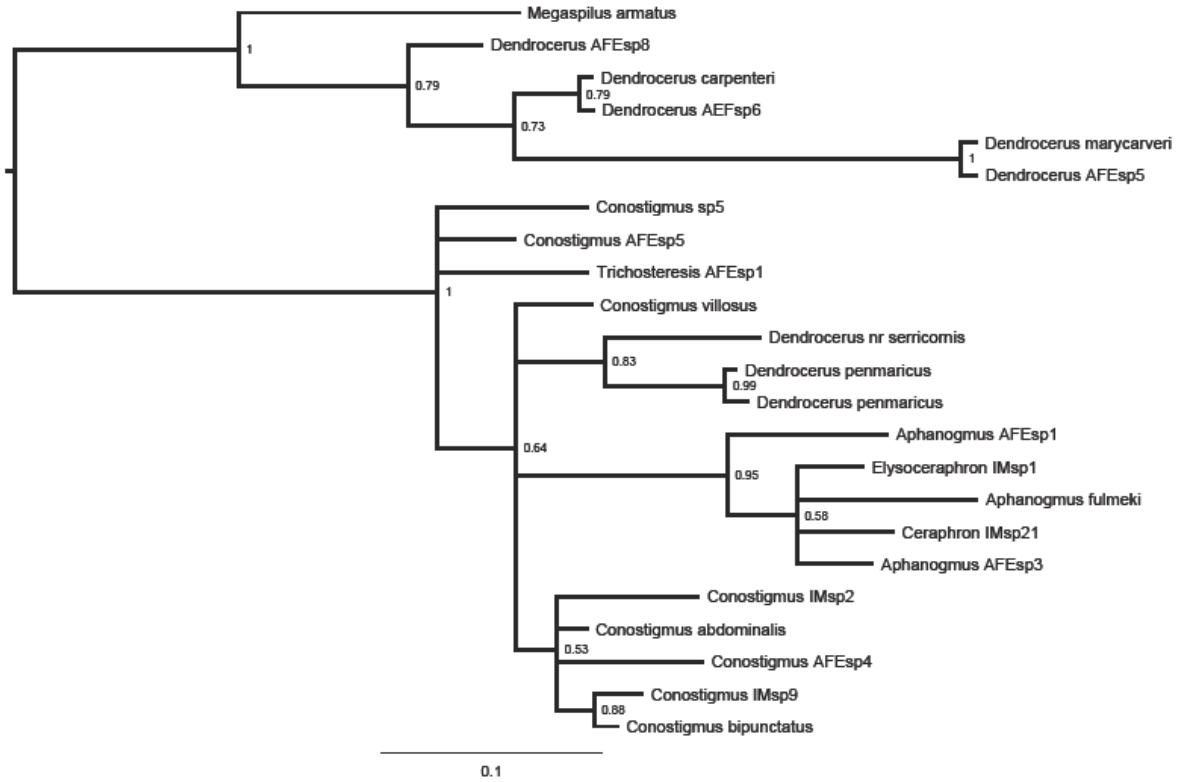

Figure 17. Topology inferred from the Bayesian analysis of exonic regions of RPS23 nuclear protein-encoding gene, posterior probabilities are listed at the nodes (11,090,000 generations).

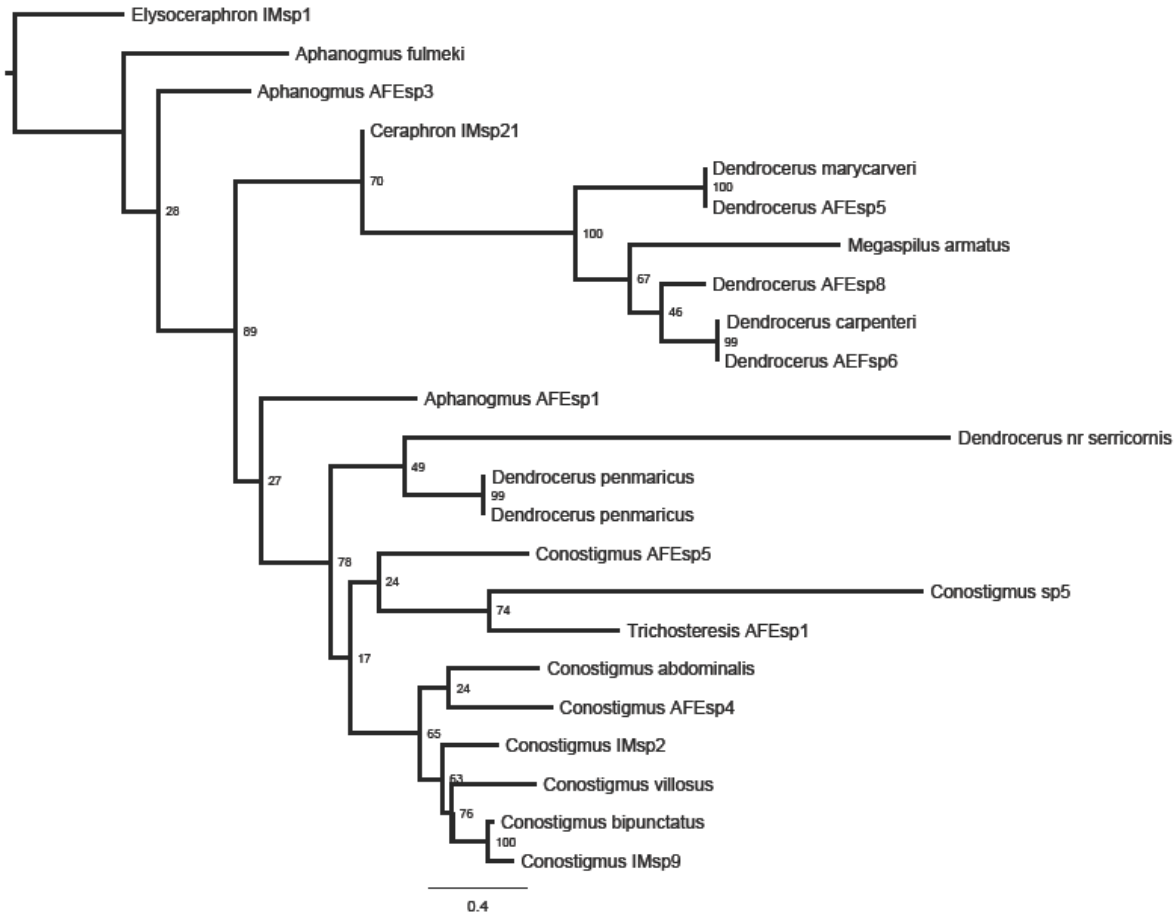

Figure 18. Most likely tree from the maximum likelihood analysis of intronic region of RPS23 nuclear protein-encoding gene, bootstrap values listed at nodes (1000 bootstrap pseudoreplicates).

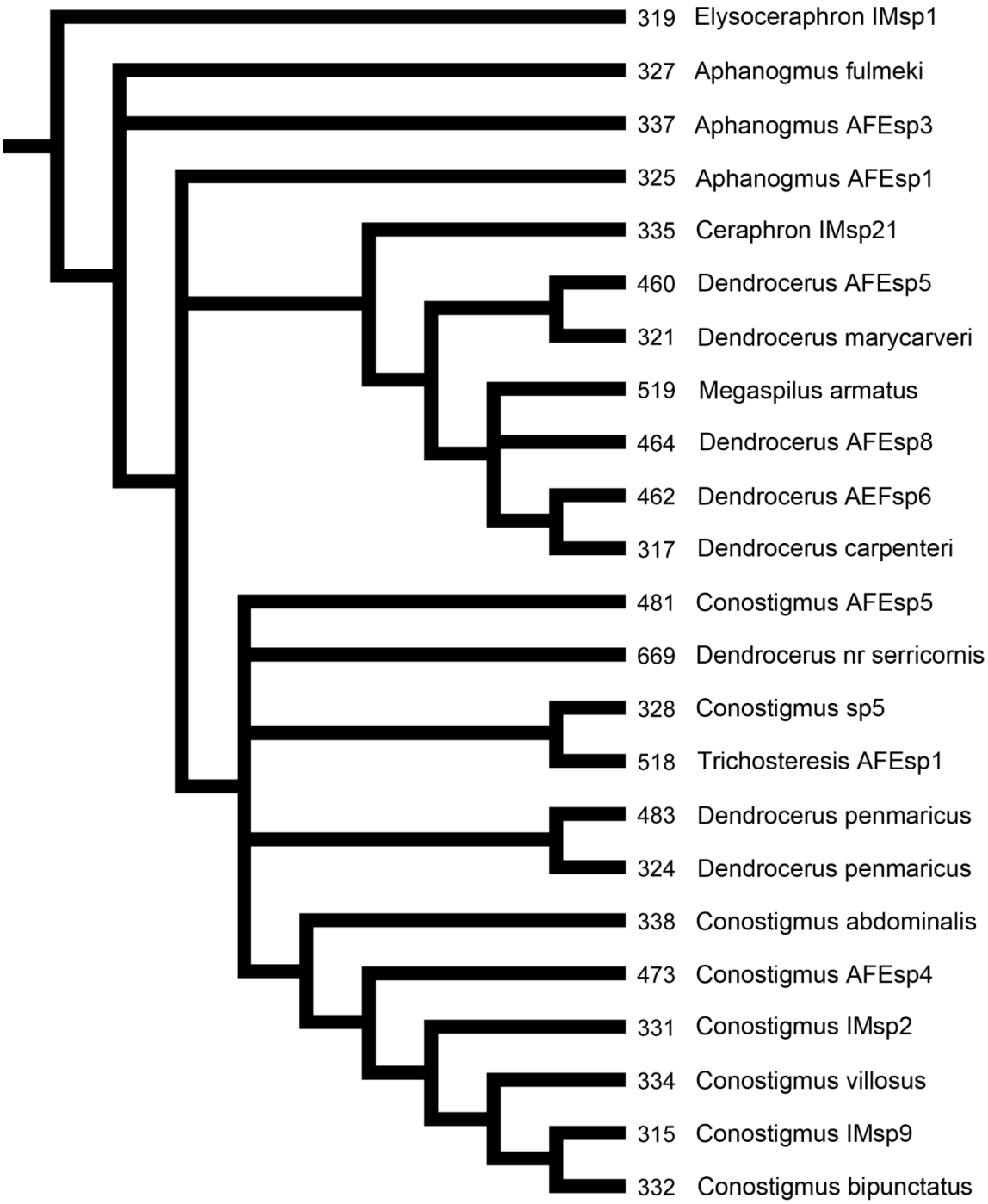

Figure 19. 50% majority rule tree from the maximum likelihood analysis of intronic regions of RPS23 nuclear protein-encoding gene (1000 bootstrap pseudoreplicates).

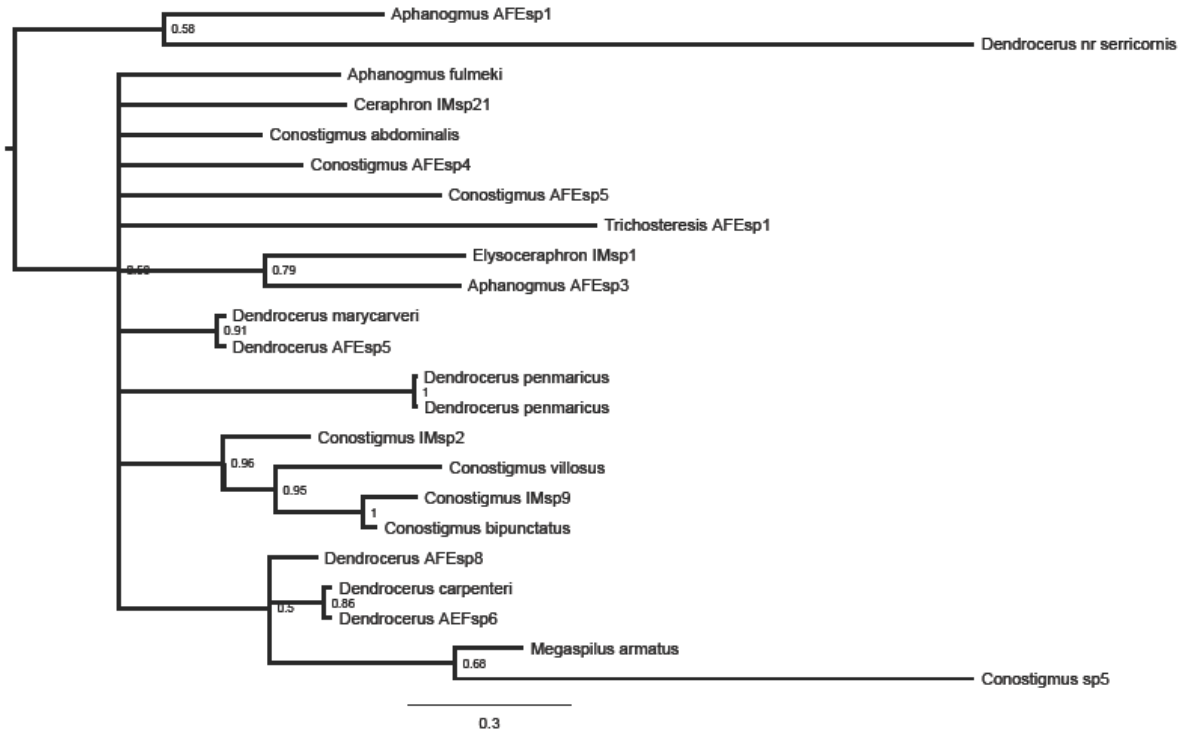

Figure 20. Topology inferred from the Bayesian analysis of intronic regions of RPS23 nuclear protein-encoding gene, posterior probabilities are listed at the nodes (11,040,000 generations).

Figure 21. Most likely tree from the maximum likelihood analysis of the concatenated dataset of 16S rRNA, 28S rRNA, COI mitochondrial protein-encoding DNA and RPS23 nuclear protein-encoding gene including intron and exons, bootstrap values listed at nodes (stopped at 800 bootstrap pseudoreplicates based on MRE bootstopping criteria).

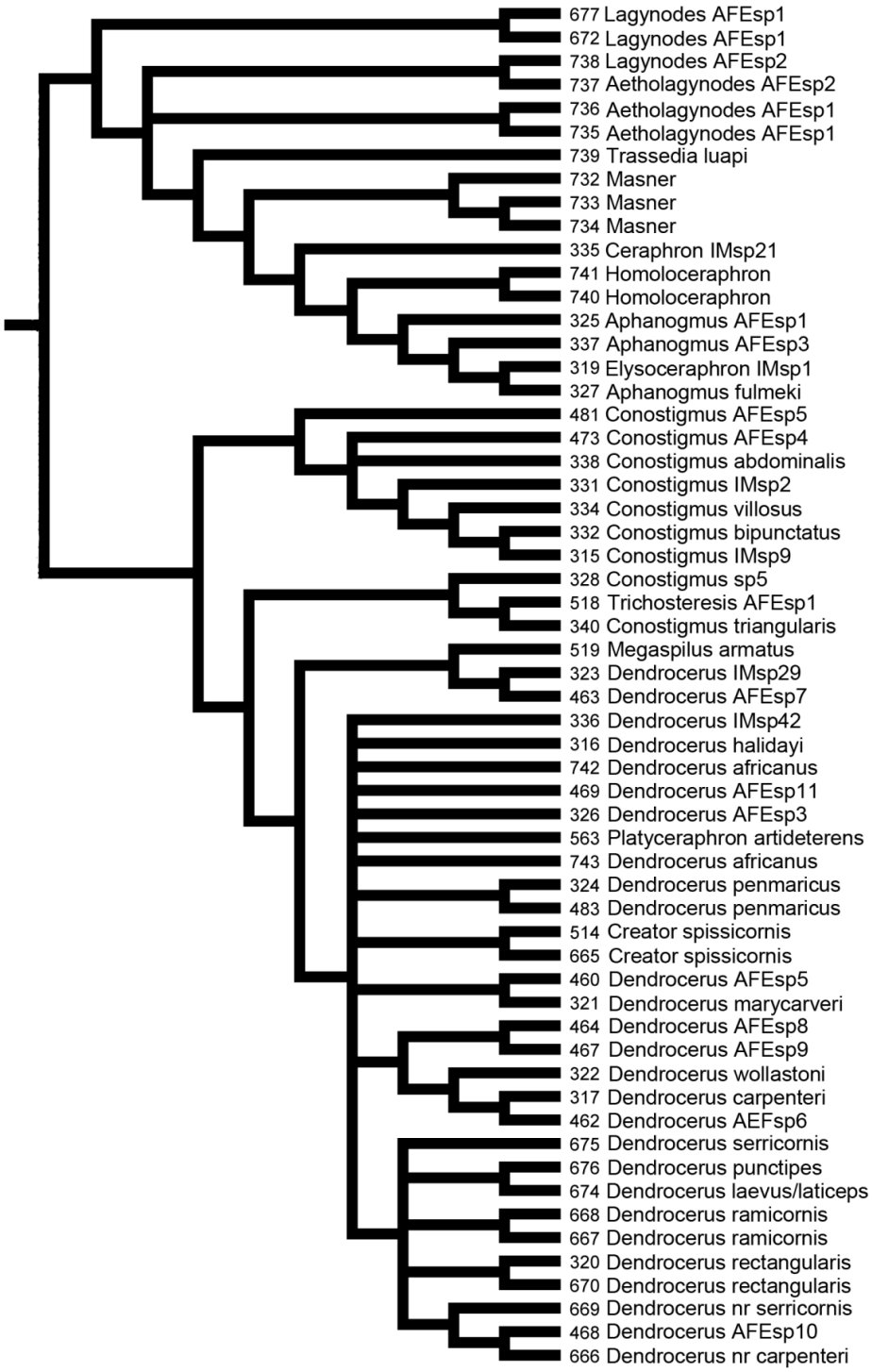

Figure 22. 50% majority rule tree from the maximum likelihood analysis of the concatenated dataset of 16S rRNA, 28S rRNA, COI mitochondrial protein-encoding DNA and RPS23 nuclear protein-encoding gene including intron and exons (stopped at 800 bootstrap pseudoreplicates based on MRE bootstopping criteria).

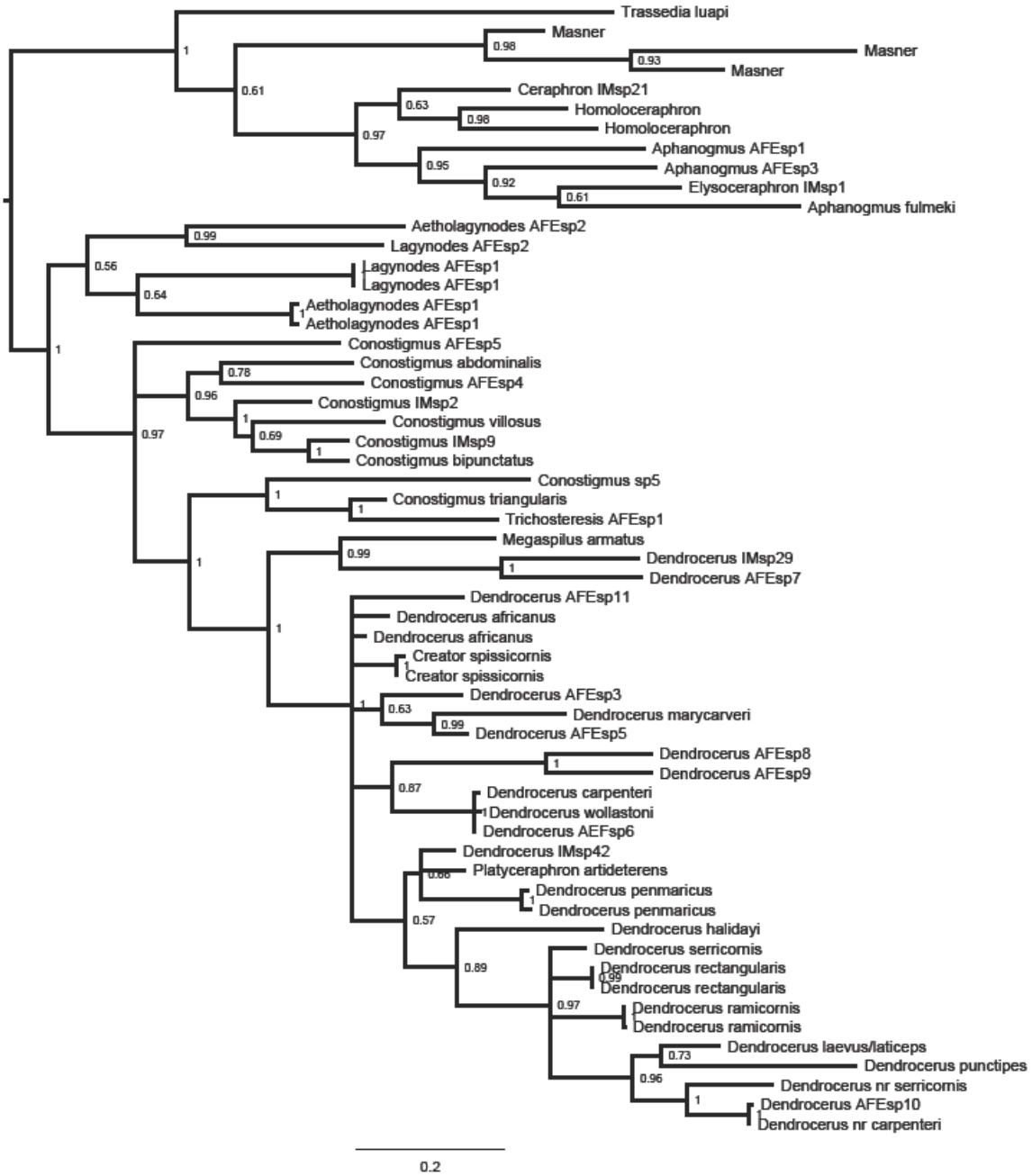

Figure 23. Topology inferred from the Bayesian analysis of the concatenated dataset of 16S rRNA, 28S rRNA, COI mitochondrial protein-encoding DNA and RPS23 nuclear protein-encoding gene including intron and exons, posterior probabilities are listed at the nodes (5,631,000 generations).